A STUDY OF 5KW WIND TURBINE PERFORMANCE IN A WIND FLOW OBSTRUCTION BUILDING USING THE CFD TECHNIQUE

KRITTAPAS KONGKAPISUTH

A DISSERTATION SUMITTED IN PARTIAL FULFILLMENT OF THE
REQUIREMENTS FOR THE DEGREE OF DOCTOR OF ENGINEERING
PROGRAM IN ENERGY AND MATERIALS ENGINEERING
(INTERNATIONAL PROGRAM)
FACULTY OF ENGINEERING
RAJAMANGALA UNIVERSITY OF TECHNOLOGY THANYABURI
ACADEMIC YEAR 2017
COPYRIGTH OF RAJAMANGALA UNIVERSITY
OF TECHNOLOGY THANYABURI

A STUDY OF 5KW WIND TURBINE PERFORMANCE IN A WIND FLOW OBSTRUCTION BUILDING USING THE CFD TECHNIQUE

KRITTAPAS KONGKAPISUTH

**A DISSERTATION SUMITTED IN PARTIAL FULFILLMENT OF THE
REQUIREMENTS FOR THE DEGREE OF DOCTOR OF ENGINEERING
PROGRAM IN ENERGY AND MATERIALS ENGINEERING
(INTERNATIONAL PROGRAM)
FACULTY OF ENGINEERING
RAJAMANGALA UNIVERSITY OF TECHNOLOGY THANYABURI
ACADEMIC YEAR 2017**

Dissertation Title	A Study of 5 kW Wind Turbine Performance in a Wind Flow Obstruction Building Using the CFD Technique
Name-Surname	Lieutenant General Krittapas Kongkapisuth
Program	Energy and Materials Engineering
Dissertation Advisor	Assistant Professor Wirachai Roynarin, Ph.D.
Academic Year	2017

DISSERTATION COMMITTEE
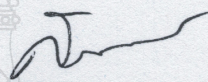
.... Chairman
(Assistant Professor Sorapong Pavasupree, Ph.D.)
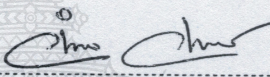
.... Committee
(Mr.Amphol Aphathanakorn, Ph.D.)

.... Committee
(Assistant Professor Jakkree Srinonchat, Ph.D.)
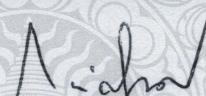
.... Committee
(Assistant Professor Kiattisak Sangpradit, Ph.D.)

.... Committee
(Assistant Professor Wirachai Roynarin, Ph.D.)

Approved by the Faculty of Engineering, Rajamangala University of Technology Thanyaburi in Partial Fulfillment of the Requirement for the Degree of Doctor of Engineering
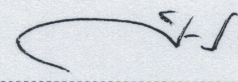
.... Dean of Faculty of Engineering
(Assistant Professor Sivakorn Angthong, Ph.D.)

March 2, 2018

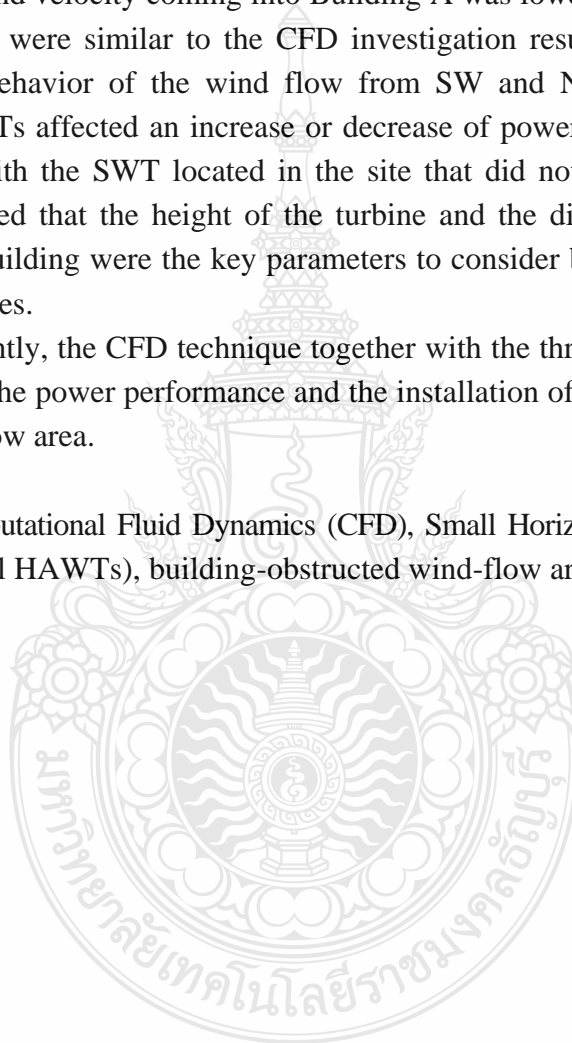|	
Dissertation Title	A Study of 5 kW Wind Turbine Performance in a Wind Flow Obstruction Building Using the CFD Technique
Name - Surname	Lieutenant General Krittapas Kongkapisuth
Program	Energy and Materials Engineering
Dissertation Advisor	Assistant Professor Wirachai Roynarin, Ph.D.
Academic Year	2017

ABSTRACT

This dissertation presents a study on techniques for a small and low wind speed turbine installation based on the small and low wind speed machine performance prediction in the wind flow obstruction area using the Computational Fluid Dynamics (CFD) technique. A Horizontal Axis Wind Turbine (HAWT) is commonly used in the wind energy sector compared to the other types of the machines. Small Wind Turbines (SWTs) in the scale of wind machines being not over 10 kW in power generation are commonly used in urban areas where are mostly surrounded by buildings that cause obstructed wind flows to the machines. The power performance of SWTs is significantly affected by the turbulence and wind shear. As a consequence, before installing SWTs in such areas, it is necessary to consider the effects of some parameters in order to reduce power loss and installation time. In this study, three units of 5 kW HAWTs installed in the Defense Energy Training Center (DETC) in Rayong Province, Thailand, were studied. The three turbulent models of CFD, comprising k-ε, k-ω, and RNG, were applied in the boundary conditions to investigate the performances and characteristics of wind flows to the machines. The wind flows being studied were from two directions, the North-East (NE) and the South-West (SW), both of which are the common wind flow directions in Thailand. Additionally, the wind velocity profile and the site information were collected and compared with the CFD data.

From the results of the CFD technique, the wind machines No.1 (WT1), No.2. (WT2), and No.3 (WT3) were compared with the wind machine located without any obstruction to the wind flow (WT0). It was found that: (1) Using the k-ε model with the wind flow from NE, the power performances of WT1, WT2, and WT3 were higher than that of WT0 by approximately 31%. For the wind flow from SW, the power performances of WT1 and WT2 were higher than that of WT0 by approximately 7%, while the power performance of WT3 was lower than that of WT0 by approximately 7%; (2) Using the k-ω model with wind flow from SW, the power performances of WT1 and WT2 were higher than that of WT0 by approximately 12%, while the power of performance of WT3 was lower than that of WT0 by approximately 2%; (3) Using the RNG model with the wind flow from SW, the power performances of WT1, WT2 were

higher than that of WT0 by approximately 9%,while the performance of WT3   was lower than that of WT0 by approximately 6%. The results of the CFD technique based on the three turbulent models showed similarities and trends in terms of power performances. Moreover, the study also measured the wind velocity behaviors in the site compared with the CFD technique results by using two anemometers which were installed at the same height of the SWTs in Building A and Building C in direction of wind flow from SW to Building A through to WT3-WT2-WT1-Building C. The measurement results from anemometers showed that the wind velocity coming into Building A was lower than that coming out of Building C, which were similar to the CFD investigation results. Therefore, the study showed that the behavior of the wind flow from SW and NE passing the buildings through to the SWTs affected an increase or decrease of power generation of the SWTs when compared with the SWT located in the site that did not obstruct the wind flow. Thus, it is suggested that the height of the turbine and the distance between the wind machine and the building were the key parameters to consider before installing this kind of the wind machines.

Consequently, the CFD technique together with the three turbulence models can be used to predict the power performance and the installation of an SWT in any building-obstructed wind-flow area.

Keywords: Computational Fluid Dynamics (CFD), Small Horizontal Axis Wind Turbines (Small HAWTs), building-obstructed wind-flow area, CFD models

Acknowledgements

Table of Contents

Table of Contents (Continued)

List of Tables

List of Figures

List of Figures (Continued)

CHAPTER 1

INTRODUCTION

1.1 Background and Statement of the Problems

The world increasingly needs more energy for daily life; fossil fuels have been used for generating energy for a long time. The environmental pollution has become a large problem, and global energy demand will increase by 1.6% annually, with nearly a 65% increase from developing countries [1]. Many countries are confronted with growing electricity demand and population; therefore, clean energy is being developed to solve this problem. Some countries aim to use 100% clean energy resources for their energy consumption [2-5], and renewable energy resources are growing fastest [6].

Thailand is the fastest-growing economy in Southeast Asia. Demand for energy is growing every day, and environmental pollution has increased because Thailand uses electricity generated from fossil fuel.

Wind energy is a renewable energy resource and clean; however, because wind energy at each site or location has different characteristics, these must be understood for improvement, which requires a long period of observation. As a result, wind turbine design has been specified by manufacturers [7]. At the end of 2016, global wind energy has grown, with an installed capacity of 486.8 GW.

Today, there are two types of wind turbine in the commercial market: the horizontal-axis wind turbine (HAWT) and the vertical-axis wind turbine (VAWT). However, the HAWT is the most frequently used for the development of electricity power generation [8-10]. However, in some locations or at some sites, the VAWT is used because some of the capabilities of the VAWT are more suitable than those of the HAWT, such as noise emissions or problems in wind direction. The VAWT can capture energy and respond to changes in wind direction more than the HAWT [11-14]. In urban areas, the buildings have a large effect due to wind direction or the roughness caused by building obstruction. These factors can create turbulent wind flow; thus, when operating close to buildings, VAWT can be suitable for urban areas. Therefore, before a wind turbine is installed at a site, it is necessary to estimate the performance and suitable location, and computational fluid dynamics (CFD) simulation techniques are suitable for optimizing the performance of wind turbines.

In this study, using three CFD turbulence models — k-Ɛ, k-ω, and the renormalization group k-e model (RNG) model — a validation technique is presented for site measurement in the study area — the Defence Energy Training Centre (DETC) at Rayong Province, Thailand, which is defined as a building-obstructed wind flow area — to investigate the power performance effect of three 5-kW HAWTs at the site. Consequently, this technique can be an applicable tool for prediction of power performance effects and investigation of appropriate designs for wind turbine projects in urban or building-obstructed wind flow areas.

1.2 General Overview

1.2.1 Renewable Energy

Fossil fuel is increasing carbon dioxide (CO_2) emissions, but renewable energy can reduce CO_2 from fossil fuels [15-16]. Generally, the kinds of renewable energy resource are often divided into the following categories.

Solar energy. An inexhaustible source of free energy on Earth is the Sun [17]. Nearly four million exajoules (1 EJ = 1018 J) and, annually, 5×10^4 EJ [18] are available.

Wind energy. One of the oldest renewable energy sources is wind energy, which is created by differences of temperature at different locations on the earth and the revolution of Earth around the sun. Since 2000, wind energy has been captured by large wind machine farms, which have grown by up to 21% per year [19]. Only 0.22% of wind machine farms has been captured by small wind machines [20].

Biomass energy. Bioenergy can be produced from a variety of organic material components; solid state, liquid state, and gas state are available from biomass [21-25]. Through a variety of processes, biomass can be a convenient raw material to produce electricity and stock [26-28].

Geothermal energy. For thousands of years, geothermal energy has used by humans, and it is a clean, renewable energy source. Geothermal energy is created form the temperature of volcanic activity under the earth's surface. Geothermal energy has reliability and low cost for generating power [29].

Hydrogen energy. Hydrogen is generated from many raw materials such as water, coal, biomass, and biogas. Hydrogen can be catalogued as renewable energy. Today, more than 50 million tons of hydrogen is generated globally, and 95% of that hydrogen is generated from fossil fuels [30].

Ocean energy. Ocean energy can be classified into four groups: ocean thermal energy conversion (OTEC), tidal current power, ocean current power, and wave power. Because of the uncertainty of the environmental impact, few types of ocean converter have been tested [31-33].

Hydropower energy. More than 160 countries worldwide use hydropower to generate electricity. Dams have been constructed to create elevation for generating electricity; after generating electricity, the water is available for irrigation and other purposes [34].

1.2.2 Wind Energy

Heating of the atmosphere from the sun and the rotation of the earth can produce wind, and this wind energy includes kinetic energy. The wind flow patterns on the earth depend on terrain. Wind energy power is the third power of wind speed, therefore. The advantages and disadvantages of wind power are as follows.

Advantages

1) Wind energy can be found everywhere on the earth, and wind machine convertors are inexpensive to produce.

2) Wind machines produce energy without generating pollution and with minimal maintenance.

3) The area under the wind turbine is only used for the tower of the wind turbine. Therefore, the area under the wind turbine tower can be used for agricultural purposes.

4) Most wind turbine farms are in remote areas where grid line power is not available.

5) In developing countries, wind turbine power is suitable for installation because grid lines are not conveniently available.

6) Although wind turbine systems use electricity from grid lines for beginning startup and control, the electricity production from wind turbine machines is more than grid-supplied power.

Disadvantages

1) Because the wind velocity is not stable and wind machines require sufficient wind speeds to generate electricity, wind machines must be supplemented with an alternative source.

2) Accidents, such as birds hitting wind turbine blades, and the disturbance of marine life in offshore installations are problems.

3) Because of the height of wind turbines, they cannot be installed in urban areas.

4) Some production line processes, such as wind turbine blade processes, of wind turbines can generate pollution.

5) To harvest dependable amounts of energy from wind, a large number of turbines must be installed in sufficient quantities in rural locations. These locations must have appropriate atmospheric wind current conditions to ensure a higher probability of power production.

1.2.3 Wind Turbine

The kinetic energy from wind velocity is captured by wind turbine blades and converted to electricity production. A wind turbine machine has the following main components.

Anemometer. The anemometer is used for measuring the velocity of wind and the transfer of wind velocity data to the wind turbine controller for control of the wind machine system.

Wind turbine blade. A wind turbine blade is used for capturing the kinetic energy of the wind and transferring it to the shaft of the generator.

Coupling and Brake. The coupling and brake are used to stop the spinning of the rotor of a wind turbine machine.

Controller. A controller is used for controlling the operation of the wind turbine machine system and such characteristics of wind turbine machines as the direction of the wind turbine blade and wind turbine's direction for capturing kinetic energy from the wind.

Gearbox. A gearbox is used for changing the speed of the wind turbine shaft; generally, a generator needs high speed to generate electricity. When wind turbine blades generate low speed, the gear box increases the speed from low to high.

Nacelle with drive train. The nacelle holds all components in the turbine machinery that are connected between the wind turbine blade shaft and the wind turbine tower.

Pitch. Pitch is used for controlling the wind turbine blade when it is necessary to increase or decrease the angle of attack from the wind direction.

Rotor. The rotor is used for connecting the hub and wind turbine blade.

Tower and foundation. Generally, wind turbine towers are made from tubular steel, which is used to support the nacelle.

Yaw. Wind turbine yaw is used for changing the direction of the nacelle either for capture or moving it away from the wind velocity direction.

Yaw motor. A yaw motor is used to drive the wind turbine yaw.

1.2.4. Small Wind Turbine

Wind turbines are machines for converting the kinetic energy from wind velocity. Large wind turbine machines are more commonly used, because they are inexpensive compared with small wind turbines. In 2014. wind turbine power reached approximately 369.6 GW, and this is expected to increase to 666.1 MW in 2019 [35].

When considering urban areas, large wind turbines are not suitable for installation, because of some of the problems referred to before; small wind turbines are considered more suitable for urban areas. Small-scale wind turbines can be classified into two types:

(1) Classification based on the axis of rotation: vertical-axis wind turbines (Darrieus wind turbine, Savonius Wind Turbine) and horizontal-axis wind turbines

(2) Classification based on lift and drag forces: lift type (Darrieus wind turbine) and Drag type (Savonius wind turbine)

Small wind turbines often use direct-drive generators to generate electricity. The wind machine uses the tail for changing direction, while large wind turbine machines use a yaw system.

1.2.5 Wind Turbine Site

Complex terrains have significant wind speeds, various wind directions, and the turbulence of wind flow. Since the 1970s, the turbulence flow from complex terrains has been studied [36], and two-dimensional [37] and three-dimensional analysis was reported [38]. The pressure gradient along the streamline due to upstream and downstream flow has been demonstrated by several theories [39]. The power production from a wind turbine system is proportional to the cube of the wind speed; in other words, if the wind speed increases 60%, the annual production of energy generated from wind turbine systems is 36%. When the tower of a wind turbine is high, it can generate more power than a short tower, because upper levels above the terrains have more wind speed than bottom levels.

1.2.6 Site Measurement

In some conditions, the design of wind turbine systems and experimental testing data can be different from the site measurement data. The complexity of such installation areas as hills, mountains, and buildings is significant for power generation. Real power data generated from real sites can be calculated in terms of "plant factor". This value is important for energy prediction.

1.2.7 Wind Turbulence

The turbulence of wind is the most significant factor for safety in wind turbine design [40]. Wind turbulence is generated from the friction with the surface of the earth or hills, trees, buildings, etc. The wind turbine's responding to wind turbulence can cause fatigue, vibration, sounds, etc. from the wind turbine machine, and the standard tool used is a turbulence model [41]. The characteristic of the turbulence model is a function of the changing pressure and flow velocity in fluid dynamics behaviour flow.

1.2.8 Urban Areas

An urban area is a human settlement with high population and complex infrastructure. Wind flow in urban areas is complex, and the wind velocity distribution and direction and the velocity gradient turbulence considerably change with building shape and urban configuration [42]. In addition, the wind velocity increases as the buildings become higher in relation to the surrounding urban canyons, introducing more acceleration [43].

High-rise buildings or surrounding trees can be represented abstractly by the wind flow effect, including downward deflection, upward deflection, low-velocity eddies, and counter-current effects.

1.2.9 Urban Building Shape Effect on Wind Flow

Fluctuating wind speeds due to the effects of building shapes have a significant effect on the generated wind power. Some building shapes will increase or decrease the velocity of wind flow depending on the changing direction of wind flow. The patterns of wind flow are complex due to turbulent flow, vortex flow, gusts of wind, Venturi effect, etc.

1.2.10 Venturi Effect

The Venturi effect is named after Giovanni Battista Venturi (1746–1822), an Italian physicist. The principal of the Venturi effect is that a fluid's velocity increases and its static pressure decreases when flowing through a constricted area, affecting some of its applications. Obstruction of wind flow by buildings is a common occurrence in urban areas. The wind blowing through narrow spaces of buildings in an urban area is seemingly faster and stronger than elsewhere. This "channelling" effect is just one form of a larger fluid flow principle — the Venturi effect. The Venturi effect states that, in a situation with constant mechanical energy, the velocity of a fluid passing through a constricted area will increase, and its static pressure will decrease. The effect utilises both the principle of continuity and the principle of conservation of mechanical energy. The principle that states that, within a specified flow field, a decrease in pressure occurs when there is an increase in velocity, is also known as Bernoulli's principle. Hence, the pressure difference described by the Venturi effect is utilised in many different devices that can be used in a variety of applications. In other words, the Venturi effect is the reduction in fluid pressure that results when a fluid flows through a constricted section, and the theory states that, in a situation with constant mechanical energy, the velocity of a fluid passing through a constricted area will increase and its static pressure will decrease. The effect can be observed in nature and industry. The severity of the Venturi effect is a function of the width, length, height, and size of openings in the canyon [44].

1.2.11 Computational Fluid Dynamics

A powerful tool to model fluid flow situations is CFD. The mathematical model and physical model are included in the CFD simulation method. CFD are simulated before validation tests [45]. The simulations have greater potential for accurate solutions than other methodologies. However, the CFD method requires an understanding of fundamental physics equations and fundamental mathematical models for creating the boundary or initial conditions of the CFD method.

1.3 Purpose of this Study

In this study, three turbulence models (k-ε, k-ω, and RNG model) for the CFD simulation technique were used to validate results of site measurements from the study area (the DETC) to investigate the power performance effect of three 5-kW HAWTs by proving incoming and outgoing wind velocity behaviour in the study area. It is expected that this CFD simulation technique could be used for predicting small wind turbines' power performance before installing the turbines in a building-obstructed wind flow area. The objective of this study are as follows.

1.3.1 To investigate the power performance of three 5-kW HAWTs in a building-obstructed wind flow area, DETC, compared with the power performance of a 5-kW HAWT installed in an unobstructed of wind flow area at DETC by using CFD, k-ε, k-ω, and RNG turbulence models.

1.3.2 To investigate the characteristics of wind flow or wind velocity behavior in DETC by a site measurement technique of wind flow over the buildings to the turbines at the site.

1.3.3 To validate the power performance effect of the turbines from the CFD investigation by comparing it with site measurements based on measured data in the study area to confirm that the CFD technique is reliable and can be applied to predict the power performance of small wind turbines in a building-obstructed wind flow area.

1.3.4 To recommend installing small wind turbines in a building-obstructed wind flow area, as well as to use the CFD technique for predicting their power performance before installing them in such an area.

1.4 Scope of this Study

1.4.1 The site of the study, the DETC, is considered a building-obstructed wind flow area that is located near the beach at Rayong province, Thailand.

1.4.2 At the site, there are three 5-kW HAWTs (THUNYA-5 kW HAWTs model) installed, surrounded by four main buildings. The wind flows across the site in the main directions of wind flow in Thailand, namely, SW and NE.

1.4.3 The main tools of the study are three CFD turbulence models (k-ε, k-ω, and RNG) and the CFDesign V.7 commercial software program and a wind speed measuring instrument (anemometer), namely, the Professional Touch Screen Weather Center With PC Interface, Model No: AW002, FREQ: 443MHz to measure wind speed for site measurement.

1.4.4 The CFD simulation technique applies the Navier–Stokes equation and continuity equation in the appropriate initial conditions, and also the boundary conditions in the 3-D model of control volume. Each turbulence model includes two main conditions. First is the fixed condition obtained from the buildings and the ground. Second is the moving condition obtained from the wind turbine rotors and the air. A wind velocity of 4.5 m/s was selected as the inlet condition, and a wind gage pressure of 0 Pa was selected as the outlet condition. In addition, ideal air was used as the working fluid, and the k-ε, k-ω, and RNG turbulence models were used for the simulation process.

1.4.5 The CFD technique used the k-ε model as wind flow from the NE and the SW and used the k-ω and RNG as wind flow from the SW at an incoming wind speed of 4.5 m/s.

1.4.6 Wind speed at the site was measured by a wind speed instrument (anemometer), the Professional Touch Screen Weather Center With PC Interface, Model No: AW002, FREQ: 443MHz, which was mounted on the roofs of two buildings (Building A and Building C) at the same height as the wind turbines' hub-height, 18 m, in the direction of the wind flow from the SW to Building A-wind turbines-Building C to investigate the behaviour of the wind velocity profile.

1.4.7 The behaviours of the wind velocity profile were compared by using the investigation results from the CFD technique and site measurement technique for validating the CFD technique.

1.5 Benefit of this Study

1.5.1 This CFD technique can be used to predict the power performance and installation of small wind turbines before installing them in a building-obstructed wind flow area.

1.5.2 This CFD technique can save cost and time in wind turbine projects in a building-obstructed wind flow area.

1.6 Dissertation Overview

CHAPTER 1 INTRODUCTION

The first chapter presents the background and a general statement of the study, as well as its purpose, scope, and overview.

CHAPTER 2 THEORY AND LITERATURE REVIEW

The second chapter outlines the theories and previous research needed to explain the parameters to gain more understanding of small-wind-turbine power performance when the turbines are installed in a building-obstructed wind flow area.

CHAPTER 3 MATERIALS AND METHODS

The third chapter describes the overall methods, materials, and techniques needed for the analysis of the CFD turbulence models (k-Ɛ, k-ω, and RNG) used in this work to investigate small wind turbines' power performance as they are installed in a building-obstructed wind flow area. In addition, site measurement based on the data measurement technique is reported for validating the CFD technique.

CHAPTER 4 RESULTS AND DISCUSSION

The fourth chapter presents the effect of the small wind turbines' power performance as wind flows across a building-obstructed wind flow to the turbines at an incoming wind speed of 4.5 m/s from both directions when using CFD technique. The CFD turbulence models (k-Ɛ, k-ω, and RNG) for CFD are used, as are site measurements based on the measured data as wind flows from the SW. In addition, both behaviours of the wind velocity profile are compared to validate the CFD technique.

CHAPTER 5 CONCLUSIONS

The fifth chapter presents conclusions and recommendations for small wind turbines installed in a building-obstructed wind flow area, as well as the used of the CFD technique for predicting the small wind turbines' behaviour before installing them into such areas.

CHAPTER 2
THEORY AND LITERATURE REVIEW

Urban regions have complex aerodynamic characteristics. The wind velocity is difficult to predict, due to the roughness; the gradient of wind flow behaviour based on changes from the urban ground; or the building shape, urban heat, etc. [46-47]. In the gaps between buildings there might be some effect from wind flow velocity, and it might increase the wind velocity by the Venturi or channelling effect, in some cases to typhoon-class wind speeds level [48]. The general information, theory, and literature review of each topic concerned with the power performance effect of small HAWTs located in a building-obstructed wind flow area are described.

2.1 Understanding of Energy and Power

2.1.1 Energy

Energy is work done that can be defined as changes of position in physical systems. The basic types of energy are potential energy and kinetic energy. The potential and kinetic energy can be divided into the forms below.

- Mechanical energy; relating to the object's motion.
- Chemical energy; relating to the bond of elements, molecular or atomic.
- Thermal energy; relating to the vibration of atoms or molecules.
- Electrical energy; relating to the movement of electrons in atoms.
- Radiation energy; relating to electromagnetic energy.
- Nuclear energy; relating to the energy stored in the nucleus of an atom.
- Gravitational energy; relating to the position level of objects.

The five renewable energy types are: solar energy, wind energy, biomass energy, hydropower energy, and geothermal energy. However, although the renewable energy sources provide free and clean energy, for some types of renewable energy source, energy conversion and storage are difficult and complex. From the law of energy, energy cannot create and destroy, it only can be changed from one form to another [49]. The energy conservation equation describes the form of the changing of energy. When considering a closed system and controlling the volume of the system, the energy transferring input and output of the system always must be equal [50]. This can be described by the continuity equation of conservation of mass in and out of the closed system.

$$\rho A_1 V_1 = \rho A_2 V_2 \tag{2.1}$$

where ρ is fluid density, A_1 is the section area of inlet, A_2 is the section area of outlet, and V_1 and V_2 are the velocities of fluid flow for the two areas, respectively.

When considering the statement of fluid motion at different positions, Bernoulli's equation can be developed as below.

$$P_1 + 0.5\rho v_1^2 + \rho g h_1 = P_2 + 0.5\rho v_2^2 + \rho g h_2 \qquad (2.2)$$

where P_1 is the inlet pressure energy, $0.5\rho v_1^2$ is the inlet kinetic energy, $\rho g h_1$ is the inlet potential energy, P_2 is the outlet pressure energy, $0.5\rho v_2^2$ is the outlet kinetic energy, and $\rho g h_2$ is the outlet potential energy. The units of energy measurement used are the International System of Units (SI) joule and British thermal unit (BTU) kilocalories. The unit convertor can convert between SI units and BTU units: 1 J = 0.2388 cal, 1 cal = 4.1868 J, 1 BTU = 1.055, and kJ = 0.252 kcal.

2.1.2 Power

The work is done by the time called "power"; the unit of power is described in terms of joules per second or watts. When considering the difference between energy and power, the energy is only measured in joules, while the power is measured in joules per time. The horsepower is one of the power units. Conversion between watts and horsepower can be described as 746 W is equal to 1 HP.

2.2 Understanding of Renewable Energy

When reducing the use of fossil fuels, renewable energy is considered as a clean, sustainable, free energy source that can reduce greenhouse gas emissions. Wind energy and solar energy are the two types most often used to generate electricity [51]. The five common renewable energy sources are biomass, hydropower, solar energy, geothermal energy, and wind energy [52]. For other resources, such as ocean energy, few technologies have been developed [53]. However, demand and technology for each resource should be balanced.

Renewable energy resources exist all over the world. In some areas, wind energy is promising, whereas, in some areas, solar radiation has the greatest potential. Thus, different renewable technologies should be selected for different areas. Renewable energy never runs out, requires less maintenance, and has a low cost of operation. Although renewable energy has many advantages, it has some disadvantages, such as the need to generate higher quantities and not relying on supply and demand.

2.3 Understanding of Wind Energy and Related Topics

2.3.1 Wind Energy

To generate power from renewable energy, wind energy is utilised most. Wind energy is mechanical energy as kinetic energy is converted to electric power by wind machines [54]. Wind energy is a clean energy resource and can reduce greenhouse gas emissions. Because wind energy is inexhaustible, it has been used historically to power ships, watering systems, etc. [55]. Wind power is the third power of the wind

speed, which is used to produce electrical power by means of wind turbine machines. The wind turbine machine blades capture the kinetic energy from the wind and convert it to drive the wind machine's shaft, which connects to the generator. The three main parameters of wind power are wind speed, air density, and swept area [56]. Because the power from the wind turbine is the cube of the wind speed, a small increase in wind speed results in a large increase in power. Wind turbine power is given in the equation below.

$$P = \frac{1}{2}\rho AV^3 \tag{2.3}$$

Where, ρ is density of air (1.225 kg/m^3), A is rotor swept area, and V is wind speed. Air density varies with elevation and temperature: high temperature produces low air density, while low temperature produces high air density. As Eq. 2.3 shows, when air density is high, the power generation from wind machines will be high [57]. The swept area of a wind turbine machine is πr^2, which means that a little increase in blade length can cause a large increase in the wind turbine power [58]. If considering the increase of rotor blade diameter and increasing wind speed, doubling the diameter can increase power output four time, while double the wind speed increases power output eight times [59]. Thus, wind turbines should be located where wind speeds are high and there are few obstacles, such as trees or buildings. Obstacles can disrupt airflow, generates high turbulent access to reduce turbine life. High turbulence and wind shear of offshore wind turbine sites are less than those of onshore wind turbine sites.

The wind class of a wind turbine is based on three parameters indicated by The International Electro technical Commission (IEC), as shows in Table 2.1.

Table 2.1 IEC Wind Class (m/s)

Type	I (High Wind)	II (Medium Wind)	III (Low Wind)	IV (Very Low Wind)
Reference Wind Speed	50.0	42.5	37.5	30.0
Annual Average Wind Speed (Max)	10.0	8.5	7.5	6.0
50-year Return Gust	70.0	59.5	52.5	42.0

2.3.2 Wind Turbine

A wind turbine is a device to convert wind kinetic energy to electric power. The wind turbine blade is the first device that captures kinetic wind energy, which is then transferred by mechanical work to the generator shaft, which will generate the electricity. Finally, the electricity is transferred to the grid line. The significant

parameters of wind turbine power generation are wind speed flow and swept area of the wind turbine machine. The power curve of the wind turbine machine is plotted by the characteristics of wind speed and quantity power output that can indicate wind turbine efficiency [60]. The maximum of a wind turbine machine was calculated by Albert Betz and equals 59.3%, and this is called the Betz limit or Betz's law. This is the power coefficient and is defined as: $C_{p,max} = 0.59$.

Currently, wind turbine machines have two configurations, depending on the rotation axis of the rotor: HAWTs and VAWTs, as Figure 2.1.
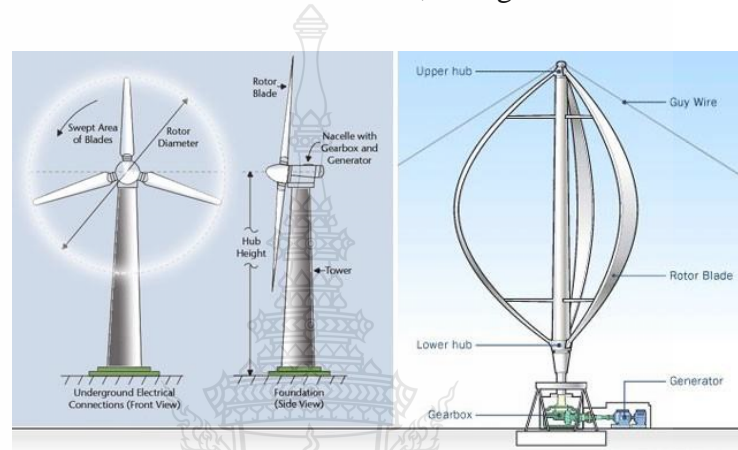
Figure 2.1 Horizontal-Axis and Vertical-Axis Wind Turbines [61]

Generally, the generators of HAWTs are located on the top of wind machine tower, inside the nacelles, while the generators of VAWTs are located on the bottom of the wind machine tower. Small HAWTs use tails for responding and changing direction from the wind direction, while large wind turbine machines use a yaw mechanism for responding and changing direction [62]. VAWTs can capture all wind directions; therefore, the tail and yaw mechanisms are not installed in VAWTs.

A gear box is used for increasing the rotating speed of the wind turbine shaft. Generally, the gear box of VAWTs can be placed near the ground to reduce tower moment over turning, while HAWTs located at the top tower can generate a large moment of tower turning when wind turbine's capture wind force.

Normally, the wind turbines can have four sizes depending on site: micro turbines, small wind turbines, and medium wind turbines are used for domestic applications, while large wind turbines are used for power plant systems. Micro wind turbines and small wind turbines are mostly used for battery-charging storage that is not connect to the grid line system, while medium wind turbines and large wind turbines connect to the grid line system.

Wind turbines can be installed onshore and offshore. Currently, onshore wind turbines are not as fast growing as offshore wind turbines, because onshore is difficult to find high and quality wind speeds although large landscape for installation.

The main parts of the small HAWT are shown in Figure 2.2, including a wind turbine blade connected to the shaft of the generator. The shaft connects to the gear box for increasing the speed of the rotor when connected with a high-speed generator while sometimes not to the gear box when used for a low speed generator (permanent magnet generator, or PMG). The nacelle also includes a yaw system for changing the wind turbine blade direction. The tail of the small wind turbine is used for capturing wind direction and will adjust the direction of the wind turbine machine. The tower is used for supporting and connecting between the wind turbine hub and the ground.
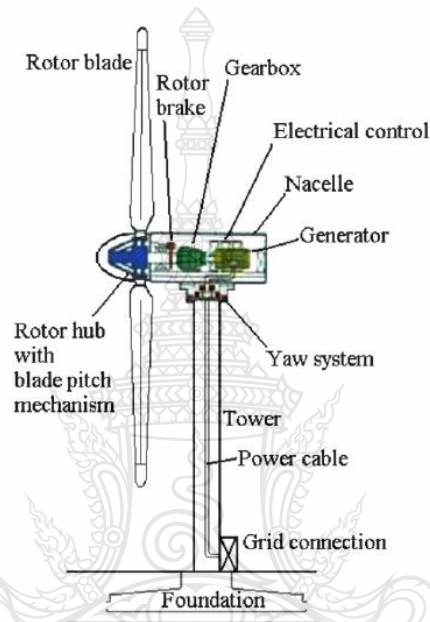
Figure 2.2 Major Components of a HAWT [63]

The wind turbine blade is used for capturing the force from the wind flow; when considering the cross-section, the airfoil profile is mostly used for design. The aerodynamic characteristics from the airfoil profile generate the lift force that is converted to the wind turbine rotor. The major component characteristics of the airfoil profile are shown in Figure 2.3.
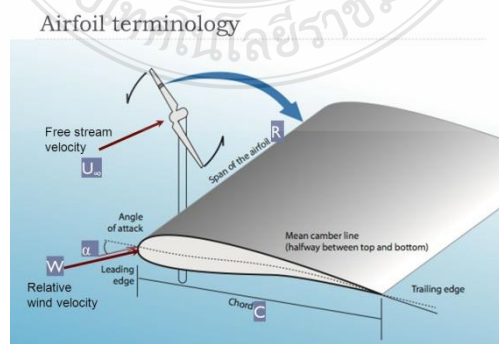
Figure 2.3 Main Parameters of an Airfoil [64]

23

The characteristics of an airfoil can generate the pressure differences, Then, force R will be generated as shown in Figure 2.4.

Lift force is the force that is vertical to the wind flow direction.

$$R_L = C_L \frac{1}{2}\rho A V^2 \qquad (2.4)$$

Drag force is the force that is parallel to the wind flow direction.

$$R_D = C_D \frac{1}{2}\rho A V^2 \qquad (2.5)$$
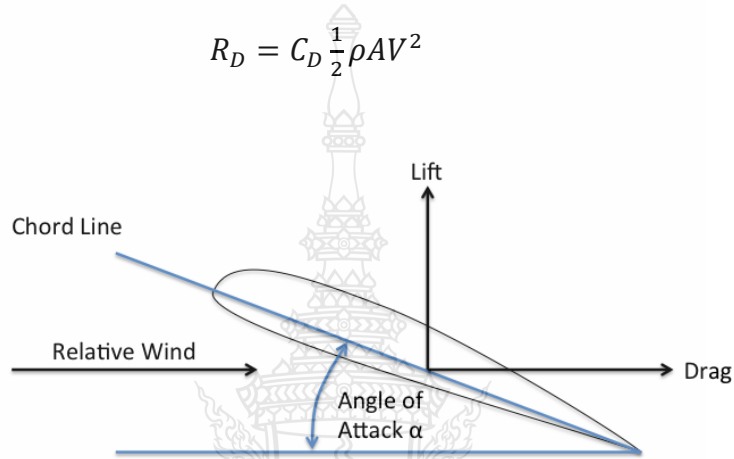
Figure 2.4 Airfoil Lift and Drag [65]

The torque generated from the rotor's rotation can be expressed as:

$$F = \frac{1}{2}\rho A V^2 \qquad (2.6)$$

where F is force from wind flow.

Hence, the torque of the rotor will be:

$$T = \frac{1}{2}\rho A V^2 R \qquad (2.7)$$

where R is the radius of the rotor.

The ratio between the velocity of the rotor tip and the wind velocity is called the tip speed ratio:

$$\lambda = \frac{R\Omega}{V} \qquad (2.8)$$

where Ω is the angular velocity.

where ρ is the density of air, V is the velocity of undisturbed air flow, A is the projected airfoil area *(chord x span)* and C_L, C_D are the lift and drag coefficients

24

The wind turbine power curve (power output vs. wind speed) is the electrical power that can be generated at different wind speeds, as shown in Figure 2.5. This power curve plotted only the steady-state wind flow velocity condition and does not include the turbulence of the wind flow condition. Furthermore, the characteristic of the real site installation of the wind turbine also affects the performance of the system.
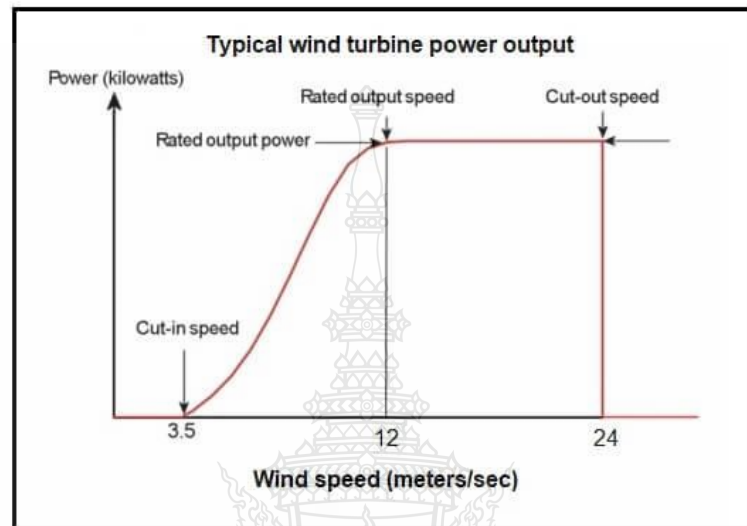
Figure 2.5 Typical Wind Turbine Power Output with Steady Wind Speed [66]

The *cut-in* wind speed point indicates that the minimum wind speed that can overcome the friction force of the rotor's rotation and cause the rotor to rotate and produces the electrical power. The *rated* wind speed point indicates the maximum power output that can generate the electrical power. The cut-out wind speed point indicates the maximum wind speed at which the wind turbine will stop the rotor from rotating to avoid damage from high wind speeds.

Turbine wind class is one of the factors that must be considered during the complex process of planning a wind power plant. If there is no change in wind direction with height, high turbulence will lower the power curve near the rated speed. Conversely, high turbulence will enhance power performance near the cut-in speed due to the wind speed distribution and the shape of the power curve. Wind turbines are classified by the wind speed, Class I to Class IV, with A or B referring to the turbulence, as shown in Table 2.2.

Table 2.2 Wind Turbines Class I A-B to Class IV A-B

Class	Avg. Wind Speed (m/s)	Turbulence	Class	Avg. Wind Speed (m/s)	Turbulence
IA	10	18%	IIIA	7.5	18%
IB	10	16%	IIIB	7.5	16%
IIA	8.5	18%	IVA	6	18%
IIB	8.5	16%	IVB	6	16%

The manufacturer's power curve, as shown in Figure 2.6, is derived from test data in ideal wind flow conditions and at the real site installation. Although some installation real site parameters may be close to ideal conditions, the power production from the real site still different from the manufacturer's power curve due to the turbulence of wind flow from the real landscape. Therefore, expected energy production at turbine locations requires adjustment to reflect performance based on the real conditions experienced at the site.
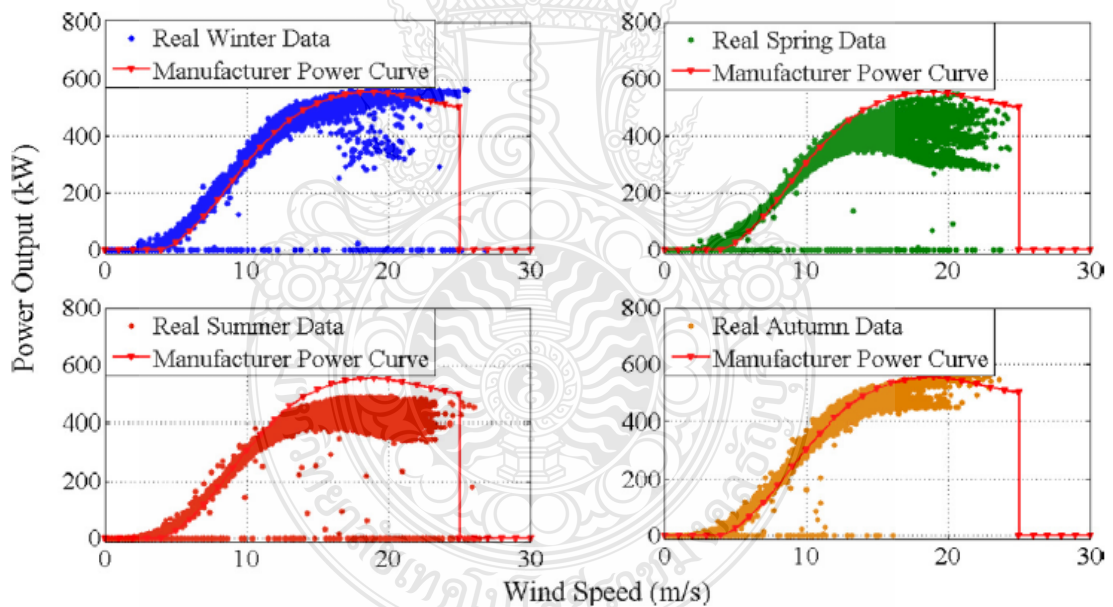
Figure 2.6 Power Curve Between Manufacturer and Site Installation [67]

The electric power output of a wind-to-electric conversion system can be expressed as

$$P_e = \frac{1}{2}\rho\eta_g\eta_m\eta_p A C_p V^3 \tag{2.9}$$

where P_e = electric power output, when; η_g and η_m = efficiencies of the electric generator and the mechanical interface, respectively; and η_p = efficiency of the power conditioning equipment. The product of these efficiencies and the coefficient of performance usually will be in the range of 20% to 35%. The electrical equipment needed for wind-to-electric conversion depends, above all, on whether the aero turbine is operated at a constant speed, nearly constant speed, or variable speed. With constant-speed and nearly-constant-speed operation, the power coefficient C_p becomes a function of wind speed. If the variable-speed mode is used, it is possible to operate the turbine at a constant optimum C_p over a range of wind speeds, thus extracting a larger fraction of the energy in the wind [68].

2.3.3 Turbulence of Wind

The characteristics of the turbulence of wind flow are based on fluid dynamics, changing pressure, and changing wind flow velocity. Turbulence is the fluctuation of wind flow in a short time scale, which is similar to dynamic load. The fatigue is generated when the dynamics load occurs; therefore, the wind turbine blade and some components of the wind turbine machine must be carefully designed. One turbulence model dimension is the turbulence intensity measured over short intervals of wind direction, as shown in Eq. 2.10.

$$I = \frac{\sigma_u}{\bar{u}} \tag{2.10}$$

Where $\bar{u}$ is wind velocity and σ_u is the standard deviation ratio at the same point and averaged over same time period.

Generally, obstacles and topography will create turbulence for many reasons, such as the boundary layer of the friction on the ground of the Earth. Normally, the velocity of wind flow will increase when the height from the ground increases, but, in complex terrain, it does not increase regularly due to turbulence. The fluctuation of wind flow is due to the turbulent flow, which includes three dimensions: along the flow of wind (stream wise), across the flow of wind (cross-stream), and vertically with the flow of the wind. The turbulent flow is essentially unpredictable. Wind shear is one cause of the turbulent flow.

The function of wind velocity and height from the ground is called wind shear. In theory, one can assume the wind velocity at ground is equal to zero due to the friction of the ground, and the velocity profile will distribute along the height from the ground. Thus, when designing a wind turbine power plant, the wind shear profile is one significant parameter for plant design. Figure 2.7 shows the wind speed changes with respect to height.
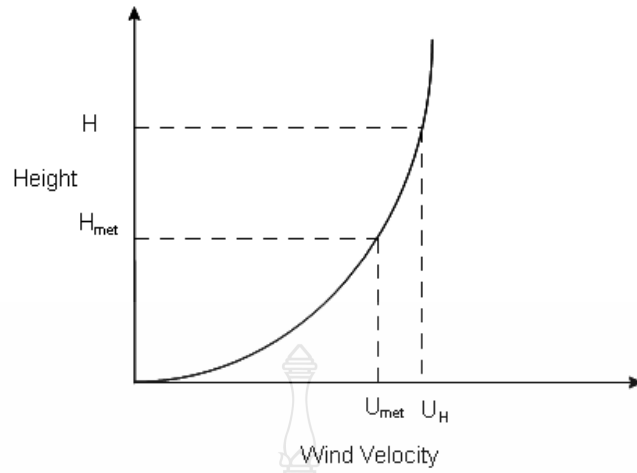
Figure 2.7 Wind Flow in Boundary Layer [69]

For a steady turbulent shear flow, the mean velocity profile in a small region near the surface is described by the relationship called the Wall law.

$$\frac{u_t}{u^*} = \frac{1}{2} ln \left(\frac{z}{z_0}\right) + B \tag{2.11}$$

where u^* is the friction velocity, u_t is the dimensionless velocity, B is an empirical constant related to the thickness of the viscous sublayer (B = 5.2 in a boundary layer over a smooth flat plane; for rough walls, smaller values of B are obtained) [70]. The constant z_0 called roughness is the frontier between the logarithmic zone and the inner $k - \varepsilon$ zone. When wind speed changes direction with increased height above ground, it is known as the shear gradient. The wind shear formula is shown below.

$$U = U_{ref} \left(\frac{h}{h_{ref}}\right)^\alpha \tag{2.12}$$

where U and U_{ref} represent the wind speed at height h, h and h_{ref} represent the height of interest and the reference height, respectively, and α is the wind shear coefficient, which depends on factors such as height, time, and location. In relation to a mild shear gradient ($\alpha \leq 0.1$), wind conditions are generally uniform across a turbine's rotor plane, provided a condition with a sharp shear gradient ($\alpha \geq 0.3$) is maintained.

The power law is the most common method to describe the average wind speed as a function of height h above the ground, which is defined as follows:

$$\frac{V_2}{V_1} = \left(\frac{h_2}{h_1}\right)^\alpha \tag{2.13}$$

in which V_2, V_1 are wind speeds at h_2, h_1 heights, and α is the wind shear coefficient, which depends on factors such as height, time, and location. This coefficient is normally considered to be 0.15-0.3, as shown in Figure 2.8.
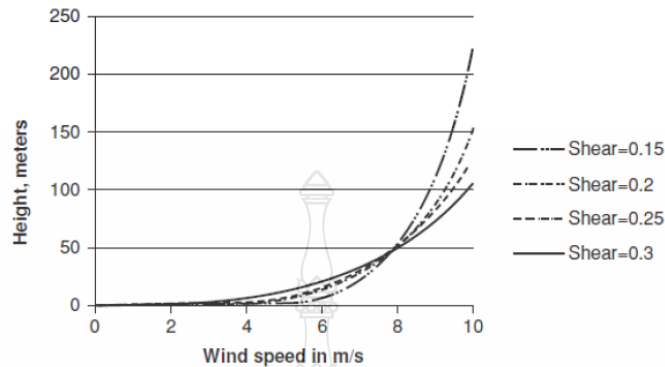
Figure 2.8 Wind Speed with Respect to Height for Different Values of Shear; the Average Wind Speed is 8 m/s at a Height of 50 m [70]

The kinetic energy and viscous damping in a fluid flow can be predicted with the dimensionless Reynolds number. The turbulence intensity is described as turbulence quantified as the horizontal wind speed divided by the average wind speed. The turbulence intensity be high when wind speeds fluctuate rapidly. Conversely, turbulence intensity is low when the wind flow is in a steady-state condition [71].

Because the turbulent effect can affect turbine loads, fatigue load, noise propagation, etc., the power performance of the wind turbine machine is a function of turbulent flow. It is necessary to improve power performance by investigating turbulence intensity [72]

Obstruction by buildings affects the power output of wind machines. The obstruction generates boundary layers of wind flow that can reduce the power performance because of turbulent wind flow. Therefore, the wind turbine machine should consider building obstruction when installed in urban areas [73-74].

In urban area, wind flow around obstacles, as shown in the Figure 2.9, increases speed when passing around the sides and over the top of the obstacles, while the wind velocity behind the obstacle is decreasing and highly turbulent. Vortices are generated on the side of, at the top of, and behind the obstacle due to turbulent flow.
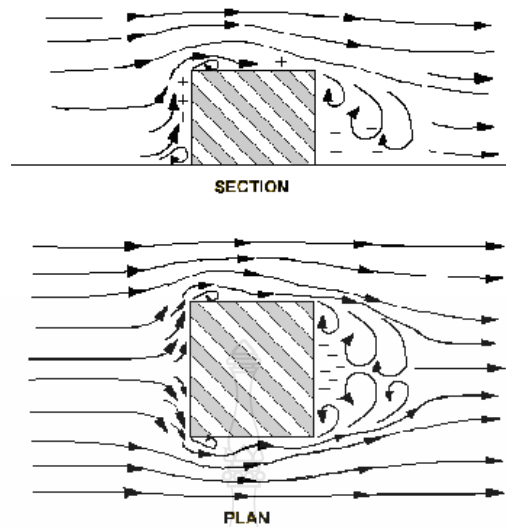
Figure 2.9 Wind Flow Around an Obstacle [75]

Obstacles, such as trees and buildings, can drastically reduce wind quality. Therefore, they could provide a power curve of different turbulence levels combined with the site measurement data testing to create more-accurate power production [76].

2.3.4 Wind Obstacles

When the wind blows without obstruction, it will flow in a smooth or laminar pattern, but when wind blows over a feature such as trees, buildings, high walls, and other structures, it can create a zone of turbulence. The wind cannot be seen, but the wind can be predicted, including how it will react to local effects. The reduction in wind velocity near the surface is a function of surface roughness, so wind velocity profiles are quite different for different terrain types [77]. Rough, irregular ground and manmade obstacles on the ground retard movement of the air near the surface, reducing wind velocity [78-79]. Because of low surface roughness on the relatively smooth water surface, wind speed does not increase as much with height above sea level as it does on land. Over a city or rough terrain, the wind gradient effect could cause a reduction of 40% to 50% of the geostrophic wind speed aloft; over open water or ice, the reduction may be only 20% to 30% [80-81].

Proper selection of a wind turbine site is critical to economic development of wind power and must take into consideration a number of factors. In close proximity, both downwind and upwind from the obstacle, the wind will get smoother. To find steady winds or to escape from the turbulence zone, for the downwind turbulence zone, estimate the height of the obstacle, multiply it by 7, and that is how far downwind is necessary. For the upwind turbulence zone, estimate the height of the obstacle, multiply it by 3, and that is how far upwind is necessary.

30

For the wind turbine site, it is important to evaluate whether nearby obstacles will cause turbulence to disrupt wind flow access to wind turbines. An industry rule of thumb is that the distance between a turbine and the nearest obstacle should be at least twice the turbine height, unless the turbine is more than twice the height of the obstacle, in which case the distance can be less. The best locations in terms of wind resources are typically high on mountains, in large open fields, or on the edge of bodies of water.

2.3.5 Wind Turbine Site

Wind speed is a critical factor of wind turbine performance and, thus, for selecting the wind turbine site. The wind flow pattern is never steady; it varies with the time of day, season, height above the surface, and features of the terrain. A suitable site for wind turbine performance is in windy areas and far from obstacles to wind flow. The International Electro technical Commission (IEC) sets international standards for the wind speeds in each wind class, as shown in Table 2.3.

Table 2.3 IEC Wind Classes

	I (High Wind)	II (Medium Wind)	III (Low Wind)	IV (Very Low Wind)
Reference Wind Speed	50 m/s	42.5 m/s	37.5 m/s	30 m/s
Annual Average Wind Speed (Max)	10 m/s	8.5 m/s	7.5 m/s	6 m/s
50-year Return Gust	70 m/s	5.5 m/s	52.5 m/s	42 m/s
1-year Return Gust	52.5 m/s	44.6 m/s	39.4 m/s	31.5 m/s

The wind power class for wind turbines is used to consider the quality of the wind turbine site and the average wind speed of that site. The higher the wind power class number, the more effective the wind turbine performance. Wind speed is usually measured in meters per second or miles per hour for rating wind turbine sites. The wind power classes for wind turbine site as shown in Table 2.4.

Table 2.4 Wind Power Class for Wind Turbine Site

Wind Speed (m/s)	Wind Speed (mph)	Quality of Site	Power Class
4	8.9	Not Acceptable	1
5	11.2	Poor	1
6	13.4	Moderate	2
7	15.7	Good	3
7.5	16.8	Very Good	4
8	17.9	Excellent	5
8.5	19	Excellent	6
9	20.1	Excellent-HI	7

2.3.6 Wind Turbines in Urban Areas

Wind energy development in urban areas will be an important issue for future sustainable cities [82]. In urban areas, siting wind turbines is an option for on-site energy generation, but there are many factors that need to be considered before the installation of the wind turbines, because wind resources in urban areas are uncertain where they can be weak and turbulent [83-84]. The performance of wind turbines in urban areas is only effective when there is adequate wind supply. Therefore, buildings showing either undisturbed or, even better, accelerated wind flows would be estimated to enlarge their wind energy potential, as also found by Arriago (2009), mentioning buildings higher than their directly adjacent buildings.

The built environment has a significant influence on the urban wind performance. Wind turbines are mainly problematic to model in urban areas because of the wind flows' impact with their multiple wind turbines, which significantly reduce the wind turbines' efficiency. However, the trees, buildings, and other obstacles on the ground affect the wind speed and turbulence intensity over the built environment, specifically leading to the low mean wind speeds and high levels of turbulence. This is an additional cause of the restart limitation of wind turbines and reduction in output [85-87].

The wind performance differs depending on different inlet directions. Different urban areas have their own best wind inlet direction for high wind collection [88]. The installation of wind turbines in the building obstacle airflow areas can result in low energy yield from the low mean wind speeds in urban areas as well as environmental effects [89]. Due to obstacles with different characteristic interference to wind flow, wind conditions in urban sites are complex, and the flexibility of wind turbines in this situation has not been verified in terms of real power production or of structural compatibility with the buildings. As a result, the wind profile in urban locations is rather different from the typical log-law-based profile used in open topography [90].

The most-significant characteristic of a wind turbine is its performance. Obstacles affect to airflow predictability and cause irregular power performance of wind turbines, which was not adequately considered in earlier research [91].

The geometric landscapes of urban arrangements and their designs have significant effects on wind speed, direction, and frequency. There are three main kinds of effect of wind within urban regions.

(1) Due to the differences in building height within the urban shade layer, buildings can employ main frictional drag upon wind speed, which generates turbulence and gives immediate changes in both direction and speed of the wind. Eventually, this decelerates the average wind speed within urban regions in comparison with country regions, which might see greater speed winds.

(2) Where the geometric topographies of high structures can slow wind speeds, they can channel airflow into urban gaps. This leads to a rise in wind speed as a result of the overpressure of airflow between buildings (this consequence is the Venturi effect) and can increase the incidence of turbulent winds.

(3) As an effect of temperature rises within cities, convection can generate contained low pressure cells within urban areas in rural regions, which can influence surface inflow from remoter rural regions into the urban metropolises. This can lead to a better regularity and raise wind speed.

Most buildings are closely spaced; thus, airflow between them is affected, and wind speed is improved. However, the effect of this depends on the height of the buildings and the amount of space between them. Generally spaced buildings can act as single buildings or isolated blocks; in contrast, as the gap decreases between buildings, airflow becomes more and more subject to overpressure, and thus the Venturi effect can cause variation the occurrence of airflow by constructing a complex pattern of changes in wind direction and speed. Usually, the urban arrangement is designed in such a way that wind speeds are often unexpected and turbulence as a result of frictional drag.

Moreover, the adjustments to airflow by urban buildings and the possible Venturi effect caused by this means that there are vast variations in wind speed direction, velocity, and occurrence, as a result of geometric features of urban regions.

2.3.7 Small Wind Turbines in Urban Areas

Small wind turbines are used for micro-generation, and they may have vertical and horizontal axis. Although there is not a unique classification for small wind turbines, IEC explains there are turbines having a rotor swept area of less than 200 m^2, associated to a rated power of around 50 kW, producing a voltage below 1,000 V AC or 1,500 V DC [66]. The U.S. Department of Energy's National Renewable Energy Laboratory describes small wind turbines as those smaller than or equivalent to 100 kW [92].

However, numerous nations have their own classifications of small wind turbines. The difference of the upper capability maximum of small wind turbines ranges from 15 kW to 100 kW for the five largest small wind states [93]. Small wind turbine frequently has direct-drive generator, direct-current output, aero-elastic blades, and lifetime bearing.

The most common small wind turbine is the HAWT. Small wind turbines, below 100 kW, might be used for a variety of applications, including on- or off-grid houses, telecom towers, offshore stages, urban schools and hospitals, remote monitoring, and other resolutions that contain energy where there is no electric grid or where the grid is unstable.

Small wind turbines might be as small as a 50-W generator for ship or motorcade use [94]. Essentially, wind turbines are located where there is high wind, and also a wind turbine requires wind flow uniformly in the same direction, therefore, eddies, swirls, and turbulence are difficulties. The rotor cannot extract energy from turbulent wind, and the frequently changing wind direction due to turbulence results in extreme wear and failure of the turbine. This means that the turbine needs to located high enough to catch robust winds and overhead turbulent air. Small wind turbines are suitable for urban locations, because the environmental influence is limited maintenance costs are low, and the technology is simple, advanced, and reliable [95].

There is a need for small wind turbines in urban areas due to the space limits and lower levels of primary energy resources; renewable-based distributed-generation technologies in urban regions are generally employed as micro and small-scale systems [96]. The typical assessment of small wind turbine performance in urban regions as the steady-state performance assessment is based on the use of the manufacturer's power curve and annual circulations of hourly average wind speeds for the prediction of wind turbine energy production [97].

In urban regions, small HAWTs are frequently fixed on a tower to raise them above any nearby obstacles. They are frequently developed based on actual wind measurement and can approximate flow properties such as mean wind speed and turbulence levels at a possible turbine location, taking into account the size and remoteness to any obstacle. Small wind turbines undergo turbulence and infrequently generate major amounts of power, especially in towns and cities. Turbulence is a complex process and can have a significant impact on the power output of wind turbines. This is mainly essential for small wind turbines, which, in practice, are normally installed close to buildings, trees, and other obstacles [98].

The urban landscape and related landscape complexities currently create significant challenges to the placement of small wind turbines. Wind flow in urban regions causes many significant issues, such as energy performance of urban wind energy and the complex morphology of wind flow in urban regions. A significant amount of uncertainty is attributable to the lack of consideration about how turbulence within urban environments affects turbine efficiency. The analysis establishes that the proposed methodologies could provide a means for installers to predict power performance correctly for a wind turbine based on (wind speed) standard deviation and TI clarifications [99].

Numerous uncertainties and mistakes are associated with geometrical model precision, inflow conditions, turbulence models, discretisation schemes, and numerical approaches Reynolds-averaged Navier-Strokes (RANS) Large eddy simulation (LES) , and Direct numerical simulation (DNS). CFD techniques must be able to predict wind flow in an urban location, and numerical simulations must be able to help to calculate the influence of different parameters considered in order to develop the reliability of the results. However, in terms of energy yield achieved from small wind turbines, installation in complex topography is not mentioned [100].

Consequently, the urban landscape and related topographical complexities cause important challenges to the placement of small wind turbines within urban regions due to wind resources, which in urban regions are complex. Generally, there is a slight power that a wind turbine can use, because the obstruction environment frequently has excessive turbulence and low velocity. However, some features of the building location can focus wind flow: building edges or passages under elevated or between two buildings. Researchers found that the focus effect of buildings and the heights of buildings could increase wind power by increasing the wind power density by three to eight times under the given conditions [101].

2.3.8 Building Features Effect

The main reason of such urban winds is the relaying of the overriding wind field by the buildings themselves. The urban impact on wind is demonstrated in several ways: some features raise wind speed, whereas others drop it, and all act to vary wind direction from the dominant weather pattern. The full impact of urban regions on the wind field has numerous features, including roughness effects. Roughness acts to slow the wind, through aerodynamic drag, and to raise its turbulence. Its influences are associated with the height of the roughness features: trees, buildings, etc. The excessive effects of urban winds resulting from the wide variation of building characters, sizes, heights, separations, and directions with respect to flow patterns and to each other create complex wind flows within a city. Such wind flows are called urban canyon winds, because high-rise lined streets act similar to canyon barriers. When wind hits the face of the building, the flow separates and is diverted into numerous streams, the direction and number depending on the angle of wind frequency related to building edges and the "flatness" of the upwind building surface.

Building-obstructed wind flow unavoidably causes irregular power performance of a wind turbine [102]. Generally, small wind turbines couple slight power from the wind resources because the building's obstruction environment frequently has excessive turbulence and a low velocity of wind flow. However, some structures of the building environment can focus the wind flow. Building edges, passages under the elevated structure or between the two buildings, etc. can improve wind power utilisation by increasing the wind power density.

2.3.9 Venturi Effect

The Venturi effect is the rise of the fluid speed due to a decrease of the flow cross-section [103]. This effect was originally defined for confined flows [104], but the same terminology has been used for non-confined flow or open flows, e.g., to describe the increase of wind speed in passages between buildings [105]. Often, the wind speed in the passages between buildings increases due to the decrease of the flow section. Indeed, as the passage width decreases, the resistance for flow through the passage increases, and more wind will flow around and over the building passage. The high resistance of the passage partly blocks the flow through the passage and diverts a large part of the oncoming wind over and around the buildings and the passages. This Venturi effect an explicit characteristic of non-confined flows [106-109].

2.3.10 Site Measurement

When wind flows over an obstacle, the separation of the airstream occurs at the front corner of an obstacle, reattachment appears at the centre, and the backflow emerges in sequence [110]. The amount of electricity at wind turbine installed in a building-obstructed wind flow area can generate depends on the local wind speed and characteristics of the wind flow to the turbines. The location of a wind turbine is, therefore, crucial for maximising its overall performance. Although the power carried by the wind is proportional to the cube of the wind speed, the actual power output delivered by a wind turbine is more complex in such areas. Anemometers are used to measure the average, minimum, and maximum wind speed, as well as the amount of turbulence at the site. If two anemometers are put at different heights on the same mast, this provides useful additional information about the wind shear – the difference in wind speed at different heights, and can also provide useful information about the intensity of any wind turbulence at the site. Wind direction can be measured using a separate weathervane, wind vane, or direction indicator, but some anemometers include a direction indicator as well. The pole, anemometer, and wind vane equipment are often referred to as a meteorological mast, or "met mast" for short. Information on wind speed and direction is collected by a data logger and can be analysed using computer software.

Wind speed measurement shows significant potential for approximating the power potential of a wind plant, according to Zhang et al. [111]. Wind resource assessment includes [112]:

- Onsite wind situation measurement
- Associations between onsite atmospheric towers to fill in lost data
- Associations between long-term meteorological condition stations and short-term onsite atmospheric towers
- Examination of the wind shear and its distinctions
- Demonstrating the distribution of wind situations
- Estimation of the offered energy at the site

2.4 Understanding of CFD

2.4.1 General Overview of CFD of the Study

CFD is a subdivision of fluid mechanics that provides numerical analysis and algorithms to solve and analyse problems that contain fluid flows. It has been in use since the early 1900s, and it as an instrument for evaluating airflow. CFD is the use of functional mathematics, physics, and computational software to visualise in what way gas or liquid flows. Computers are used to achieve the calculations essential to simulate the interface of liquids and gases with surfaces distinct by boundary conditions; with high-speed supercomputers, improved solutions can be achieved.

CFD is based on the Navier–Stokes equations. These equations define how the velocity, pressure, temperature, and density of a moving fluid can be associated; consequently, CFD is a convenient tool for analysing thermal properties and modelling air flow. CFD software involves evidence about the size, content, and layout of the data for calculating what will occur, quantitatively, when fluids flow, and is used for problems of mechanical movement, such as wind turbine power performance. CFD techniques can predict wind flow in an urban location, and numerical simulations can assist to measure the influence of different measured parameters to increase the reliability of the results.

However, CFD-based estimates are never 100% reliable, because the input data might contain too abundant imprecision, the obtainable computer power might be too slight for high numerical precision, and the methodical understanding base may be insufficient. Numerous doubts and mistakes are associated with geometrical model precision, inflow conditions, turbulence models, discretisation schemes and numerical approaches (RANS, LES, DNS).

In addition to the extensive range of length and time scales and the associated computational cost, the governing equations of fluid dynamics enclose a nonlinear convection term and a nonlinear and nonlocal pressure gradient term. These nonlinear equations must be solved mathematically with the appropriate boundary and initial conditions [87]. In this study, the appropriate of CFD software, boundary conditions, meshing, the convergence, and the turbulence model are as follows.

2.4.1.1 CFDesignV.7 Software

CFDesignV.7 software turns a 3-D computer-aided design (CAD) workstation into a fully interactive flow bench, thermal test rig, and wind tunnel. Three-dimensional assemblies become associative, zero-cost prototypes revealing critical engineering information not available from physical tests. If a design change is made to the model, the same change is seen immediately in CFD. An effective simulation starts with good CAD techniques both in terms of model integrity and proper creation of the flow region. The first step is to design the CAD model for the flow analysis. This means modelling the flow geometry and optimising the model for simulation. Materials are physical substances and are the foundation of the CFD analysis. There are two distinct material types available in an analysis: fluids and solids.

2.4.1.2 Boundary Conditions

The boundary conditions describe the inputs of the simulation model. Some conditions, such as similar velocity and volumetric flow rate, describe in what way a fluid arrives or leaves the model. Other conditions, such as similar film coefficient and heat flux, describe the transaction of energy concerning the model and its surroundings. Boundary conditions associate the simulation model with its surroundings. Without them, the simulation is not definite, and in some cases cannot progress. Boundary conditions can be as definite as any steady-state or transient ones. Steady-state boundary conditions persevere through the simulation. Transient boundary conditions vary with time and are frequently used to simulate an occasion or a cyclical phenomenon.

2.4.1.3 Meshing

Preceding a CFD analysis, the geometry is fragmented into small parts called elements. The corner of each element is a node. The calculation is achieved at the nodes. These elements and nodes create the mesh. In 3-D models, most elements are tetrahedral, a four-sided, triangular-faced element. In 2-D models, most elements are triangles, as shown in Figure 2.10.

Figure 2.10 Tetrahedral Triangle Elements

The CFD achieves a complete topological interrogation of the analysis geometry and defines the mesh size and distribution on every edge, surface, and volume in the model. Geometric curving, gradients, and proximity to adjacent geometry are all measured when assigning element sizes and mesh distributions. Enhanced solution robustness and good mesh transitions lead to a well-posed mathematical model. It does not matter which selection mode (volume, surface, or edge) is stimulated. Significantly simplified setup of analysis models results in less time spent assigning mesh sizes. In more-efficient mesh distributions, the mesh is fine where required and coarse where it can be enhanced, and solution precision is due to better mesh quality and mesh transitions.

2.4.1.4 Convergence

Convergence is based on the convergence observer. Every CFD analysis is made up of multiple iterations. The iteration is a numerical sweep through the entire model. The convergence of multiple iterations is shown in Figure 2.11.
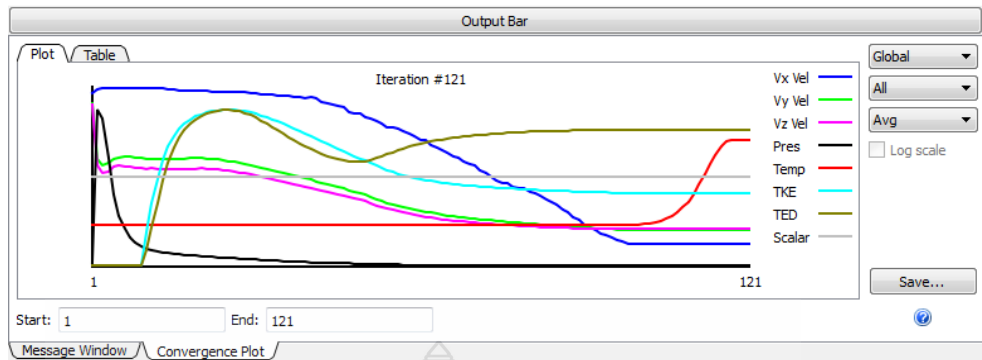
Figure 2.11 Convergence of Multiple Iterations [113]

Early in the analysis, many results are adjusted from iteration. The convergence lines may oscillate up and down. Horizontal convergence lines indicate when the results stop fluctuating and that the solution is "converged". The convergence requirement can be stretched so previously results can be evaluated quantitatively. Trends can be considered qualitatively previously in the analysis, and complete convergence is extended.

        2.4.1.5 Turbulence Model

        The turbulence model container generates a large variance in the results. Turbulence models are essential because there are not large or affordable enough computers to capture every scale of motion directly. Also, CFD users characteristically need a steady-state rather than a complete-time-accurate one that captures every little vortex. As a result, there are unsteady motions affecting the flow that cannot directly be resolved; consequently, they must be modelled. Turbulence models are mostly classified according to which governing equations they apply within these broader categories, and they are further broken down by the number of additional transport equations one must solve to calculate the model influences. In some cases, the turbulence model has a huge effect on the results achieved from CFD.

        For the flow of fluid above the flat plate, as shown in Figure 2.12, the uniform velocity fluid hits the leading edge of the flat plate, and a laminar boundary layer begins to develop. The flow in this region is predictable because, after some distance, small disordered oscillations begin to develop in the fluid field, and the flow begins to make the transition to turbulence, eventually becoming completely turbulent. The transition between these three regions can be defined in terms of the Reynolds number, $Re = \rho \vartheta L / \mu$, where ρ is the fluid density, ϑ is the velocity, L is the characteristic length, and μ is the fluid dynamic viscosity. It is expected that the fluid is Newtonian; the viscosity is constant with respect to shear rate. This is close or identical because a wide range of fluids in engineering are significant, such as air or water, because density will vary with respect to pressure, although it is assumed that the fluid is weak compressible fluid, which means the Mach number is less than 0.3.

39
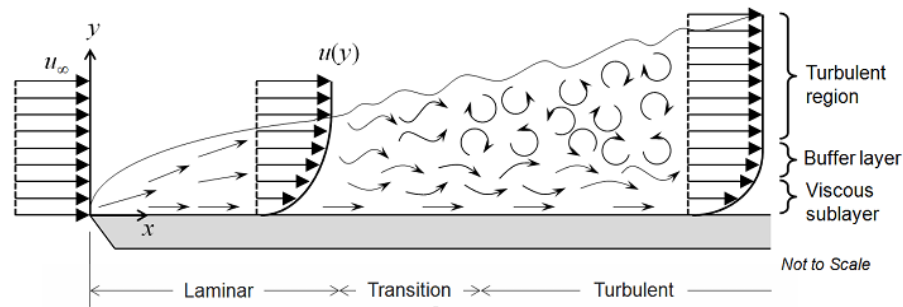
Figure 2.12 Turbulence of Fluid Over a Flat Plate [114]

The CFD turbulence models, such as the standard k-ε model (SKE), the RNG, the realisable k-ε model (RKE), and the shear stress transport k-ω model (SST) are all two-equation (2E) eddy viscosity models. In these 2E models, the Reynolds stress term is expressed by the turbulent viscosity. The turbulent viscosity is based on the solutions of the equations for turbulent kinetic energy (k) and specific dissipation rate (ω) or turbulent dissipation rate (ε). The 2E models have advantages of computing efficiency, but the accuracy is limited by the hypothesis of isotropic eddy viscosity.

k-epsilon model

The k-epsilon model solves for two variables: k, the turbulent kinetic energy, and epsilon, the rate of dissipation of kinetic energy. Wall functions are used in this model, so the flow in the buffer region is not simulated. The k-epsilon model is widely held for industrial applications due to its good convergence rate and relatively little memory supply. It does not exactly calculate flow fields that show adverse pressure gradients, strong curvature to the flow, or jet flow. It does perform well for external flow problems around complex geometries.

k-omega model

The k-omega model is like the k-epsilon, but it solves for omega, the specific rate of dissipation of kinetic energy. It also uses wall functions, and consequently has similar memory supplies. Moreover, it has more difficulty converging and is rather sensitive to the initial estimate at the solution. Hence, the k-epsilon model is frequently used first to find an initial condition for solving the k-omega model. The k-omega model is suitable in numerous cases where the k-epsilon model is not accurate, such as internal flows, flows that exhibit strong curvature, separated flows, and jets.

Low Reynolds number k-epsilon

The low Reynolds number k-epsilon is like the k-epsilon model but does not use wall functions; it solves the flow everywhere. It is a logical extension to k-epsilon and has many of its benefits but consumes more memory. It is frequently suitable to use the k-epsilon model to compute a good initial condition for solving the low Reynolds number k-epsilon model. Meanwhile, it ensures that, without using wall functions, lift and drag forces and heat flux can be modelled with higher precision.

40

Renormalisation group k-epsilon

Assessments of the performances of numerous Reynolds-averaged Navier–Stokes (RANS) models for simulating wind flows over complex topographies showed that the RNG k–ε model provided enhanced agreement with the field data over the standard k– ε model [115]. Consequently, the current CFD simulations of wind flows above complex topographies are achieved based on the RNG k– ε model. The solutions derivative from the standard k–ε model cannot be directly used for the RNG k– ε model.

2.4.2 CFD in Wind Engineering

The most dependable method for wind assessment in a building environment is to measure the wind speed directly, ideally at the position and the height of the proposed wind turbine. However, measuring the wind speed at a site is both time consuming and expensive, i.e., normally not appropriate for the early stages of wind energy development. However, wind energy potential in a building environment can be exploited in a proper condition with improvement of computer science, CFD simulation with complex building configuration, or city models becoming accessible [116]. Because CFD is a simulation of fluid mechanics for solving and analysing fluid flows, CFD modelling is becoming an important tool in the wind industry to study wind flow patterns. Accurate CFD simulations of wind flow are essential for the selection of wind farm locations as well as the design of appropriate wind turbines [117]. They can be functional to calculate accurate wind turbine performance with the slightest or optimal cost and time scale. The CFD result can be associated with the experimental method. In computational modelling of turbulent flows, the suitable model that fulfils the type of obstruction can calculate fluid velocity and the greatest of related problems for engineering design, which include fluid flows [118]. Additionally, the CFD methodology can be effectively applied with the least cost and time related to the experimental method [119], and CFD techniques can be a consistent substitute for less costly and faster resource calculations of wind turbine applications; moreover, they afford to the governing flow mechanism [120]. Modern CFD tools are critical for modelling wind flows over complex urban topographies [121]. They offer location-specific, height-specific, and time-specific wind data and give an approximation of the wind power.

Theoretical research on wind engineering can be divided into two classes: analytical calculation and numerical calculation. But it is still difficult to fully solve a flow problem by an analytical calculating method. This method is usually based on experimental data from lots of wind tunnel tests. Recently, due to computer technology developing rapidly, CFD has become more and more useful in wind engineering research. This method is more economical than experimental methods, because it requires no experimental devices and saves effort [122]. The accuracy of CFD methods is highly dependent on the mathematic model chosen, so the study of CFD methods has become important. Various computational models exist, each with its own strengths and weaknesses, that attempt to predict accurately the performance of a wind turbine. Being able to predict wind turbine performance numerically makes it possible to reduce the expensive and exhaustive wind tunnel and field experimental tests. The major benefit is that

computational studies are more economical, versatile, and higher resolution than costly experiments [123]. In the numerical research, the 3-D unsteady flow analysis is done using CFD; there is in both the level and the shape of the 3-D predictions and the experimental measurements, which gives confidence that the 3-D CFD is acceptably capturing the necessary flow physics of the aerodynamics, but it is computationally intensive [124].

CFD methods are frequently used to advance computational resource ability and have extended the stage where analysis of complex phenomena, such as multiphase, free surface, and highly turbulent flows, is likely for an enormous number of design differences in a reasonable timescale [125]. Recently, developments of CFD codes have shown that simulations of this nature are in good agreement with experimental data [126]. This gives confidence to the reliability of the numerical results. The CFD program is used to transport the simulations of a finite-volume method and is also used for the spatial discretisation of the governing equations. The numerical method must be authorised. The study must be associated with the experimental method [127], and the flow feature in small wind turbines will be investigated. Maturing CFD technology is making more wind flow simulation experiments accessible, which can be authorised by site measurement or field measurement. Project design for any wind project should not be too work intensive, while the cost margins for project management employing CFD software will involve specialised expertise for problem setup and preprocessing and postprocessing tools [128]. Nevertheless, CFD simulations can be complex for an enormous range of computational parameters set by the user. Therefore, before undertaking any wind study scheme, a comparison of computational results with measured data must be done for the different discretisation schemes. Moreover, each scheme has to be verified alongside the several turbulence models with respect to grid dependency tests [129]. Nevertheless, the wind velocity at the wind turbines' hub height that was predicted by the standard k-Ɛ turbulence model was adopted rather than the measured data, showing that wind velocity prediction by the CFD method is accurate for wind power forecasting [130].

2.4.3 CFD Turbulence Model

CFD is a fluid mechanics simulation for solving and analysing fluid flows. It can be useful to predict wind-turbine performance exactly at the least or optimal cost and time scale. CFD results can be associated with experimental results. In the computational modelling of turbulent flows, an applicable model for the obstruction type can calculate the fluid velocity and additional related concerns for engineering designs concerning fluid flows [131]. In computational modelling of turbulent flows, a common objective is to achieve a model that can calculate the capacities of concentration, such as fluid velocity, for use in engineering designs of the system being modelled. For turbulent flows, the range of length scales and complexity of phenomena involved in turbulence make most modelling approaches excessively costly; the computational cost to decide all scales involved in turbulence is beyond what is feasible.

The principal methodology in such cases is to generate numerical models to estimated uncertain phenomena. Turbulence models are categorised based on computational expense, which relates to the variety of scales that are modelled versus resolved. If all the turbulent scales are not modelled, the computational cost is lower, but accuracy is reduced.

A CFD turbulence model has the process similar to the system of mean flow equations. It is not essential for engineers to decide the details of the turbulent fluctuations. They only need to recognise how the turbulence affects the mean flow. Useful turbulence models have wide applicability and must be accurate, simple, and economical to run. In this study, the CFD turbulence models (k-ε model, k-ω model, and RNG model) are selected.

The $k - \varepsilon$ model

Most standard models are created on the RANS equations (time averaged) —zero equation models, mixed-length models, one-equation models, two-equation models, k-ε style models (standard, RNG, realisable), k-ω models, etc. [132].

The Reynolds-averaged approach is based on decomposing the velocity as follows.

$$u_j = \overline{u_j} + \acute{u}_j \tag{2.14}$$

where $\overline{u_j}$ is the average velocity vector and $\acute{u}_j$ is the velocity vector fluctuation. The $k - \varepsilon$ model has been found to provide a more effective response to the energy production rate than the standard $k - \varepsilon$ turbulence model. The $k - \varepsilon$ model equations can be written as follows:

$$\rho(\overline{U}.\nabla)K = \nabla\left[\left(\mu + \frac{\mu_t}{\sigma_k}\right)\nabla K\right] + P_k - \rho\varepsilon \tag{2.15}$$

$$\rho(\overline{U}.\nabla)\varepsilon = \nabla\left[\left(\mu + \frac{\mu_t}{\sigma_\varepsilon}\right)\nabla\varepsilon\right] + C_{\varepsilon 1}\frac{\varepsilon}{K}P_k - C_{\varepsilon 1}\rho\frac{\varepsilon^2}{K} \tag{2.16}$$

$$\mu_t = \rho C_\mu \frac{K^2}{\varepsilon} \tag{2.17}$$

$$P_k = \mu_t[\nabla\overline{U} + (\nabla\overline{U})^t]\nabla\overline{U} \tag{2.18}$$

The standard model constants, which are applicable to the flows with high Reynolds numbers, are provided in Table 2.5. The CFD k-ε turbulence model is selected to validate the performance prediction of the turbine, as the characteristics of the CFD k-ε turbulence model is quite appropriate for the given conditions of the study:

• The CFD $k - \varepsilon$ turbulence model is the most widely used model and has been validated for applications ranging from industrial to environmental flows.

• The model is useful for the free-shear layer flows with relatively small pressure gradients in the confined flows where the Reynolds shear stresses are important.

• The model can be stated as the simplest model for which only initial and/or boundary conditions need to be supplied.

• Two equations and the von Karman constant (k), together with the eddy viscosity stress–strain relationship, constitute the k-ε model, where ε is the dissipation rate of k. Many attempts have been made to develop the two-equation models to improve the $k - \varepsilon$ model.

Table 2.5 Values of the $k - \varepsilon$ Model Constants

C_μ	$C_{\varepsilon 1}$	$C_{\varepsilon 2}$	σ_k	σ_ε
0.09	1.44	1.92	1	1.3

The $k - \omega$ model

This model is suitable for calculating the turbulence near the wall. The $k - \omega$ model is based on model transport equations for the turbulence kinetic energy, k, and the specific ω dissipation rate. These values are derived from the equations and the characteristics of the $k - \omega$ model below.

$$\frac{\partial(\rho k)}{\partial t} + div(\rho k U) = div\left[\left(\mu + \frac{\mu_t}{\sigma_k}\right) grad\ k\right] + P_k - \beta\rho\acute{k}\omega \tag{2.19}$$

$$\frac{\partial(\rho\omega)}{\partial t} + div(\rho\omega U) = div\left[\left(\mu + \frac{\mu_t}{\sigma_\omega}\right) grad\ \omega\right] + \alpha\frac{\omega}{k}P_k - \beta\rho\acute{\omega}^2 \tag{2.20}$$

When

$$\sigma_k = 1;\ \sigma_\omega = 2;\ \alpha = \frac{5}{2};\ \beta = 0.075$$

Therefore, the turbulence viscosity of this model will be:

$$\mu_t = \rho\frac{k}{\omega} \tag{2.21}$$

• One of the records is frequently used in turbulence models. It is a two-equation model and contains two additional transport equations to signify the turbulent properties of the flow.

• It is the flexibility that decides the scale of the turbulence, while the principal variable, ε, decides the energy in the turbulence.

• This permits a two-equation model to describe history effects like the convection and diffusion of turbulent energy.

The RNG model

Eddies in the range of size L and integral scale down to eddies of size $L/Re^{3/4}$, where $Re = v_{rms}L/v$ is the Reynolds number are considered. The high viscous dissipation causes very low energy. Therefore, the 3-D Navier–Stokes equations for a turbulent flow need a grid mesh on the order of $Re^{9/4}$. When it is assumed that the Re is large, the numerical solver of the computational method requirements is exceedingly high. The RNG method reduces the computational requirement by eliminating the inertial range eddies from the equations of motion, yielding equations for averaged flow quantities at an integral scale. The RNG-based $k - \varepsilon$ turbulence model is derived from the instantaneous Navier–Stokes equations, using RNG methods.

Transportation equations for the RNG model are:

$$\frac{\partial}{\partial t}(\rho k) + \frac{\partial}{\partial x_i}(\rho k u_i) = \frac{\partial}{\partial x_j}\left(\sigma_k \mu_{eff} \frac{\partial k}{\partial x_j}\rho k\right) + G_k + G_b - \rho\epsilon - Y_M + S_k \tag{2.22}$$

$$\frac{\partial}{\partial t}(\rho \epsilon) + \frac{\partial}{\partial x_i}(\rho\epsilon u_i) = \frac{\partial}{\partial x_j}\left(\sigma_k \mu_{eff} \frac{\partial \epsilon}{\partial x_j}\rho k\right) + C_{a\epsilon}\frac{\epsilon}{k}(G_k + C_{3\epsilon}G_b) - C_{2\epsilon}\rho\frac{\epsilon^2}{k} + R_\epsilon + S_\epsilon \tag{2.23}$$

The effects of smaller scales of motion when using the RNG turbulence model developed using RNG are as below.

• It can be used to derive a turbulence model similar to the k-Ɛ model and it results in a modified form of the epsilon equation, which attempts to account for the different scales of motion through changes to the production term.

• The RNG model in FLUENT provides an option to account for the effects of swirl or rotation by modifying the turbulent viscosity appropriately.

• Similar k-ε equations include an additional term in the ε equation for interaction between turbulence dissipation and mean shear, the effect of swirl on turbulence, analytical formula for turbulent Prandtl number, and differential formula for effective viscosity.

Hence, researchers should compare the CFD data result and experimental data result to investigate the different discretisation schemes.

2.4.4 The Governing Equation

The behaviour of fluid flow can be solved by governing equations that obtain the three principles of conservation: conservation of mass, conservation of momentum, and conservation of energy. When the CFD method is used for solving, the three principles of conservation will be used, and the Navier–Stokes equation will be developed in the CFD method for solving. The Navier–Stokes equation can be expressed as follows:

Continuity equation

$$\frac{\partial \rho}{\partial t} + \nabla \cdot (\rho \vec{u}) = 0 \tag{2.24}$$

Momentum equation

$$\Sigma F = ma \tag{2.25}$$

The Navier–Stokes equation:

$$\frac{\partial}{\partial t}(\rho \vec{u}) + \rho(\vec{u} \cdot \nabla \vec{u}) = -\nabla p + \nabla \cdot \tau + S_m, \tag{2.26}$$

where the stress tensor τ is related to the strain rate by

$$\tau = \mu \left(\nabla \vec{u} + (\nabla \vec{u})^T - \frac{2}{3} \delta \nabla \vec{u} \right) \tag{2.27}$$

Energy equation

$$\frac{\partial}{\partial t}(\rho h_t) - \frac{\partial \rho}{\partial t} + \nabla \cdot (\rho \vec{u} h_t) = \nabla \cdot (\vec{u} \cdot \tau) + \vec{u} \cdot S_m + S_e, \tag{2.28}$$

where the total enthalpy h_t is related to the static enthalpy h_s by

$$h_t = h_s + \frac{1}{2}\vec{u} \tag{2.29}$$

The finite volume is used for solving in the CFD commercial program. The partial differentials are carried out to approximate the solutions. Some parameters in the equation can be removed when used to simplify the equations by assuming that fluid flow is steady, isothermal, and incompressible. However, the CFD method should be validated by experimental testing or real site measurement.

CHAPTER 3

MATERIALS AND METHODS

The overall methods, materials, and techniques of this study of 5-kW wind turbine performance in a wind flow obstructing building using the CFD technique are described. The results from the CFD simulation are obtained from three CFD turbulence models (k-Ɛ, k-ω, and RNG) that affect the power performance and free spinning rotating of the three 5-kW HAWTs (WT1, WT2, and WT3) as they are installed in a building-obstructed wind flow area by comparing them with a 5-kW HAWT (WT0) as an arbitrary installation in an unobstructed area. In addition, the site measurement based on the measured data or site-estimated technique was done to obtain the results to validate the CFD simulation results.

3.1 Wind Energy Resources in Thailand

Wind data from various sources show that the study location, DETC, has low wind potential. The micro and small wind turbines with low cut-in and rated speed can be effective during medium or high wind speed of even shorter durations. Wind energy is not as easy to capture as solar, because it keeps flowing, moving, and changing, and it is harder to predict in cities due to complex physical features. Therefore, micro-siting of small wind turbines in urban areas is one requirement related to power performance of turbines in such areas. One approach is to develop the applicable tool to predict the power performance of low wind speed and turbulence at the site.

Generally, the wind potential in Thailand from the World Bank Wind Map Thailand Wind Resource Area is classified mostly in the poor-to-fair class, as shown in Figure 3.1.
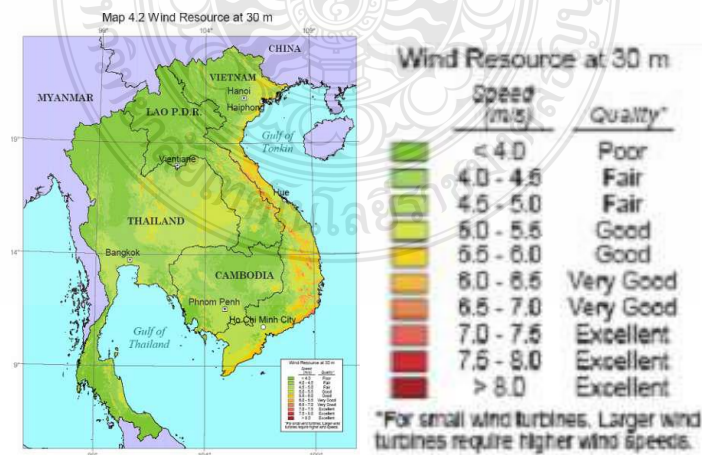
Figure 3.1 Wind Potential in Thailand [133]

The wind resource map of Southeast Asia was created for the World Bank by True Wind Solutions using Meso Map, a mesoscale atmospheric simulation system. Although the map is believed to present an accurate overall picture of wind resources in Southeast Asia, resource estimates for any location should be confirmed by measurement. To utilize wind energy to generate electricity, annual monsoon characteristics of the selected location are important. The annual monsoon characteristics of Thailand are illustrated in Figure 3.2. Direction and speed of the wind at selected locations should continuously be measured to obtain correct wind data for analyzing the potential of wind energy to generate electricity.
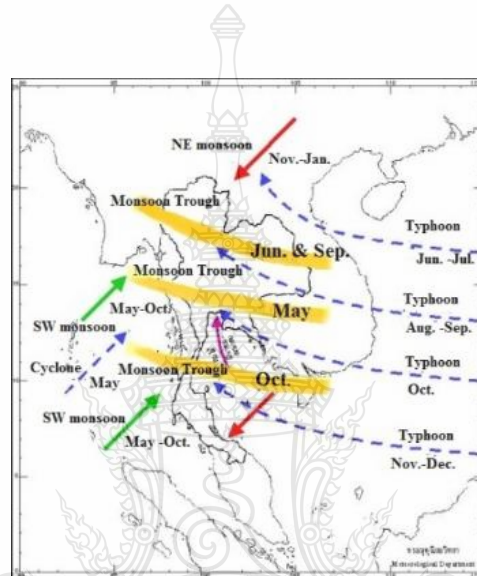
Figure 3.2 Monsoon Season in Thailand [134]

3.2 Conceptual Design

The power performance of the wind turbines depends on the torque and angular velocity. This research only focuses on the power performance and free spin rotation of the turbine rotors using the CFD technique, as well as on the wind flow velocity profile in the site measurement technique as wind flows across the buildings and the turbines in a building-obstructed wind flow area. Hence, when the rotor turbine rotates, the voltage of the PMG is generated, and the voltage varies according to the rotational speed of the rotor; thus, high speed means high power performance.

3.2.1 Model Description

The DETC in Rayong Province, Thailand, is considered a building-obstructed wind flow area. In this case, three 5-kW HAWTs, THUNYA-5-kW HAWTs (WT1, WT2, and WT3), are surrounded with four main buildings (building A, B, C, and D), as shown in Figure 3.3 and Figure 3.4. The site position is latitude 12 degrees 40 minutes north, longitude 101 degrees 2 minutes east, and the height is 3 m above sea level. The wind blows throughout the year, including the southwest monsoon season from May to October, and the north-east monsoon season from November to January.

The statistical wind-speed data, collected over the past 30 years (between 1968 and 1997) in Rayong Province by the Data-Processing Division of the Department of Meteorology, shows that the average wind speed is between 2.6 and 7.7 m/s. The highest wind speed occurs between June and August. Table 3.1 shows the model, sizing, and alignments of the buildings and the three 5-kW HAWTs in the DETC.
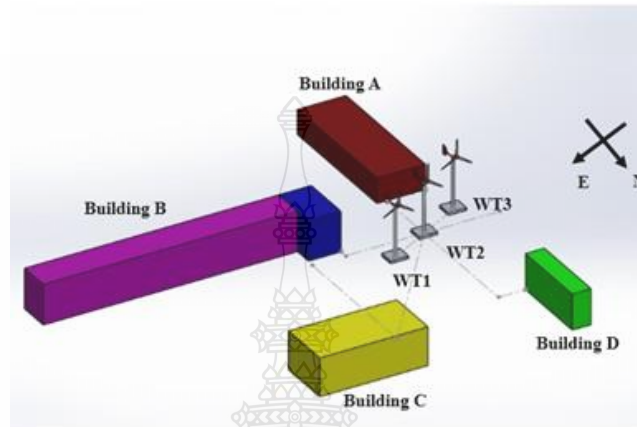
Figure 3.3 Building and 5-kW HAWTs Model in DETC

Figure 3.4 Three 5-kW HAWTs and Buildings in DETC

Table 3.1 Sizing and Alignment of the Buildings and the Wind Turbines in DTEC

Building	H (m)	W (m)	L (m)	Distance. from WT1(m)	Distance from WT2(m)	Distance from WT3(m)
A	9.25	18	51	35	24	20
B	15	12	113	25	30	45
C	9.25	18	51	60	70	87.5
D	13.3	7	30	47.5	50	55

Remarks: The wind turbines are 18 m apart. A three-dimensional model of the buildings and wind-resource data was used as input to the three CFD models and completed using the CFDesign commercial program. In this study, WT1, WT2, and WT3 represent the case study 5-kW HAWTs, whose performance prediction is investigated as the wind flows across the obstructing buildings, using the CFD k-ε, k-ω, and RNG turbulence model with the CFDesign V.7 software. The results of this study are expected to show the power performance, free spinning rotation, of WT1, WT2, and WT3 compared with the performance, free spinning rotation, of WT0, a 5-kW HAWT arbitrarily located in a site without obstructing buildings, after an incoming wind flow of 4.5 m/s through the buildings and the front turbines. Afterward, the results of the WT1, WT2, and WT3 were validated with the wind flow velocity behaviour profile from site estimation or site measurement based on the measured data results to confirm the accuracy and the recommendation of the CFD technique.

3.2.2 Wind Turbine Specifications

Table 3.2 shows the technical data of the THUNYA-5-kW HAWT, which is installed within the DETC area, and the THUNYA-5-kW HAWT is shown in Figure 3.5. The power curve of the THUNYA-5kW HAWT is shown in Figure 3.6, which describes the cut-in wind speed of the THUNYA-5-kW HAWT at 2.5 m/s, the rated wind speed at 9.5 m/s, and the average wind speed at 4.5 m/s. In addition, Figure 3.7 shows the grid-connected inverter of the THUNYA-5-kW HAWTs in the electrical control room of the DETC.

Table 3.2 Technical Data Sheets of a THUNYA-5-kW HAWT

Main data	
Hub height	18 m
Rotor diameter	6.5 m
Rated power	5 kW @ 9.5 m/s
Cut-in	2.5 m/s
Rotor speed	200 rpm
Generator speed	200 rpm
Grid connected	220 V 50 Hz
Rotor speed control	Fixed pitch
Yaw mechanism	Active (azimuth angle)
Breaking system	Auto furling
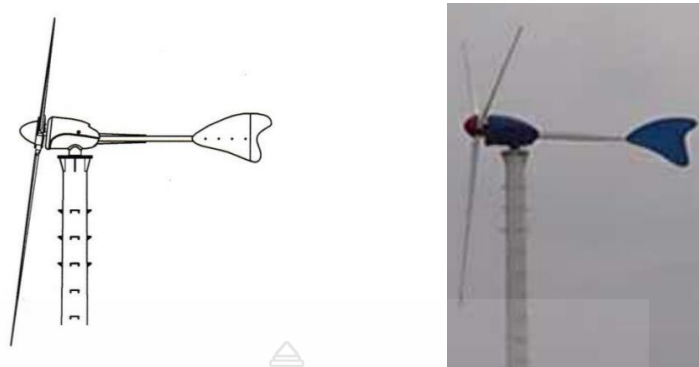
Figure. 3.5 A THUNYA-5kW HAWT in DETC
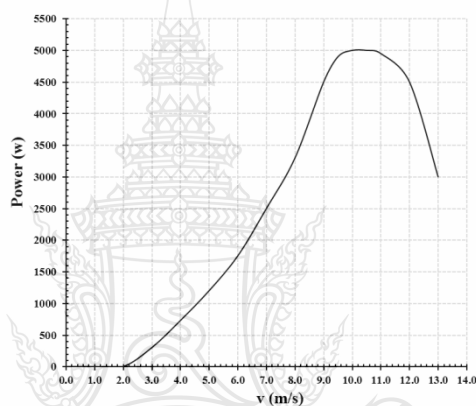
Figure 3.6 Power Curve of a THUNYA-5-kW HAWT

Figure 3.7 Grid-Connected Inverters of THUNYA-5-kW HAWTs in Electrical Control
Room of DETC

3.3 CFD Technique

3.3.1 CFD Boundary Conditions

When solving the CFD problems, the Navier–Stokes equation, continuity equations, appropriate initial conditions, and boundary conditions must be applied. Figure 3.8 shows the CFD boundary conditions of the 3-D model applied as the control volume and using CFD k-Ɛ, k-ω, and RNG turbulence models with the CFDesign V.7 software. The CFDesign setup and usability is shown in Appendix A. Each CFD turbulence model includes two main conditions: the buildings and the ground are fixed, and the wind turbine blades and the air are moving.

The fixed condition means the object or material in the 3-D model cannot move when forces act on it (which include the building, ground, nacelle, wind turbine tower, and wind turbine tailing), while the moving condition means that the object or material in the 3-D model can move when forces act on it (which include the wind turbine blade, air, and rotating region).
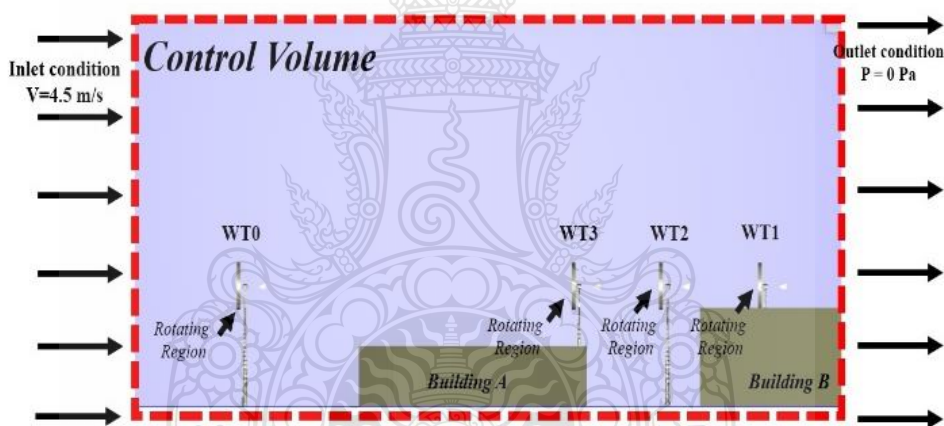
Figure 3.8 CFD Boundary Conditions as the Wind Flows from the SW

The rotating regions, which form a part of the motion module, allow for the analysis of rotating machinery. The rotating region is an envelope that surrounds a spinning device. Throughout the analysis, the rotating region rotates about its centre line, and any solid within the region rotates as well. The inlet condition of 4.5-m/s wind velocity was selected, and the outlet condition was 0-Pa wind gage pressure.

Figure 3.9 describes the rotating region of the CFD boundary conditions, which include the moving/dynamic condition and fixed/static condition. The moving conditions include the rotating region and turbine blade, as both parts can move when the force of the wind velocity acts on them. However, the fixed condition includes the turbine tailing and turbine tower, as both parts cannot move when the force of the wind acts on them.
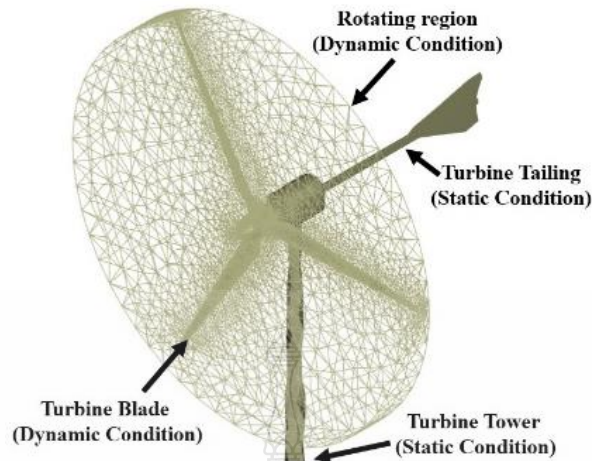
Figure 3.9 Rotating Region of the CFD Boundary Condition

       This model produces a steady-state solution accounting for some of the interaction between the two frames. The quasi-steady approximation decreases when the passing flow speed is large, relative to the turbine speed at the interface. The boundary conditions and control volume parameters are shown in Table 3.3.

       Table 3.3 also shows the model parameters applied in the CFD control volume model, with the inlet side selected by the wind velocity and the outlet side selected by the pressure. Ideal air was used as the working fluid, and the k-ε, k-ω, and RNG turbulence model was applied for simulation.

Table 3.3 CFD Model Parameters

Parameter name	Unit	Parameter Value
Inlet velocity	m/s	4.5
Inlet total temperature	K	320
Angular velocity	Rad/s	Free spin
Working fluid		Ideal air
Fluid density	kg/m^3	1.225
Turbulence model		k-ε, k-ω, RNG
Outlet	Pa	0

       Figure 3.10 shows the grid dependency of the 3-D model at 4.5 m/s of wind velocity inlet condition. When the model is constructed with 0.25 million (coarse mesh) grid elements, the turbine has a rotation of 141 rpm, while the construction with 0.7 million grid elements (medium mesh) increases the rotation of the turbine to 168 rpm, but the curve in this period does not show convergence because the slope of the curve is high. The curve shows convergence at a grid number of about 3.5 million elements (fine mesh), and the grid convergence at 4.5 m/s of the wind velocity inlet condition is shown in Table 3.4.
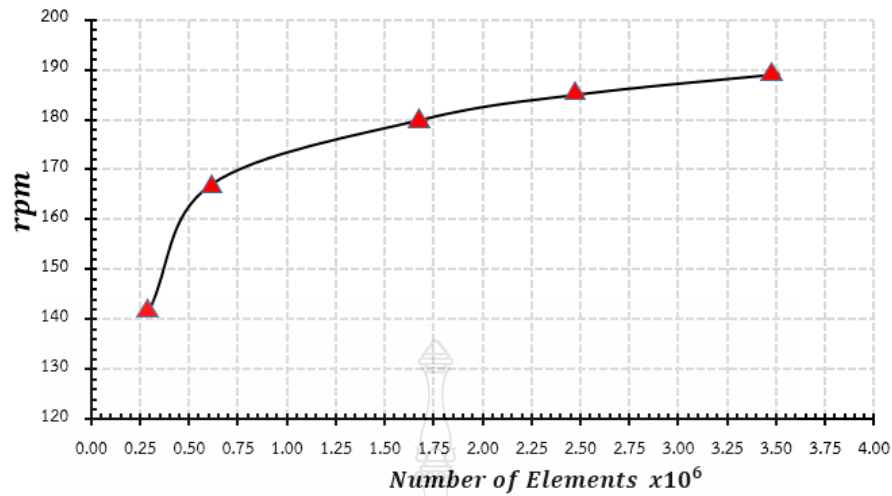
Figure 3.10 Grid Dependency of the 3-D Model at 4.5 m/s of Wind Velocity Inlet
Condition

Table 3.4 Grid Convergence at 4.5-m/s Wind Velocity Inlet Condition

Grid number$\times 10^6$.	Blade velocity (rpm)
0.25	141
0.50	162
0.75	170
1.00	172
1.50	178
2.50	185
3.50	189

3.3.2 CFD Model Description of Mesh Refinement Study

CFD modelling was conducted to assess the wind flows and estimate the energy output system, accounting for the specific geometries of the obstacle flows. The site geometry was modelled using CAD. The wind conditions were expressed on the geometry model to estimate the flow conditions resulting from the interaction between the wind flow, building structures, ground roughness, and wind turbines. A detailed explanation is presented below.

CFD uses a Eulerian fluid flow field specification. The domain is discretised using cell-vertex numeric (finite volume) elements. These may be unstructured tetrahedral elements, which are used to capture the complex geometry of the rotating domains and to allow automatic meshing for any future geometry modifications.

The CFD mesh adaptation system was used to refine the mesh in specified high-volume velocity gradients for investigation. Three mesh adaptation steps were undertaken for each model: coarse mesh, medium mesh, and fine mesh.

Figure 3.11 shows the CFD tetrahedron meshing of the wind turbine blade. The CFD model generated 0.9 million elements for the wind turbine blade. Figure 3.1.1(a), (b), and (c) show coarse mesh, medium mesh, and fine mesh wind turbine blades, respectively.

(a) Coarse Mesh   (b) Medium Mesh

(c) Fine Mesh
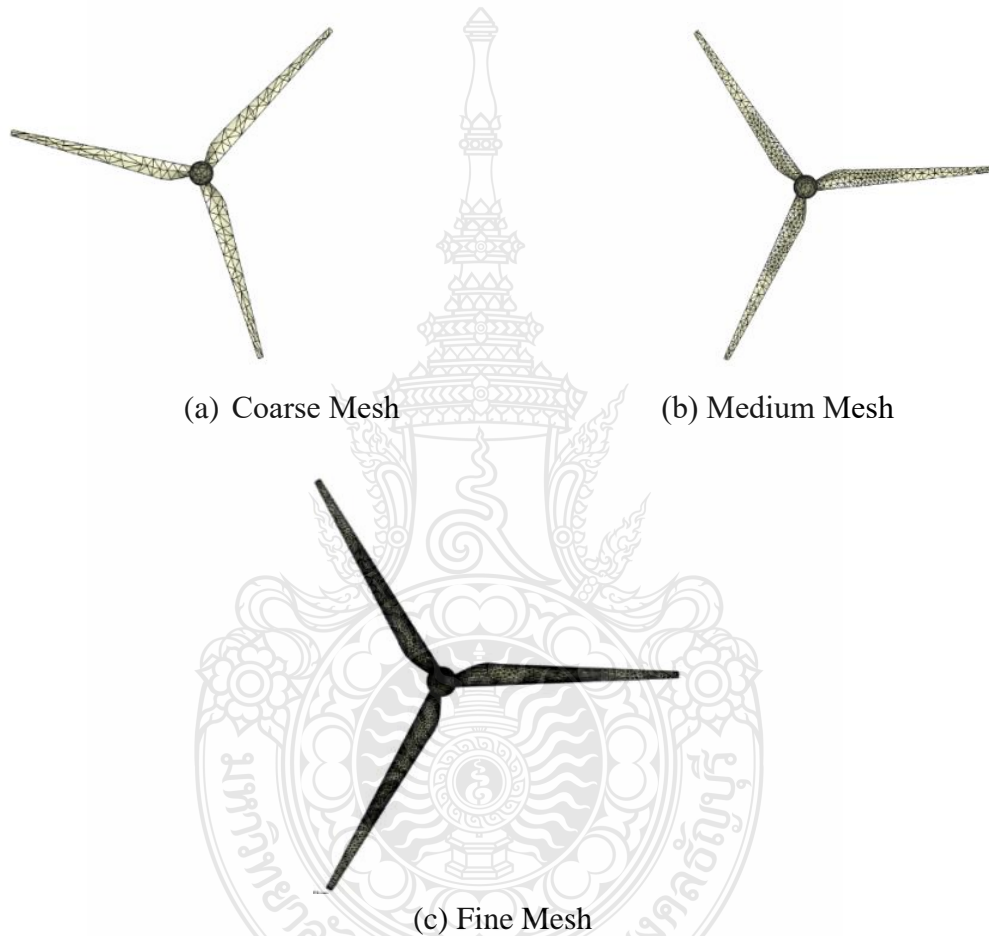
Figure 3.11 Mesh of Wind Turbine Blades in CFD

Figure 3.12 shows the CFD tetrahedron mesh model of the buildings in the DETC. The CFD model generated 1.0 million elements for the buildings, 0.9 million elements for the wind turbine blade, 0.6 million elements for the rotating region, 0.5 million elements for the air, and 0.5 million elements for the ground.
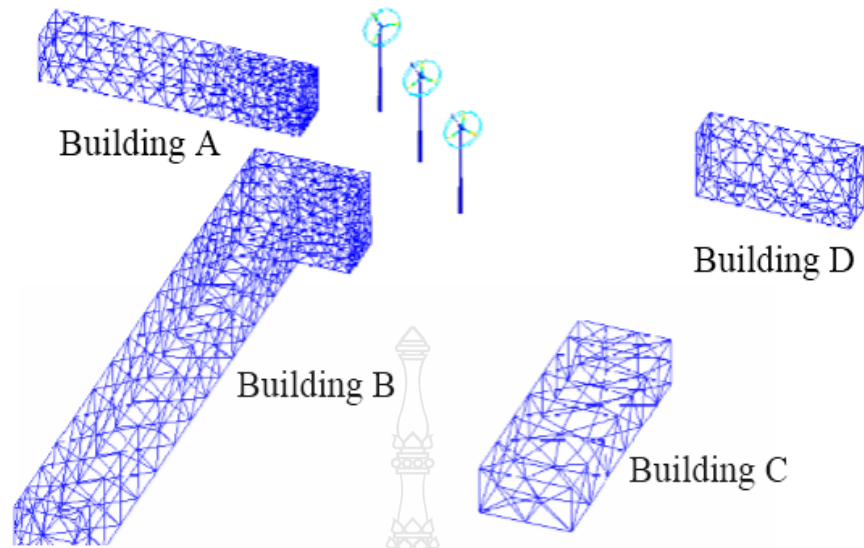
Figure 3.12 Meshing of DETC Buildings Model

3.4 Site Measurement Technique

Site estimation or site measurement based on the measured data results is used for validating the results of the three CFD turbulence models that used for simulation. The site measurement was done by measuring wind velocity with a wind speed measuring instrument, Professional Touch Screen Weather Center With PC Interface, Model No: AW002, FREQ: 443MHz. This device was used for measuring wind speed on the roof of Building A and Building C to find out the wind velocity behaviour profile from incoming wind speed at Building A compared to outgoing wind speed at Building C, as follows.

• Two sets of such instruments were mounted on a pole at the same height as the wind turbine, 18 m, on the roof of Building A and Building C, in the line of wind flow from the SW to Building A-WT3-WT2-WT1-Building C.

• Wind speed was measured with two sets of these instruments as wind flow from the SW crossed over the first instrument at Building A (incoming wind speed) to WT3-WT2-WT1 and the second instrument at Building C (outgoing wind speed).

• Incoming wind speed (Vin) was compared with outgoing wind speed (Vout) to find the wind velocity behaviour profile of site measurement for validating the wind velocity characteristic to the turbines of the CFD investigation results.

Figure 3.13 shows the activities of the instruments set up on the poles and mounted at the roofs of Building A and Building C at the same height as the wind turbines hub height, 18 m.
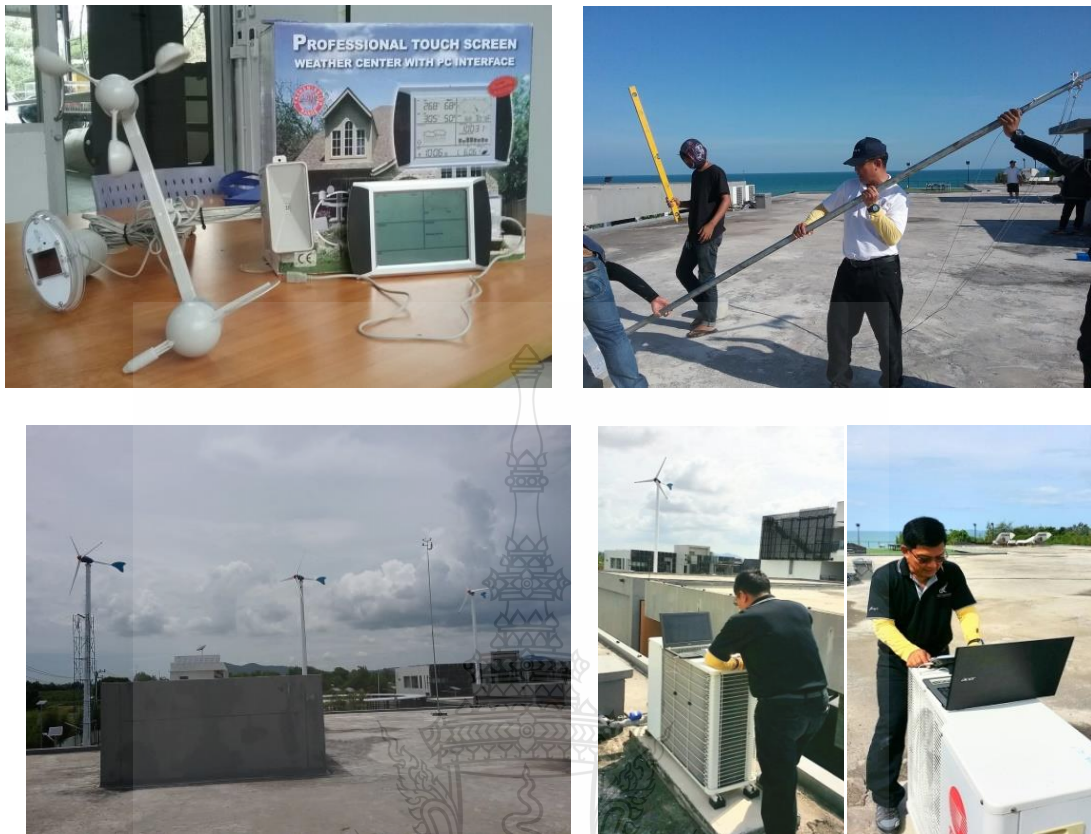
Figure 3.13 Instrument Installation for Measuring Wind Flow Velocity Behaviour
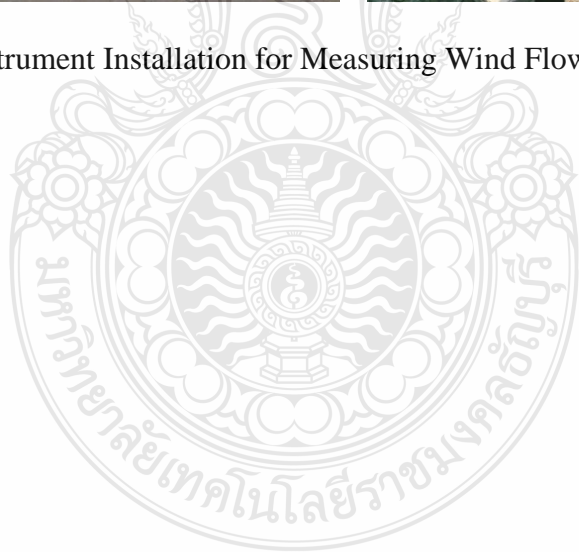
CHAPTER 4

RESULTS AND DISCUSSION

The results of the power performance effect with free spinning rotation of the small wind turbines affected by an incoming wind speed at 4.5-m/s flow across a building-obstructed wind flow area were obtained using three CFD turbulence models (k-Ɛ, k-ω, and RNG), and the wind flow velocity behaviour was studied using site-estimated or site-measurement-based data. In addition, the results of the techniques are compared to confirm whether the CFD simulation technique is reliable or needs more improvement.

4.1 CFD $k - \varepsilon$ Model Simulation Results and Discussion

Results

The simulation results focus on the free spin rotation of WT0, WT1, WT2, and WT3 by using the $CFD\ k - \varepsilon$ turbulence model in the two directions of wind flow from the NE and the SW that affect to the three 5-kW HAWTs' (WT1, WT2, and WT3) power performance (free spinning rotating) when compared with a 5-kW HAWT installed at the DETC unobstructed by buildings. The incoming wind speed was 4.5 m/s. Because the power performance of the wind turbines depended on the torque and angular velocity, when the rotor turbine rotation caused the PMG to generate the electrical power, the voltage varied according to the rotational speed of the rotor. Thus, high rotation meant high electrical power for the wind turbine. The results of the $CFD\ k - \varepsilon$ turbulence model simulation as follows.

4.1.1 Wind Velocity Profile

Figures 4.1 (a1)–(d2) show the wind velocity profiles of the $CFD\ k - \varepsilon$ turbulence model results from two directions of wind flow, NE and SW, at different heights, 9.25, 13.30, 15.0, and 18.0 m, of the cutting plane from the ground. The points of the cutting plane, representing the locations on the buildings' roofs, were determined by the inflow of the wind velocity, turbulence intensity, and recirculation zones. The wind velocity profile indicates that, at the higher points of the cutting plane, there is more wind velocity, and the wind flow from the NE is likely to introduce a Venturi effect between Buildings B-C and Buildings C-D. However, the wind flow from the SW predominantly brings about a Venturi effect between Buildings A-B and Buildings A-D.
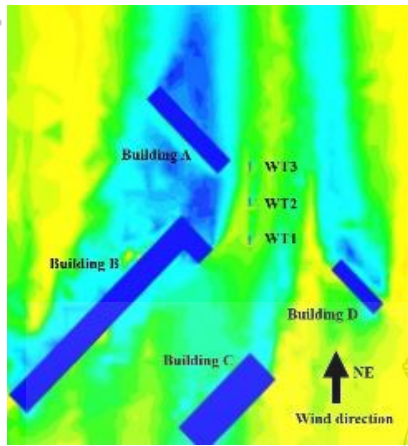
(a1)
(a1) Height 9.25 m, from NE
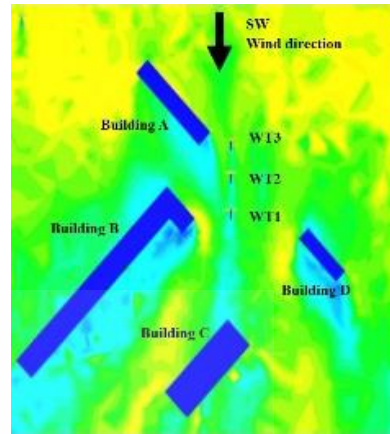
(a2)
(a2) Height 9.25 m, from SW
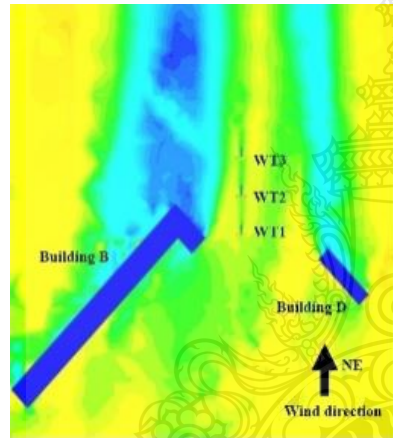
(b1)
(b1) Height 13.30 m, from NE
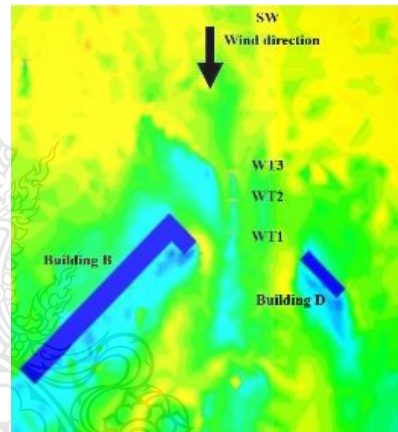
(b2)
(b2) Height 13.30 m, from SW
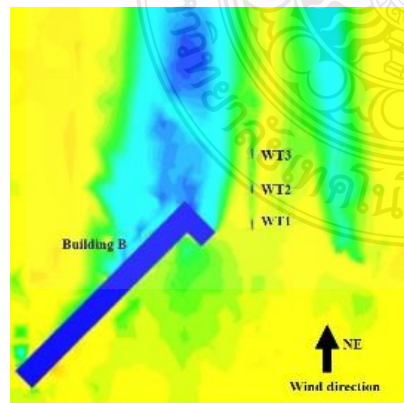
(c1)
(c1) Height 15.0 m, from NE

(c2)
(c2) Height 15.0 m, from SW

(d1)

(d1) Height 18.0 m, from NE

(d2)
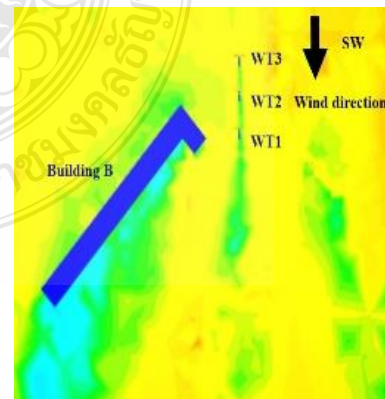
(d2) Height 18.0 m, from SW
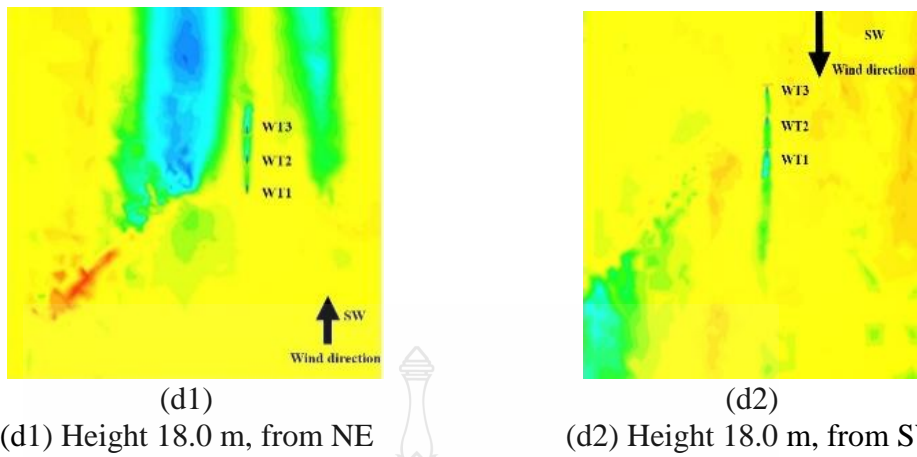
Figure 4.1 Wind Velocity Profile from the NE and the SW at Different Heights from
the Ground: (a) 9.25 m, (b) 13.30 m, (c) 15.0 m, and (d) 18.0 m

4.1.2 Wind Velocity Contour

Figures 4.2(a) and (b) show the wind velocity contour as wind flows
from two directions, the NE and the SW, indicating that, although the DETC has more
open terrain from the direction of the wind flow from the SW, as wind flows from the
NE across Building C to WT1-WT2-WT3-Building A, there is more wind velocity to
the turbines than when wind flows from the SW across Building A to WT3-WT2-WT1-
Building C.

(a) Wind Velocity Contour of Wind Flow from the NE

(b) Wind Velocity Contour of Wind Flow from the SW
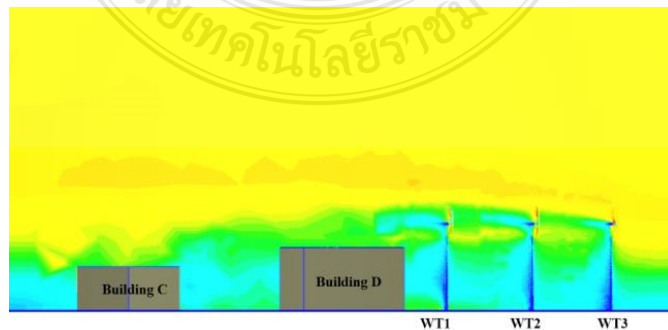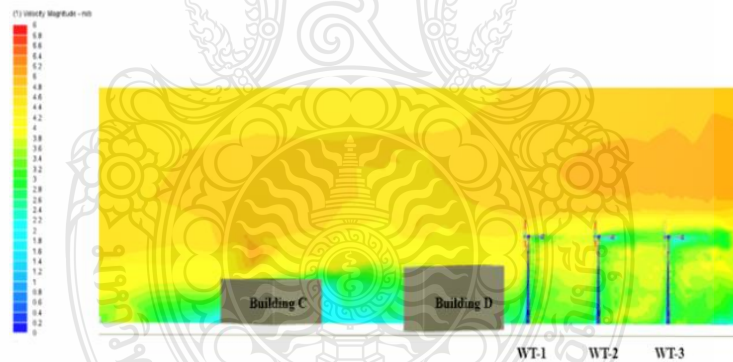
Figure 4.2 Wind Velocity Contour of Wind Flow (a) from the NE and (b) from the SW

60

4.1.3 Wind Velocity Profile Flow Over the Building

Figure 4.3 shows the profile of the wind velocity flow over the building (using Building C as an example). The result indicates that the roughness effect on the wind generates surface local wind shear gradients above a roof surface, as well as when the wind flow passes over the building, leaving a low wind-speed region immediately above the roof and then transitioning steeply to a higher wind speed zone. Consequently, a steep wind shear gradient causes increasing wind speed at the turbine.
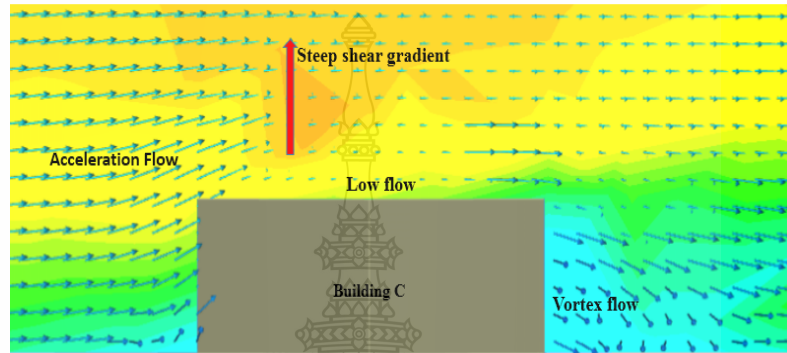
Figure 4.3 Air Accelerating Over the Building and Creating a Steep Shear Gradient

4.1.4 Vortex Flow Vectors

Figures 4.4(a1)–(d) show the vortex flow vectors at WT1, WT2, WT3, and WT0 as wind flows from NE and SW. The results indicate that the vortex flow is seen at WT1, WT2, and WT3 from both directions, but it is not seen at WT0 due to WT1, WT2, and WT3 installed near the buildings and the turbines themselves, whereas WT0 is an arbitrary installation in an unobstructed area. Consequently, vortex flow decreases the power performance of the wind turbines.
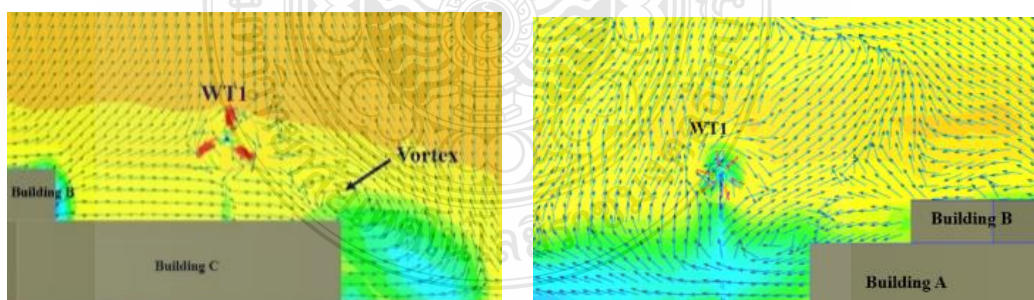
(a1)Vortex Flow at WT1 from the NE   (a2) Vortex flow at WT1 from the SW
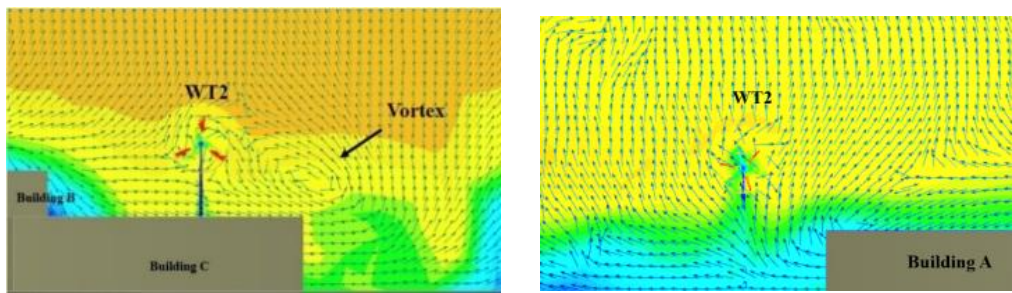
(b1) Vortex Flow at WT2 from the NE   (b2) Vortex Flow at WT52 from the SW
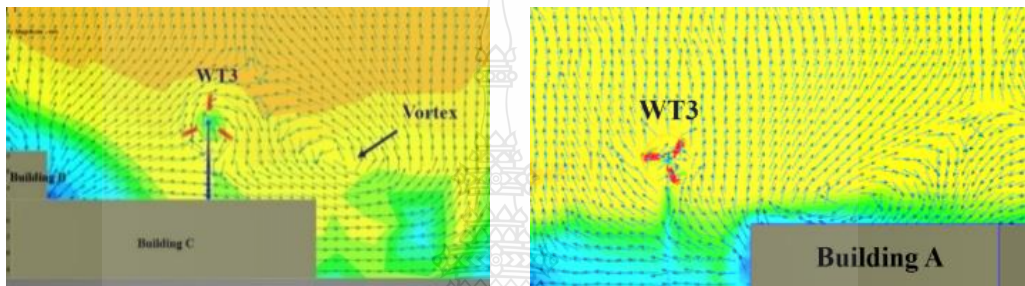
(c1) Vortex Flow at WT3 from the NE   (c2) Vortex Flow at WT3 from the SW
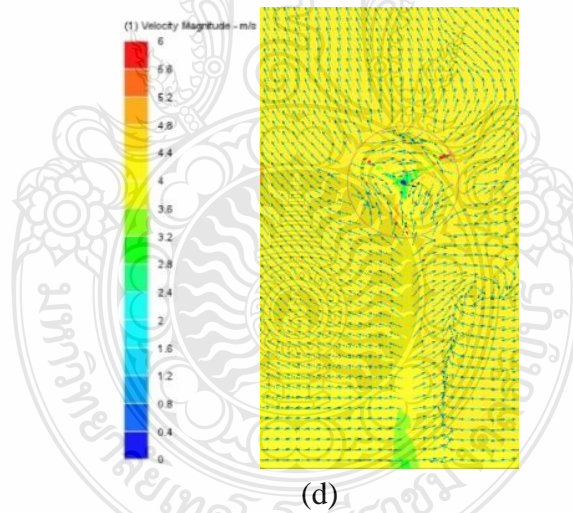
(d) No Vortex Flow at WT0, as Wind Flow from Both Directions

Figure 4.4 Vortex Flow Vectors to Wind Turbines from Two Directions

4.1.5 Grid Dependency and Grid Convergence

The grid dependency of the 3-D model at 4.5 m/s of wind velocity inlet condition is shown in Figure 3.10, as well as grid convergence at 4.5 m/s of wind velocity inlet condition as shown in Table 3.4.

4.1.6 Calculation of Power Performance of Wind Turbine

The calculation of the power performance effect, free spinning rotating, of wind turbine can calculate as follows (using WT1 as the example when the wind flow from the SW):

$$\frac{x_i}{100} = \frac{N_{WT0} - N_{WT1}}{N_{WT0}}$$

$$\frac{x_i}{100} = \frac{216 - 200}{216}$$

$$x_i = +7.73\%$$

4.1.7 CFD k-Ɛ Model Simulation Results

The results of the wind turbine's power performance were calculated by torque and the angular velocity of the rotor. In this study, using the CFD simulation technique for investigating the wind turbine's power performance in the free spin rotor condition, the angular velocity of the turbine is the result of the power performance of the wind turbines. Consequently, high angular velocity means high power performance.

Table 4.1 is the result of the power performance, with free spinning rotation, of WT0, WT1, WT2, and WT3 using the CFD k-Ɛ turbulence model with wind flow from both directions, NE and SW, at an incoming wind speed of 4.5 m/s (see Appendix B and C). The result indicates that, as wind flows from the NE, the power performance, with free spinning rotation, of WT1>WT3>WT2>WT0, while, as wind flows from the SW, the power performance, with free spinning rotation, of WT1>WT2>WT0>WT3.

Table 4.1 Power Performance, with Free Spinning Rotation, of WT0-WT3 Using CFD k-Ɛ Model as Wind Flows from Two Directions at an Incoming Wind Speed of 4.5 m/s

Direction	WTs	RPM/Voltage	Ampere	Watt
NE	WT0	95	10.53	1,000.00
	WT1	130	10.70	1,391.20
	WT2	118	10.72	1,264.70
	WT3	120	10.71	1,285.30
SW	WT0	95	10.53	1,000.00
	WT1	102	10.52	1,073.00
	WT2	104	10.78	1,056.80
	WT3	101	9.16	925.00

Remark: A THUNYA 5kW HAWT's generator designed 1 rpm = 1 V

Figure 4.5 and Table 4.2 show comparisons of the power performance effects, with free spinning rotation, of WT1, WT2, and WT3 with WT0 by using the CFD k-ℰ turbulence model as the wind flows from the NE and the SW at an incoming wind speed of 4.5 m/s. The results indicate that the power performances, with free spinning rotation, of WT1, WT2, and WT3 are both higher and lower than WT0.
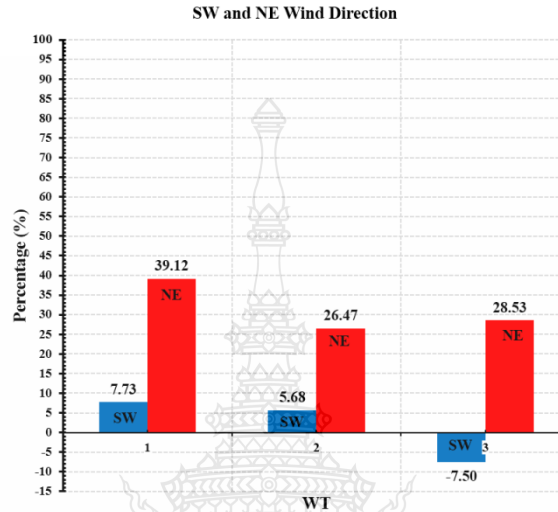
Figure 4.5 Comparison of Power Performance, Free Spinning Rotation, of WT1-WT3 with WT0, as Wind Flows from Two Directions at an Incoming Wind Speed of 4.5 m/s

Table 4.2 Comparison of Power Performance, Free Spinning Rotation, of WT1-WT3 with WT0, as Wind Flows from Two Directions at an Incoming Wind Speed of 4.5 m/s

Wind Turbine No.	Effect of Wind Turbine Power (NE) (%)	Effect of Wind Turbine Power (SW) (%)
WT0	100.00	100.00
WT1	139.12	107.73
WT2	126.47	105.68
WT3	128.53	92.50

The results of the CFD k-ℰ turbulence model simulation show that the power performance effect, with free spinning rotation, of WT1, WT2, and WT3 as wind flows from the NE and the SW increased and decreased when compared with WT0 due to the influence of the building-obstructed wind flow effect, as follows:

- As wind flows from the NE, the power performance effect, with free spinning rotation, of WT1, WT2, and WT3 is higher than that of WT0 by 39.12%, 26.47%, and 28.53%, respectively.
- As wind flows from the SW, the power performance effect, with free spinning rotation, of WT1 and WT2 is higher than that of WT0 by 7.73% and 5.68%, respectively, while the power performance effect, with free spinning rotation, of WT3 is lower than that of WT0 by 7.50%.

Discussion

4.1.8 CFD k-Ɛ Model Simulation Results Discussion

Normally, the geometric features of the buildings and their layouts have major effects on wind turbines' power performance. The buildings create turbulence and cause unexpected changes in the wind's speed, direction, and frequency. In addition, the geometric features of the buildings can decrease the wind speed; however, they can also channel the wind flow into the buildings' canyon and lead to an increase in the wind speed, because the Venturi effect can cause wind flow overpressure between buildings, and this can increase the frequency of turbulent winds. If the temperature increases within the building-obstructed area, it can create a low-pressure cell and lead to increased wind speed and frequency. Moreover, widely spaced buildings can act as single isolated blocks; therefore, if the gap decreases between the buildings, the wind flow will likely become more prone to overpressure. Thus, the Venturi effect can change the airflow frequencies by producing a complex pattern of changes in the wind direction and speed.

Compared with WT0, because the incoming wind flow from the NE creates a Venturi effect by channelling the incoming wind flow into the building canyons between Buildings B-C and C-D, Buildings B and C create a steep wind shear gradient that leads to an increase in power performance effect, with free spinning rotation, of WT1, WT2, and WT3, higher than WT0 by approximately 31%. Because the incoming wind flow from the SW creates a Venturi effect by channelling the incoming wind flow into the building canyon between Buildings A-B and A-D, Buildings A and B create a steep wind shear gradient that leads to an increased power performance effect, with free spinning rotation, of WT1 and WT2, higher than WT0 by approximately 7%. The power performance effect, with free spinning rotation, of WT3 decreased to lower than WT0 by approximately 7%, because WT3 is not in the building canyon of the incoming wind flow and is not influenced by local steep wind shear gradients from the buildings. Also, Building A increases the vortex flow effect to WT3.

Consequently, it is evident that the geometric features and layout of the obstructing buildings, as well as the ratio of the wind turbines' hub height and the distance of buildings and front turbines to the turbines are factors to shape and influence the wind flow pattern to the turbines, causing increased and decreased power performance effectiveness.

4.2 *CFD* $k - \varepsilon,\ k - \omega,$ **and RNG Simulation Results and Discussion**

Results

4.2.1 Wind Velocity Profile

Figures 4.6(a1)-(d3) show the wind velocity profiles of the CFD k-ε, k-ω, and RNG turbulence model results as wind flows to WT3, WT2, and WT1 with incoming wind speed of 4.5 m/s from the SW at heights 9.25, 13.30, 15.0, and 18.0 m from the cutting plane of the ground. The points of the cutting plane, representing the locations on the buildings' roofs, were determined by the inflow of the wind velocity, the turbulence intensity, and the recirculation zones. The wind velocity profiles from the three CFD turbulence models are indicated as follows. At the higher points of the cutting plane from all CFD turbulence models, more wind velocity displayed the same characteristics. The buildings' influence was likely to introduce a Venturi effect between Buildings A-B and A-D, and local steep wind shear gradients from Buildings A and B caused an increased wind speed to WT2 and WT1.

@ 9.25 m (a1) k-ε Model   (a2) k-ω Model   (a3) RNG Model

@ 13.30 m (b1) k-ε Model   (b2) k-ω Model   (b3) RNG Model

@ 15.0 m (c1) k-ε Model   (c2) k-ω Model   (c3) RNG Model

@ 18.0 m (d1) k-ε Model   (d2) k-ω Model   (d3) RNG Model
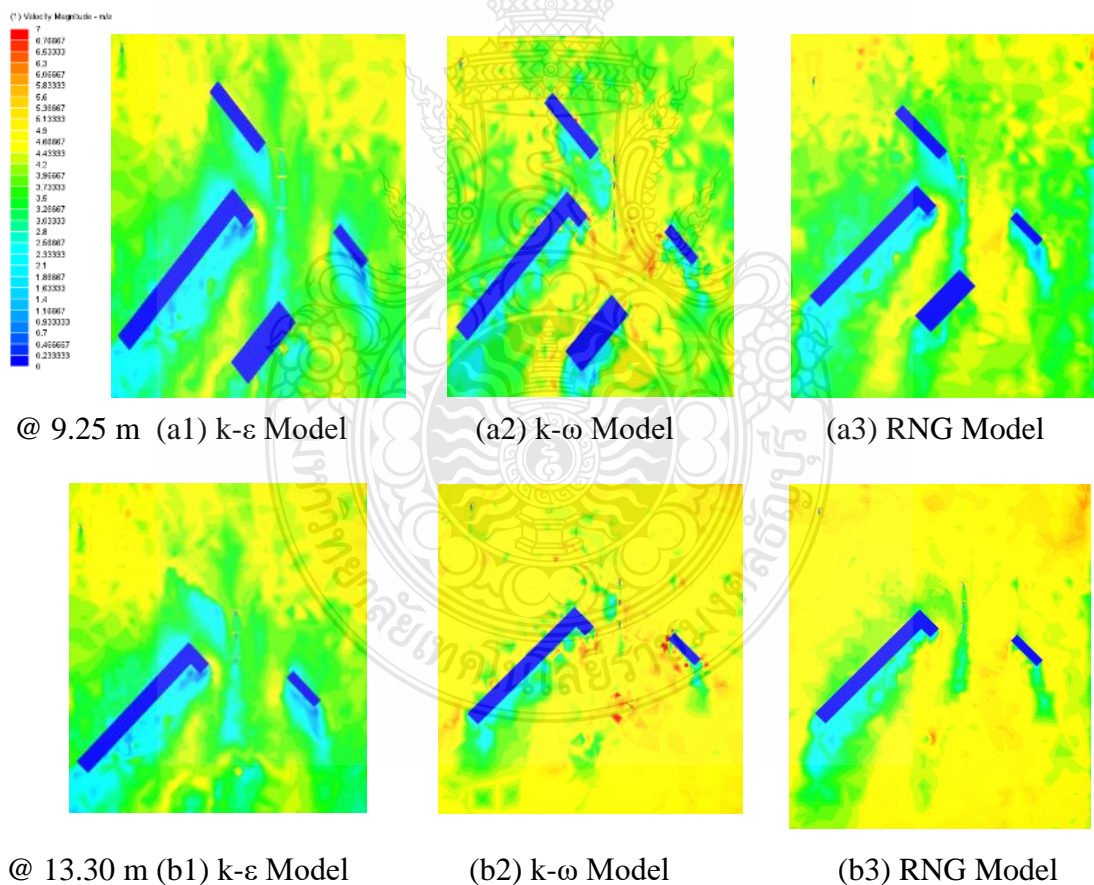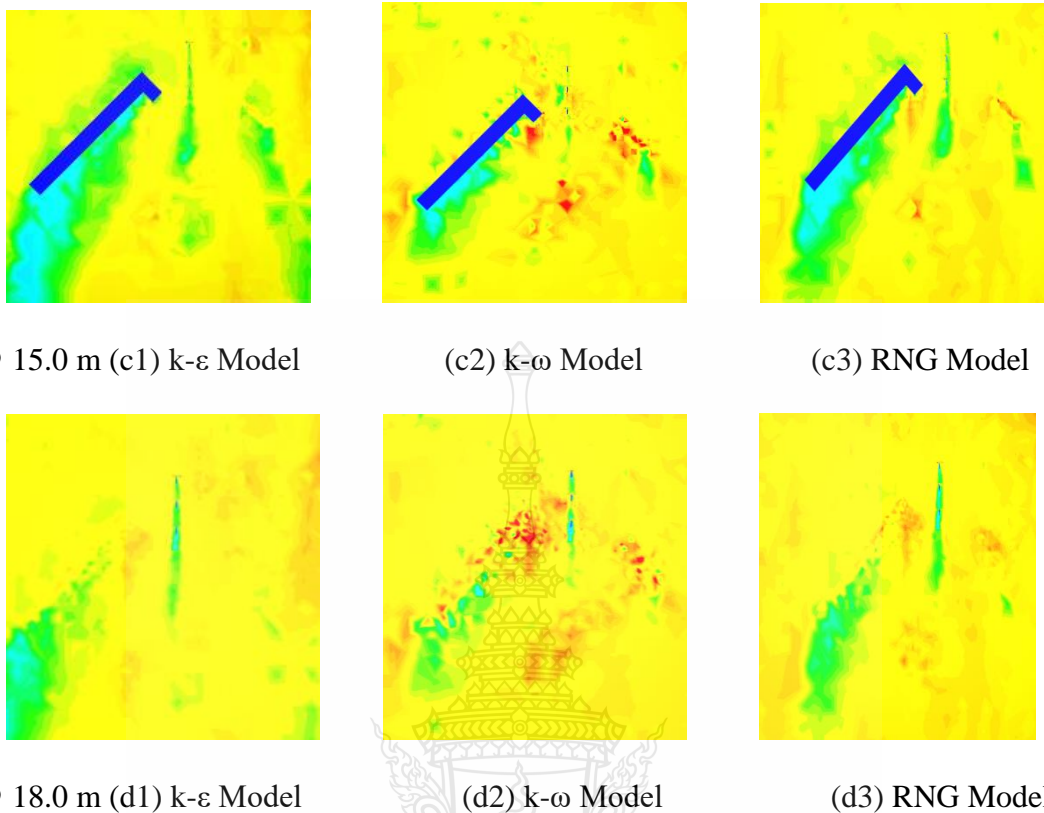
Figure 4.6 Wind Flow Profile Results from CFD k-ε, k-ω, and RNG Turbulence Model Simulation, at Height (a) 9.25 m, (b) 13.30 m, (c) 15.0 m, and (d) 18.0 m

4.2.2 Wind Velocity Contour

Figures 4.7(a)-(c) show the wind velocity contour of wind flow from CFD k-ε, k-ω, and RNG turbulence models as wind flows from the SW with incoming wind speed of 4.5 m/s to Building A-WT3-WT2-WT1-Building C. The results of the three CFD turbulence models indicate that, even though there was more open terrain near WT3, the wind velocity at WT3 was likely less than the wind velocity at WT2 and WT1.
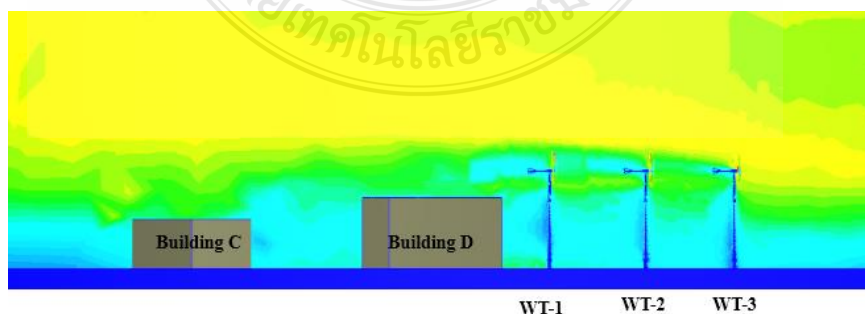
(a) Wind Velocity Contour of Wind Flow from k-ε Model
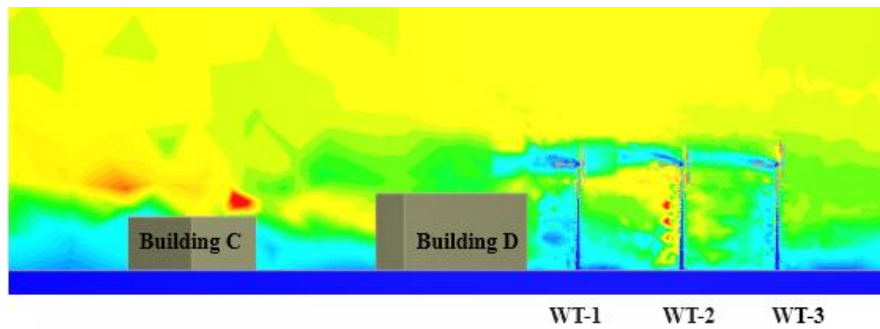
(b) Wind Velocity Contour of Wind Flow from k-ω Model
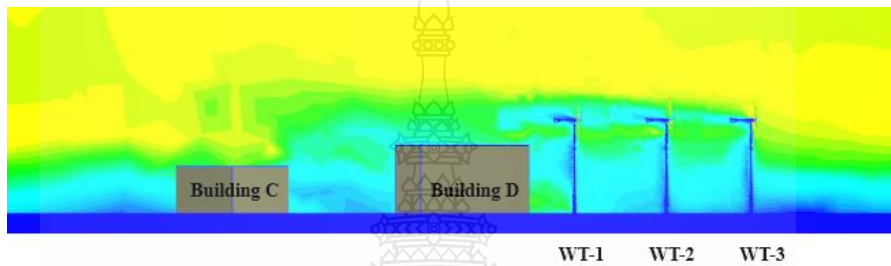
(c) Wind Velocity Contour of Wind Flow from RNG Model

Figure 4.7 Wind Velocity Contour of Wind Flow (a) from k-Ɛ Model, (b) from k-ω Model, and (c) from RNG Model

4.2.3 Vortex Flow Vectors

Figures 4.8(a1)-(d) show the vortex-flow vectors at the wind turbines of the three CFD turbulence models as wind flows with incoming wind speed of 4.5 m/s from the SW to the turbines. The results indicate that, when the air flows across the building, a vector direction of wind can cause a vortex beside the wind turbines. The vortex flows of the three CFD turbulence models are seen in WT1, WT2, and WT3 with the same characteristic, but no vortex flow is seen at WT0, as WT0 is an arbitrary installation in an unobstructed area.

@ WT1 (a1) k-ε Model   (a2) k-ω Model   (a3) RNG Model

68

@ WT2 (b1) k-ε Model (b2) k-ω Model (b3) RNG Model

@ WT3 (c1) k-ε Model (c2) k-ω Model (c3) RNG Model

(d) No Vortex Flow at WT0
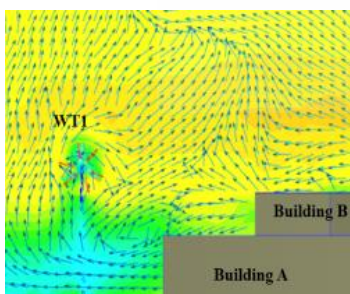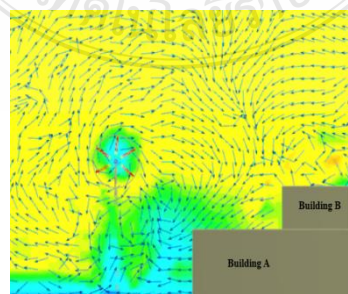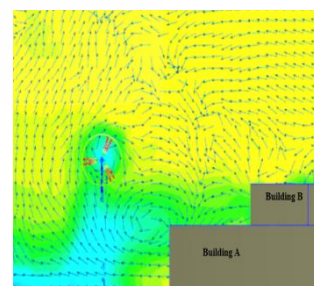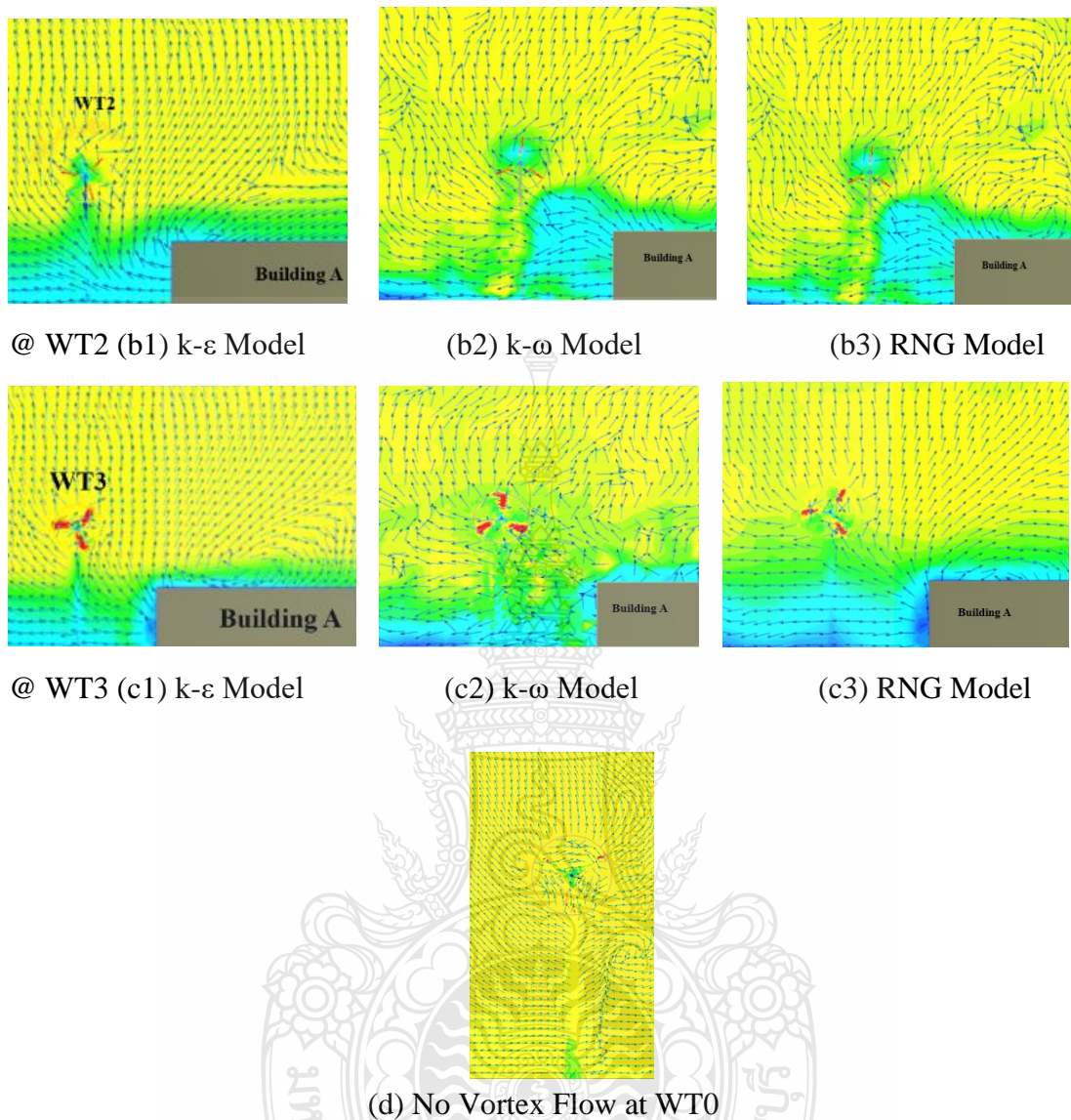
Figure 4.8 Vortex Flow Vectors to Wind Turbines from the three CFD Turbulence
     Model Simulations

   4.2.4 CFD k-Ɛ, k-ω, and RNG Model Simulation Results
     Table 4.3 is the result of power performance, with free spinning rotation,
of WT0, WT1, WT2, and WT3 by using the CFD k-ε, k-ω, and RNG turbulence models
at an incoming wind speed of 4.5 m/s (see Appendix C, D, and E). The results indicate
that, using the k-ε turbulence model, the power performance, with free spinning
rotation, of WT1>WT2>WT0>WT3, while, using the CFD k-ω and RNG turbulence
models, the power performance, with free spinning rotation, of WT2>WT1>WT0>WT3.
Consequently, the three CFD turbulence models signify the same behaviour profile of
power performance, with free spinning rotation, of WT1 and WT2>WT0 and WT3<WT0.

Table 4.3 Power Performance, with Free Spinning Rotation, of WT0-WT3 Using CFD k-Ɛ, k-ω, and RNG Turbulence Models as Wind Flows from the SW at an Incoming Wind Speed of 4.5 m/s

CFD model	WTs	RPM/Voltage	Ampere	Watt
k-Ɛ turbulence model	WT0	95	10.53	1,000.00
	WT1	102	10.52	1,073.00
	WT2	104	10.78	1,056.80
	WT3	101	9.16	925.00
k-ω turbulence model	WT0	93	10.16	945.00
	WT1	104	9.98	1,037.99
	WT2	109	9.93	1,082.40
	WT3	93	9.96	926.10
RNG turbulence model	WT0	98	10.51	1,030.00
	WT1	104	10.54	1,096.02
	WT2	109	10.45	1,139.28
	WT3	93	10.52	978.50

Remark: A THUNYA 5kW HAWT's generator designed 1 rpm = 1 V

Figure 4.9 and Table 4.4 show the comparison of power performance effect, with free spinning rotation, of WT1, WT2, and WT3 with WT0 by using CFD k-Ɛ, k-ω, and RNG turbulence model simulation results as the wind flows from the SW at an incoming wind speed of 4.5 m/s. The results indicate that the power performances, with free spinning rotation, of WT1, WT2, and WT3 are both higher and lower than WT0. WT1 and WT2 are higher than WT0, and WT3 is lower than WT0. Consequently, the profiles of the wind turbines' power performance, with free spinning rotation, from each CFD turbulence model show the same behaviour.
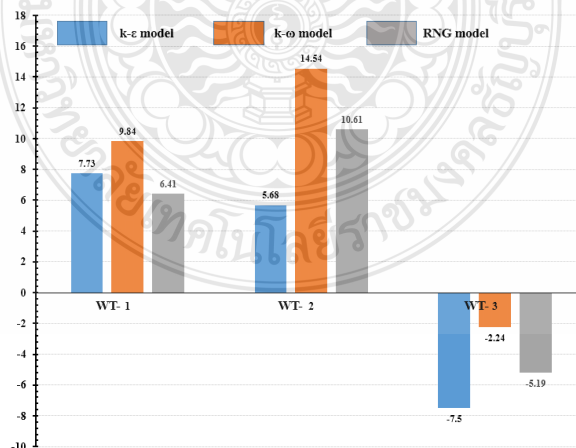
Figure 4.9 Comparison of Power Performance Effect, with Free Spinning Rotation, of WT1-WT3 with WT0 by Using CFD k-Ɛ, k-ω, and RNG Turbulence Model as Wind Flows from the SW at an Incoming Wind Speed of 4.5 m/s

Table 4.4 Comparison of Power Performance Effect, with Free Spinning Rotation, of WT1-WT3 with WT0 Using CFD k-Ɛ, k-ω, and RNG Turbulence Model as Wind Flows from the SW at an Incoming Wind Speed of 4.5 m/s

Wind Turbine No.	WT Power Effect (k-ε)(%)	WT Power Effect (k-ω) (%)	WT Power Effect RNG (%)
WT0	100.00	100.00	100.00
WT1	107.73	109.84	106.48
WT2	105.68	114.54	110.62
WT3	92.50	97.76	94.11

Figure 4.9 and Table 4.4 are the comparison results of the CFD k-Ɛ, k-ω, and RNG turbulence models. Simulations show that the power performance effects, with free spinning rotation, of WT1, WT2, and WT3 compared with WT0 are as follows.

- Using the k-ε model, the power performance effects, with free spinning rotation, of WT1 and WT2 increased by 7.73% and 5.68%, respectively, while the power performance effect, with free spinning rotation, of WT3 decreased by 7.50%.

- Using the k-ω model, the power performance effects, with free spinning rotation, of WT1 and WT2 increased by 9.84% and 14.54%, respectively, while the power performance effect, with free spinning rotation, of WT3 decreased by 2.24%.

- Using the RNG model, the power performance effects, with free spinning rotation, of WT1 and WT2 increased by 6.48% and 10.62%, respectively, while the power performance effect, with free spinning rotation, of WT3 decreased by 5.89%.

An increased or decreased of power performance effect, with free spinning rotation, of WT1, WT2, and WT3 occurred after the wind flowed across the buildings to the turbines. Consequently, the CFD k-Ɛ, k-ω, and RNG turbulence model simulation profile characteristics appear similar due to the following results: (1) Using the k-Ɛ model, the power performance effects, with free spinning rotation, of WT1 and WT2 are higher than WT0 by approximately 7%, while WT3 is lower than WT0 approximately by 7%. (2) Using the k-ω model, the power performance effects, with free spinning rotation, of WT1 and WT2 are higher than WT0 by approximately 12%, while WT3 is lower than WT0 by approximately 2%. (3) Using the k-ω model, the power performance effects, with free spinning rotation, of WT1 and WT2 are higher than WT0 by approximately 9%, while WT3 is lower than WT0 by approximately 6%.

Discussion

4.2.5 $CFD\ k-\varepsilon,\ k-\omega,$ and RNG Model Simulation Results Discussion

The results of the CFD k k-ω, and RNG turbulence model simulation profiles are the same as the results of the CFD k-Ɛ turbulence model as wind flows from the SW, as in Section 4.1.7. Therefore, as wind flows from the SW, the effect increases or decreases the power performances, with free spinning rotation, of WT1, WT2, and WT3 from the CFD k-Ɛ, k-ω, and RNG turbulence model simulations. The reasons are the same as for the increased or decreased power performances, with free spinning rotation, of WT1, WT2, and WT3 from the CFD k-Ɛ turbulence model simulation. The results of the CFD k-Ɛ, k-ω, and RNG turbulence model profiles of power performances, with free spinning rotation, of WT1, WT2, and WT3 are similar for the following reason:

• The power performance effect, with free spinning rotation, at WT3 is decreased probably by the wake region or vortex flow from Building A due to the position of WT3 close to Building A.

• The power performance effect, with free spinning rotation, at WT2 is increased probably by a Venturi effect created from the gap between Buildings A-B and A-D, and by a local steep wind shear gradient from Building A.

• The power performance at WT1 is increased probably by a Venturi effect created from Buildings A-B and A-D, and a local steep wind shear gradient from Buildings A and B.

• The results of the CFD k-Ɛ, k-ω, and RNG turbulence model profiles of power performances, with free spinning rotation, of WT1, WT2, and WT3 are similar and affirm this technique is highly reliable.

In summary, building-obstructed wind flow areas create wind power with both low and high energy yields due to the Venturi effect, steep wind shear gradients, vortices, etc. that cause increase and decrease in wind turbine power performance. Moreover, the CFD turbulence model simulation technique is reliable for predicting wind turbine power performance in a building-obstructed wind flow area.

4.3 Site Measurement Results and Discussion

Results

4.3.1 Wind Velocity Behaviour in the Site

Table 4.5 shows the measurement results of incoming and outgoing wind speeds from the site measurement technique that was done by the Professional Touch Screen Weather Center With PC Interface, Model No: AW002, FREQ: 443MHz. The setup of the two instruments is shown in Figure 4.10. They were used to measure wind speed at the same height of the wind turbines' hub height on the roofs of Buildings A and C as wind flows from the SW at an incoming wind speed (Vin) to Building A across WT3-WT2-WT1 to Building C at an outgoing wind speed (Vout).
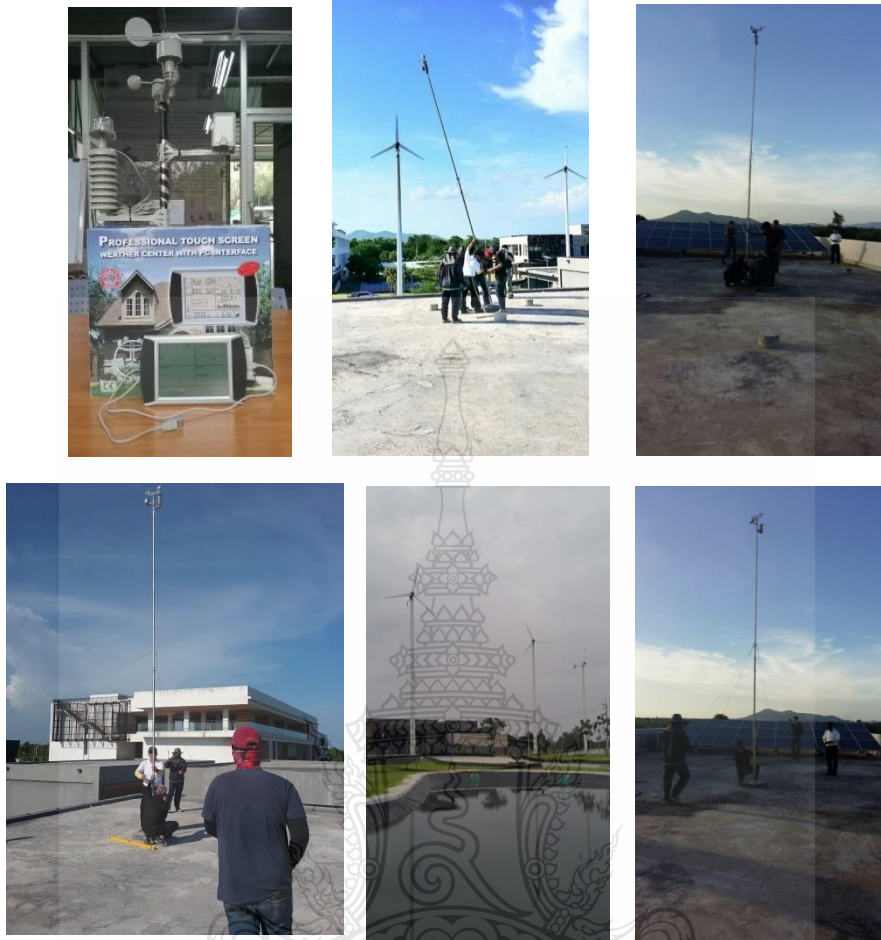
Figure 4.10 The Setting Up of Two Wind Speed Measuring Instruments

Table 4.5 The Measuring Results of Vin and Vout as Wind Flow from the SW

Time	Building A Vin, m/s	Building C Vout, m/s	Time	Building A Vin, m/s	Building C Vout, m/s
1030	2.7	4.1	1300	4.5	5.4
1035	2.7	3.7	1305	4.4	5.1
1040	3.4	4.8	1310	4.1	5.8
1045	2.7	4.8	1315	4.4	5.1
1050	2.0	3.7	1320	3.4	4.1
1055	3.4	4.4	1325	3.7	4.8
1100	3.4	4.1	1330	5.1	4.4
1105	3.1	4.1	1335	3.4	4.4
1110	2.7	4.1	1340	4.8	4.1
1115	3.7	4.1	1345	4.4	3.7
1120	2.7	4.8	1350	3.1	3.7
1125	3.7	3.7	1355	5.1	4.1
1130	3.1	3.7	1400	3.4	5.1

4.3.2 Small Wind Turbine Characteristics in the Site Conditions

By monitoring the small wind turbines' characteristics in the site measurement ambient conditions, it was found that the small wind turbines are sensitive to turbulence, as shown in Figure 4.11, because they always stop rotating before changing the rotor to the normal direction for following the recent turbulence vector, and often the turbines do not reach the matching maximum rpm with recent wind velocity. In the CFD condition, the small wind turbines are fixed in the normal direction to the SW and never stop rotating for responding to the normal direction of the recent turbulence vector, and they also always cause the turbines' rotation to reach the matching maximum rpm with recent wind velocity. However, the behaviour of the wind flow velocity profile, as shown in Figure 4.12, describes the experimental results of the site measurement based on the measured data of incoming wind velocity at the roof of Building A (Vin) compared with outgoing wind speed at the roof of Building C (Vout) as the wind flows from the SW to Building A-WT3-WT2-WT1- Building C. The results indicate that Vin at Building A is lower than Vout at Building C.

Figure 4.11 Usual Direction of Wind Turbines in DETC Along with Turbulence
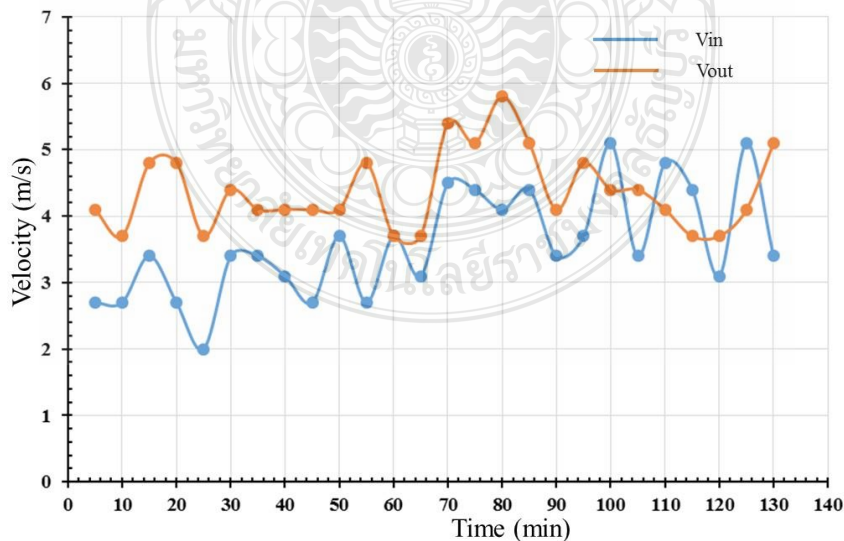
Figure 4.12 Behaviour of Wind Velocity Profile (Vin < Vout) as Wind Flow from the SW Passed Over the Buildings and three 5-kW HAWTs

74

Discussion

4.3.3 Behaviour of Wind Velocity in CFD and Site Measurement Comparison

Figure 4.12 and Table 4.5 indicate that the behaviour of the wind velocity profile of the site measurement and CFD investigation are similar. This means the accuracy of the CFD technique is validated by site the measurements. Consequently, the CFD technique can be used to predict the power performance of small wind turbines in a building-obstructed wind flow area.

CHAPTER 5

CONCLUSIONS

5.1 Conclusions and Recommendations

This chapter presents the detailed results of this study, which used CFD with site measurement characteristic results to corroborate each other, along with recommended further work. From the references and the results of the CFD simulations and site estimations, the conclusions and recommendations are as follows.

5.1.1 The power performance of a small wind turbine in building-obstructed wind flow both increases and decreases power performance caused by turbulence, the Venturi effect, and steep wind shear gradient.

5.1.2 When choosing a building-obstructed wind flow area to install small wind turbines, the geometric features and layout of the obstructing buildings are the major factors to be considered, as they will shape the wind flow characteristics of the small wind turbines. This is the factor to be evaluated to increase or decrease the power performance effectiveness of small wind turbines.

5.1.3 From the results of the CFD technique, wind machines WT1, WT2, and WT3 were compared with a wind machine located without obstructed wind flow (WT0). The results found by using the differences of turbulence models applied to the boundaries conditions are as follows.

(1) Using the k-ε turbulence model, as wind flows from the NE, the power performances of WT1, WT2, and WT3 are higher than that of WT0 by approximately 31%.

(2) Using the k-ε turbulence model, as wind flows from the SW, the power performances of WT1 and WT2 are higher than that of WT0 by approximately 7%, while WT3 is lower than WT0 by approximately 7%.

(3) Using the k-ω turbulence model, as wind flows from the SW, the power performances of WT1 and WT2 are higher than that of WT0 by approximately 12%, while WT3 is lower than WT0 by approximately 2%.

(4) Using the RNG turbulence model, as wind flows from the SW, the power performances of WT1 and WT2 are higher than that of WT0 by approximately 9%, while WT3 is lower than WT0 by approximately 6%.

5.1.4 The site testing results using two anemometers at the same height of the SWTs on Buildings A and C show that wind velocity at incoming wind speed on Building A is lower than outgoing wind speed at Building C, which are similar to CFD investigation results in the three turbulence models.

5.1.5 Consequently, the CFD technique in this study using turbulence models can be applied to predict the power performance of small wind turbines in building-obstructed wind flow areas.

5.1.6   The ratio of wind turbines' hub height and longer distances between wind turbines and buildings is recommended as a key parameter of this CFD technique for installing small wind turbines in a building-obstructed wind flow area.

From the above results, this study found that the three turbulence models can be used to predict the small wind turbine power performance effect from building obstruction. The turbulence model results show both an increase and a decrease of the wind turbine performance in building-obstructed wind flows, and the results of each CFD model are appropriate, depending on the boundary conditions.

5.2 Implications for Practice and Future Research

Further work is proposed to enhance the CFD, k-ε, k-ω, and RNG turbulence model to simulate each direction and to gather more results caused by changing wind direction of wind flow patterns. A greater distance from the buildings to the wind machine or extending the wind turbine tower in cases where the wind machine is close to a building are recommended. However, the appropriate distance and height of the wind machine could be well predicted using the CFD technique in comparing the results of turbulence models. Long-term site measurements and investigations are needed for comparison with CFD results. Further research is recommended to study building-obstructed wind flow to achieve higher performance for small wind machines located in obstructed wind flows.
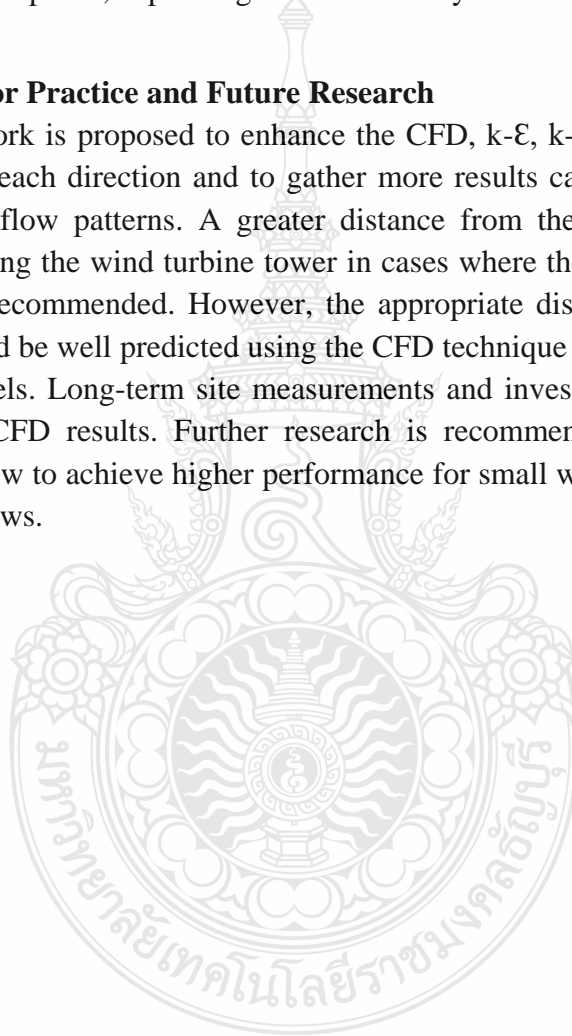
List of Bibliography

[1]   Arslan, O. (2010). Technoeconomic analysis of electricity generation from wind energy in Kutahya, Turkey. **Energy**, 35(1), 120–31.

[2]   International Energy Agency. (2017). **Monthly electricity statistics**. Retrieved from http://www. iea.org/ statistics/monthlystatistics/

[3]   Morris, C. & Jungjohann, A. (2016**). Energy democracy Germany's energiewende to renewables, German state already has 120 percent renewable power**. Retrieved from http:// www. renewablesinternational.net/german-state-already-has-120-percentrenewable power/150/537/79680/

[4]   Robbie, E. (2015). **Aspen is third U.S. city to reach 100% renewable energy**. Retrieved from http:// www. aspentimes.com/news/17972193-113/aspen-is-third-us-city-to-reach-100

[5]   Watts, J. (2016). **Uruguay makes dramatic shift to nearly 95% electricity from clean energy**. Retrieved from http://www.theguardian.com/environment/2015/dec/03/uruguaymakes- dramatic-shift-to-nearly-95-clean-energy

[6]   Gipe, P. (2004). **Wind power: renewable energy for home, farm, and business**. Chelsea Green Publisher.

[7]   Manwell, JF., McGowan, J.G., & Rogers, A.L. (2009). **Wind energy explained: theory, design and application**. 2nd ed. Amherst, USA: John Wiley & Sons.

[8]   Abdulrahman M., & Wood, D. (2017). Investigating the power-COE trade-off for wind farm layout optimization considering commercial turbine selection and hub height variation. **Renew Energy**, 102, 78-267.

[9]   Castellani, F., Astolfi, D., Sdringola, P., Proietti, S., & Terzi, L. (2017). Analyzing wind turbine directional behavior: SCADA data mining techniques for efficiency and power assessment. **Appl Energy**, 185 (Part 2), 1076–86.

[10] Song, D., Yang, J., Cai, Z., Dong, M., Su, M., & Wang, Y. (2017). Wind estimation with a non-standard extended Kalman filter and its application on maximum power extraction for variable speed wind turbines. **Appl Energy**, 190, 85-670.

[11] Saleh, H., Aly, A.A.E.A., & Abdel-Hady, S. (2012). Assessment of different methods used to estimate Weibull distribution parameters for wind speed in Zafarana wind farm, Suez Gulf, Egypt. **Energy**, 44(1), 9-710.

[12] Shu, Z.R., Li, Q.S., & Chan, P.W. (2015). Statistical analysis of wind characteristics and wind energy potential in Hong Kong. **Energy Convers Manage**, 101, 57-644.

[13] Masseran, N., & Markov. (2015). Chain model for the stochastic behaviors of wind-direction data. **Energy Convers Manage**, 92, 74-266.

List of Bibliography (Continued)

[14] Alavi, O., Sedaghat, A., & Mostafaeipour, A. (2016). Sensitivity analysis of different wind speed distribution models with actual and truncated wind data: a case study for Kerman, Iran. **Energy Convers Manage**, 120, 51–61.

[15] GWEC. (2016). **Global wind statistics**. Global Wind Energy Council.

[16] Lind, A., Rosenberg, E., Seljom, P., Espegren, K., Fidje, A., & Lindberg, K. (2013). **Analysis of the EU renewable energy directive by a techno-economic optimisation model, Energy Policy 60(2013)364e377**. Retrieved from http://dx.doi.org/10.1016/ j.enpol.2013.05. 053.

[17] Blaschke, T., Biberacher, M., Gadocha, S., & , I. (2013). Energy landscapes: meeting energy demands and human aspirations. **Biomass- Bioenergy**, 55, 3–16.

[18] World Energy Outlook. (2016). **International Energy Agency; 2012**. Retrieved from http://www.Worlden ergyoutlook.org/weo2012/

[19] International Energy Agency. (2016). **The global wind energy outlook. Global wind energy council**. Retrieved from http://files. gwec.net/files/ GlobalWind Energy Outlook2016.

[20] World Wind Energy Association (2016). **Small wind world report**, 1–16.

[21] IEA. (2014). International Energy Agency. **World Energy Outlook**, OECD/IEA, Paris.

[22] UNDP. (2002). **World Energy Assessment : Energy and Challenge**. United Nations Development Program. UNDP, New York.

[23] WEC. (2011). **Survey of Energy Resources 2010: Bioenergy, World Energy Council.** Retrieved from www.worldenergy.org/publications. verified January 10, 2011.

[24] IPCC. (2007). **Intergovernmental Panel on Climate Change**. Climate Change 2007: Mitigation of Climate Change. Contribution of Working Group III to the Fourth Assessment Report of the Intergovernmental Panel on Climate Change. [B. Metz, O.R. Davidson, P.R. Bosch, R. Dave, L.A. Meyer (eds)], Cambridge University Press, Cambridge, UK, pp. 851.

[25] IPCC. (2011). **Intergovernmental Panel on Climate Change, Special reports on renewable energy sources**. Summary for policy makers, in: 11th Session of Working Group III of the IPCC, Abu Dhabi, United Arab Emirates, 5e8, May 2011.

[26] Klass, D.L. (1998). **Biomass for Renewable Energy, Fuels, and Chemicals, Academic Press/lsevier**, London.

[27] F. Rosillo-Calle, P. de Groot, Hemstock, S.L., & Woods, J. (2007). **The Biomass Assessment Handbook: Bioenergy for a Sustainable Environment.** Earthscan, London.

[28] E. Ntona, G., Arabatzis, G.L., Kyriakopoulos. (2015). Energy saving: views and attitudes of students in secondary education, Renew. Sustain. **Energy Rev**. 46 (2015)1e15.

[29] Bertani, R. (2016). **Geothermal power generation in the world 2010–2014**, update report. Geothermics 60, 31–43. Retrieved from http://dx. doi.org/ 10.1016/ j.geothermics. 2015.11.003.

[30] Zhang, J.Z., Li, J., Li, Y., & Zhao, Y. (2014). **Hydrogen generation, storage and utilization**. John Wiley & Sons.

[31] Inger, R., Attrill, M.J., Bearhop, S., Broderick, A.C., James Grecian, W., & Hodgson, D.J. (2009). Marine renewable energy: potential benefits to biodiversity? An urgent call for research. **J Appl Ecol**, 46, 53-1145.

[32] Frid, C., Andonegi, E., Depestele, J., Judd, A., Rihan, D., & Rogers, S.I. (2012). The environmental interactions of tidal and wave energy generation devices. **Environ Impact Assess Rev**, 32, 9-133.

[33] Boehlert, G.W., & Gill, A.B. (2010). Environmental and ecological effects of ocean renewable energy development: a current synthesis. **Oceanography**, 23, 68–81.

[34] Adhau, S.P., Moharil, R.M., & Adhau, P.G. (2012). Mini-hydro power generation on existing irrigation projects: case study of Indian sites. **Renewable and Sustainable Energy Reviews**, 16, 95-4785.

[35] Global. (2014). **Market Forecast for 2015–2019**. Retrieved from http://www.gwec.net/ global-figures/market-forecast-2012-2016/.

[36] Taylor, P.A., & Gent, P.R., (1974). A model of atmospheric boundary layer flow above an isolated two-dimensional hill: an example of flow over gentle topography. **Bound.-Layer Meteorol**, 7, 349–362.

[37] Jackson, P.S., & Hunt, J.C.R. (1975). Turbulent wind flow over a low hill. **Quart.J. Roy. Meteorol. Soc.**, 101, 929–955.

[38] Mason, P.J., & Sykes, R.I. (1979). Flow over an isolated hill of moderate slope. **Quart. J. Roy. Meteorol. Soc.,** 105, 383–395.

[39] Jackson, P.S., & Hunt, J.C.R. (1975). Turbulent wind flow over a low hill. **Quart. J. Roy.Meteorol. Soc.**, 101, 929–955.

[40] Hölling, M., Peinke, J., Ivanell, S. (2014). **Wind Energy—Impact of Turbulence, Research Topic sin Wind Energy, vol.2. Springer Berlin, Heidelberg.** Retrieved from http://dx.doi.org/10.1007/978-3-642-54696-9_20.

[41] Kaimal, J.C., Izumi, Y., Wyngaard, J.C., & Cote, R. (1972). Spectral characteristics of surface-layer turbulence. **Quart. J. R. Meteorol. Soc.**, 98 (417), 563–589.

List of Bibliography (Continued)

[42] S. Houda, N., Zemmouri, R., Athmani, & Belarbi, R. (2011). Effect of urban morphology on wind flow distribution in dense urban areas. **Revue des Energies Renouvelables**, Vol. 14 N°1, 85 – 94

[43] Dr. Islan Abohela, Dr. Neveen Hamza, & Dr. Steven Dudek. (2013). **Building on wind flow above a barrel vaulted roof,** Proceeding of BS 2013: 13th Conference of International Building Performance Simulation Association, Chambery, France, August, 26-28.

[44] Spirn, & Anne Whiston. (1986). **Air quality at street-level: strategies for urban design.** Prepared for: Boston Redevelopment Authority, June 1986.

[45] Runa Nivea Pinto, Asif Afzal, Navaneeth, I. M., & Ramis, M. K. **Computational Analysis of flow in Turbines**, P. A. College of engineering, Mangalore, India

[46] B. Blocken, J. Carmeliet. (2004). Pedestrian wind environment around buildings: literature review and practical examples. **J. Therm. Envelope Build. Sci**., 28, 107-159.

[47] Kim, Y.-H., Choi, D.-Y., & Chang, D.-E. (2011). Characteristics of urban meteorology in Seoul metropolitan area of Korea. **Atmosphere**, 21 (2011) 257e271 (with English Abstract).

[48] BBC News. (2012). **Man Crushed to Death by 'floating' Lorry in Leeds.** Retrieved from http://www.bbc. com/news/uk-england-leeds-16968325, February 9, 2012.

[49] Woolley, Steve. **Edexcel IGCSE Physics Revision Guide**. Pearson Education. p. 49. ISBN 9780435046736.

[50]. Charles Kittel, Walter, D. Knight, & Malvin, A. Ruderman. **Berkeley Physics**, Course Volume 1.

[51] Ahmad, S., Tahar, R.M., Muhammad-Sukki, F., Munir, A.B., & Rahim, R.A. (2015). Role of Feedin Tariff Policy in Promoting Solar Photovoltaic Investments in Malaysia: A System Dynamics Approach**. Energy**, 84, 15-808.

[52] EIA. (2017). **EIA– U.S Energy Information Administration. Renewable energy explained; 2017**. Retrieved from
https://www.eia.gov/energyexplained/index.cfm?Page=renewable_home.

[53] IEA. (2017). EIA – International Energy Agency. Topics: renewables; 2017. Retrieved from http://www.iea. org/topics/renewables/.

[54] Iov, F., Ciobotaru, & Blaabjerg, F. (2010). **Power Electronics control of wind energy in distributed power systems.** fellow IEEE, Aalborg University, Institute of Energy Technology Pontoppidanstraede 101, DK-9220 Aalborg East, Denmark, 2010.

List of Bibliography (Continued)

[55] IEEE Explore. **Analysis of Air Foils and Design of Blades for a Low-Speed 250W Horizontal Axis Wind Turbine Suitable for Coastal Areas of Bangladesh**.

[56] Danish. **The Energy in the Wind**, Wind Industry Association.

[57] Gipe &Paul. (2009). **Wind Energy Basics**. Chelsea Green Publishing Company. ISBN 978-1-60358-030-4.

[58] Tony Burton, David Sharpe, Nick Jenkins, & Ervin Bossanyi. (2001). **Wind Energy Handbook**. John Wiley & Sons, Ltd.

[59] Paul Gipe, Scams, Frauds, & Flakes. (2009)**. Fantasy wind Turbines or If it's too good to be True.** 20 July 2009.

[60] Jorge L. Acosta, Kevin Combe, Sasaˇ Z. Djokic´, Senior Member, & Ignacio Hernando-Gil. (2012). Performance Assessment of Micro and Small-Scale Wind Turbines in Urban Areas. **IEEE SYSTEMS JOURNAL**, VOL. 6, NO. 1, MARCH 2012.

[61] Youngji. (2015). **Looking inside wind turbine**. Retrieved from https://medium.com/@youngji/looking-inside-wind-turbine-9e2888fb2ee

[62] GE Power. (2013). **Products & Services**. Retrieved from https://Gepower.com.

[63] Chia, C.C., Lee, J.R., & Bang, H.J. (2008). **Structural health monitoring for a wind turbine system: A review of damage detection method.** Retrieved from https://www.researchgate.net/figure/Figure-1-A-typical-configuration-of-a-horizontal-axis-wind-turbine-system-1_230937312_fig1

[64] Osborne, L. (2016). **Wind turbine project recap wind power and blade aerodynamics**. Retrieved from http://slideplayer.com/slide/6044933/

[65] Proudly Namibian. (2017). **Angle of attack**. Retrieved from http://www.aviationchief.com/angle-of-attack.html

[66] Paul Dvorak. (2017). **Wind power engineering & development**. Retrieved from http://www.windpowerengineering.com/blog/build-wind-turbine-hurricane-speed-winds/

[67] Saeed Zolfaghari, Gholam H. Riahy, & Mehrdad Abedi. (2015). A new method to adequate assessment of wind farms' power output. **Energy Conversion and Management**, 103, 585–604

[68] Marks. **Standard Handbook for Mechanical Engineers**. Eleventh Edition, by: Eugene A. Avallpne, Theodore Baumeister III, Ali Sadegh.

[69] David Seger, & Andy Solberg. **Economizer performance: Applying CFD modeling to the data center's exterior**. Retrieved from http://searchdatacenter.techtarget.com/tip/Economizer-performance-Applying-CFD-modeling-to-the-data-centers-exterior

[70] Wan, Y., Ela, E., & Orwig, K. (2010). Development of an Equivalent Wind Plant Power-Curve Preprint. **Wind**, No June, p. 20, 2010.

<p style="text-align:center">List of Bibliography (Continued)</p>

[71] Li, Q., Murata, J., Endo, M., Maeda, T., & Kamada, Y. (2016). Study on power performance for straight-bladed vertical axis wind turbine by field and wind tunnel test. **Renew. Energy**, vol. 90, pp.291–300.

[72] Li, Q., Murata, J., Endo, M., Maeda, T., & Kamada, Y. (2016). Experimental and numerical investigation of the effect of turbulent inflow on a Horizontal Axis Wind Turbine (Part I: Power performance). **Energy**, vol. 113, pp. 713–722.

[73] Tabrizi, A. B., Whale, J., Lyons, T., & Urmee, T. (2014). Performance and safety of rooftop wind turbines: Use of CFD to gain insight into inflow conditions. **Renew. Energy**, vol.67, pp. 242–251.

[74] Balduzzi, F., Bianchini, A., Carnevale, E.A., Ferrari, L., & Magnani, S. (2011). **Feasibility analysis of a Darrieus VAWT installation in the rooftop of a building.** Int. Conf. Appl. Energy, no. May, pp. 3345–3358.

[75] KAPER. (2005). **Kite flying around wind obstacles**. Retrieved from http://www.davidhunt.me/basics/BASICS_040502_hunt_windflow.html

[76] Lundquist, Julie, Clifton, & Andrew. (2012). **How turbulence can impact power performance**. North American Windpower, September 2012

[77] Brown, G. (2001). **Sun, Wind & Light**. New York: Wiley. p.18.ISBN 0-471-34877-5.

[78] Oke, T. (1987). **Boundary Layer Climates.** London: Methuen. p. 54. ISBN 0-415-04319-0.

[79] Crawley, Stanley. (1993). **Steel Buildings**. New York: Wiley. p. 272. ISBN 0-471-84298-2.

[80] Lubosny, Zbigniew. (2003). **Wind Turbine Operation in Electric Power Systems: Advanced Modeling**. Berlin: Springer. p. 17. ISBN 3-540-40340-X

[81] Harrison, Roy. (1999). **Understanding Our Environment**. Cambridge: Royal Society of Chemistry. p. 11. ISBN 0-85404-584-8.

[82] B.Wang, L.D. Cot, L.Adolphe, S.Geoffroy, J. Morchain. (2015). Estimation of Wind Energy Over Roof of Two Perpendicular Buildings. **Energy and Buildings**, 88, 57-67.

[83] Chong, W.T., Fazlizan, A., Poh, S.C., Pan, K.C., Hew, W.P., & Hsiao, F.B. (2013). The design, simulation and testing of an urban vertical axis wind turbine with the omni-direction-guide-vane. **Applied Energy**, 112, pp. 601-609.

[84] Sunderland, K.M., Mills, G., & Conlon, M.F. (2013). Estimating the wind resource in an urban area: A case study of micro-wind generation potential in Dublin, Ireland. **Journal of Wind Engineering and Industrial Aerodynamics**, 118, pp. 44-53.

List of Bibliography (Continued)

[85] Millward-Hopkins, J., Tomlin, A., & Ma, L. (2012). The predictability of above roof wind resource in the urban roughness sublayer. **Wind Energy**, 15, 225-243.

[86] Mertens, S. (2003). The energy yield of roof mounted wind turbines. **Wind Eng**, 27 (6), 507-518.

[87] Uchida, T., & Ohya, Y. (2008). Micro-siting technique for wind turbine generators by using large-Eddy simulation. **J. Wind Eng. Ind. Aerodyn**., 96, 2121-2138.

[88] Wang, B., Cot, L.D., Adolphe, L., Geoffroy, S., & Sun, S. (2017). Cross indicator analysis between wind energy potential and urban morphology. **Renewable Energy**, 113, 989-1006

[89] Stankovic S, Campbell N, & Harries A. (2009). **Urban wind energy**. Earthscan.

[90] Balduzzi F, Bianchini A, Carnevale EA, Ferrari L, & Magnani S. Feasibility analysis of a Darrieus vertical-axis wind turbine installation in the rooftop of a building. **Appl Energy**, 97, 9-921.

[91] Amir BashirzadehTabrizi, Jonathan Whale, Thomas Lyons, & Tania Urmee. (2014). Performance And safety of rooftop wind turbines: Use of CFD to gain insight into inflow conditions. **Renewable Energy**, Volume 67, July 2014, Pages 242-251.

[92] World Wind Energy Association. (2015). **Small Wind World Report Summary**, March, 2015.

[93] NREL. (2017). **Small Wind**. Department of Energy National Renewable Energy Laboratory, U.S. Retrieved from https://www.nrel.gov/wind/smallwind.

[94] Anon. (2013). **Solar & Wind Powered Sign Lighting**. Energy Development Cooperative Ltd. Retrieved from https://www.solar-wind.co.uk/ solar_powered_sign_lights.html.

[95] Valerio Lo Brano, Vincenzo La Rocca, Giuseppina Ciulla, Edoardo Moreci, Marco Beccali Dipartimento di Energia, Ingegneria dell'Informazione, Modelli Matematici – DEIM. **Energy and economic assessment of a small Domestic wind turbine in Palermo**. IEEE explorer, University of Palermo, Palermo, Italy.

[96] Jorge L. Acosta, Kevin Combe, Sasaˇ Z. Djokic´, & Ignacio Hernando-Gil. (2012). Performance Assessment of Micro and Small-Scale Wind Turbines in Urban Areas. **IEEE Systems Journal**, 6(1), March 2012.

[97] Dhunny, A.Z., Lollchund, M.R., Rughooputh, S.D.D.V. (2017). Wind energy evaluation for a highly complex terrain using Computational Fluid Dynamics (CFD), **Renewable Energy**, 101, 1-9.

[98] McIntosh. (2008). **Product**. McLntosh laboratory, Inc-2 Chamners Street-Binghamton, NY 13903-2699. Retrieved from http://wwwmcintoshlabs.com.

List of Bibliography (Continued)

[99] IEEE Xplore. **Urban deployment of small wind turbines: Power performance and turbulence.**

[100] Hafida Daaou Nedjari, Ouahiba Guerri, & Mohamed Saighi. (2017). CFD wind turbines wake assessment in complex topography. **Energy Conversion and Management**, 138, 224-236.

[101] Lo, L., & Ip, K.Y. (2009). Investigation on the Feasibility and Enhancement Methods of Wind Power Utilization in High-Rise Buildings of Hong Kong. **Renewable Sustainable Energy Rev**., 13(2), 450-461.

[102] Amir BashirzadehTabrizi., Jonathan Whale., Thomas Lyons., & Tania Urmee. (2014). Performance and safety of rooftop wind turbines: Use of CFD to gain insight into inflow conditions. **Renewable Energy**, Vol 67, 242-251.

[103] Blocken, B., Stathopoulos, T., & Carmeliet, J. (2008). A numerical study on the existence of the Venturi-effect in passages between perpendicular buildings. **J Eng Mech –ASCE**, 134(12), pp. 1021-1028.

[104] Venturi, GB. (1799). **Experimental enquiries concerning the principle of the lateral Communication of motion in fluids: applied to the explanation of various hydraulic phenomena**. Translated from the French by Nicholson W. 1st English ed., J. Taylor, Architectural Library, High-Holborn, London.

[105] J. Gandemer. (1975). **Wind environment around buildings: aerodynamic concepts**. Proceedings of 4th international conference wind effects on buildings and structures, Cambridge University Press, Heathrow, pp. 423-432.

[106] Lawson, T.V. (1980). **Wind effects on buildings**. Applied Science Publishers, Vol 1, Ltd., London, England.

[107] Dutt, A.J. (1991). Wind flow in an urban environment. **Environ Monit Assess**, 19 (1–3), pp. 495-506.

[108] Blocken, B., Carmeliet, J., & Stathopoulos, T. (2007). CFD evaluation of the wind speed conditions in passages between buildings – effect of wall-function roughness modifications on the atmospheric boundary layer flow. **J Wind Eng Ind Aerod**, 95 (9–11), pp. 941-962.

[109] Blocken, B., Stathopoulos, T., & Carmeliet, J. **Wind environmental conditions in passages between two long narrow perpendicular buildings**.

[110] Qiang Wang, Jianwen Wang, Yali Hou , Renyu Yuan, Kun Luo , Jianren Fan. (2018). Lidar measurements. **Renewable Energy**, 115, 1118-1133.

[111] Jie Zhang, Souma Chowdhury, Achille Messac, & BriMathias Hodge. (2013). **Assessinglong-term wind conditions by combining different measure-correlate-predict algorithms**. In ASME International Design Engineering Technical Conferences, Portland, Oregon, volume 3A, August 4th- 7th 2013.

List of Bibliography (Continued)

[112] IEEE. **Wind Resource Assessment and Numerical Simulation for Wind Turbine**. Airfoils, IEEE.

[113] Autodesk Knowledge Network. (2018). **Engineering software**. Retrieved from https://knowledge.autodesk.com/support/cfd/learn-explore.

[114] Frank, P. Incropera, David, P. Dewitt, Theodore, L. Bergman, & Adrienne, S. Lavine. **Fundamentals of Heat and Mass Transfer**.

[115] Kim, H.G., Patel, V.C., & Lee, C.M. (2000). Numerical simulation of wind flow over hilly terrain. **J Wind Eng Ind Aerodyn**, 87, 45–60.

[116] Wang, B., Cot, L.D., Adolphe, L., Geoffroy, S., & Sun, S. (2017). Cross indicator analysis Between Wind energy potential and urban morphology. **Renewable Energy**, 113, 989-1006.

[117] Dhunny, A.Z., Lollchund, M.R., & Rughooputh, S.D.D.V. (2017). Wind energy evaluation for a highly complex terrain using Computational Fluid Dynamics (CFD). **Renewable Energy**, 101, 1-9.

[118] Tabrizi, A.B., Whale, J., Lyons, T., & Urmee, T. (2014). Performance and safety of rooftop Wind turbines: Use of CFD to gain insight into inflow conditions. **Renew. Energy**, vol. 67, pp. 242–251.

[119] T. Burton, D., Sharpe, N., Jenkins, E., & Bossanyi. (2001). **Wind Energy Handbook**. John Wiley & Sons, UK.

[120] Kalmikov., A., Dupon, G, Dykes, K., & Chan, C. (2010**). Wind power resource assessment in Complex urban environments: MIT campus case-study using CFD analysis**. In: AWEA 2010 WINDPOWER Conference. Dallas, USA.

[121] HE Dexin. (2006). Wind engineering and industrial aerodynamics. **Beijing**, Vol I, pp: 5-6.

[122] Zhang Guoyu, Jiang Jin, & Liu Changlu. (2009). Numcrical simulation of aerodynamic performance for wind turbines. **East China Electric Power**, VOL. 37, No. 3, pp: 0449-0452.

[123] Franklyn Kanyako, & Isam Janajreh. **Vertical Axis Wind Turbine Performance Prediction for Low Wind Speed Environment**. iEnergy Center Masdar Institute of Science and Technology Abu Dhabi, United Arab Emirates *ijanajreh@masdar.ac.ae, IEEE explorer.

[124] Danao, L.A. (2012). **The Influence of Unsteady Wind on the Performance and Aerodynamics of Vertical Axis Wind Turbines**. pp. 1–258.

[125] Menter, F.R., Langtry, R., & Völker, S. (2006). Transition modelling for general purpose CFD codes. **Flow, Turbul. Combust.**, vol. 77, no. 1–4, pp. 277–303.

List of Bibliography (Continued)

[126] Bachant, P., & Wosnik, M. (2015). **Effects of Reynolds Number on the Performance and Near-Wake Dynamics of a Vertical-Axis Cross-Flow Turbine**. Submitt to Energies.

[127] Anders Goude, Bahri Uzunoˇglu, Javier Gabriele Giovannini, Magdalena, & Antonio Fernandez. (2015). **A GUI for urban wind flow CFD analysis of small scale wind applications**. 2015 International Conference on Cyberworlds

[128] Dhunny, A.Z., Lollchund, M.R., Rughooputh, S.D.D.V. (2017). Wind energy evaluation for a highly complex terrain using Computational Fluid Dynamics (CFD). **Renewable Energy**, 101, 1-9.

[129] R. Beckers. (2006). **Small Wind Turbine Site Selection**.

[130] Li Li, Yimei Wang, & Yongqian Liu. (2013). **Wind Velocity Prediction at Wind Turbine Hub Height Based on CFD Model**. IEEE Xplore, 2013 international conference on materials for renewable energy and environment, pp.411-414.

[131] Spirn, & Anne Whiston. (1986). **Air Quality At Street-Level: Strategies For Urban Design**. Prepared for: Boston Redevelopment Authority, June 1986.

[132] IEC 61400-12-1. (2005). **Wind turbines: Part 12.1 – power performance measurements of electricity producing wind turbines**. Geneva, Switzerland, International Electrotechnical Commission.

[133] Ministry of Energy. (2018). **Wind power and its potential in Thailand**. Department of Alternative Energy Development and Efficiency. Retrieved from http://weben.dede.go.th/webmax/content/wind-power-and-its-potential-thailand

[134] GENI. (2017). **Wind energy potential in Thailand**. Global Energy Network Institute. Retrieved from http://www.geni.org/globalenergy/library/renewable-energy-resources/world/asia/wind-asia/wind-thailand.shtml.

APPENDICES
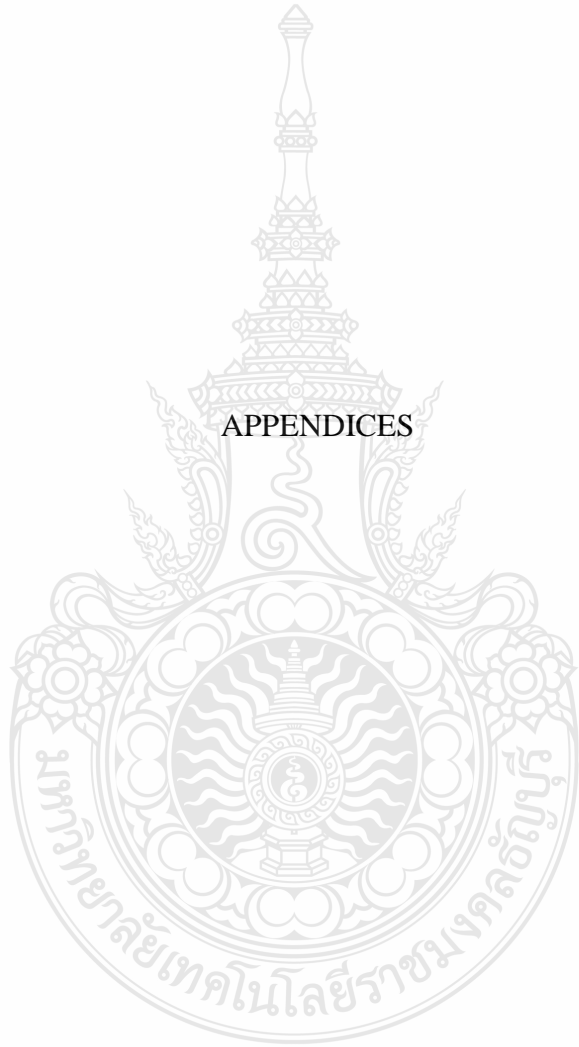
APPENDIX A
CFDesign Usability
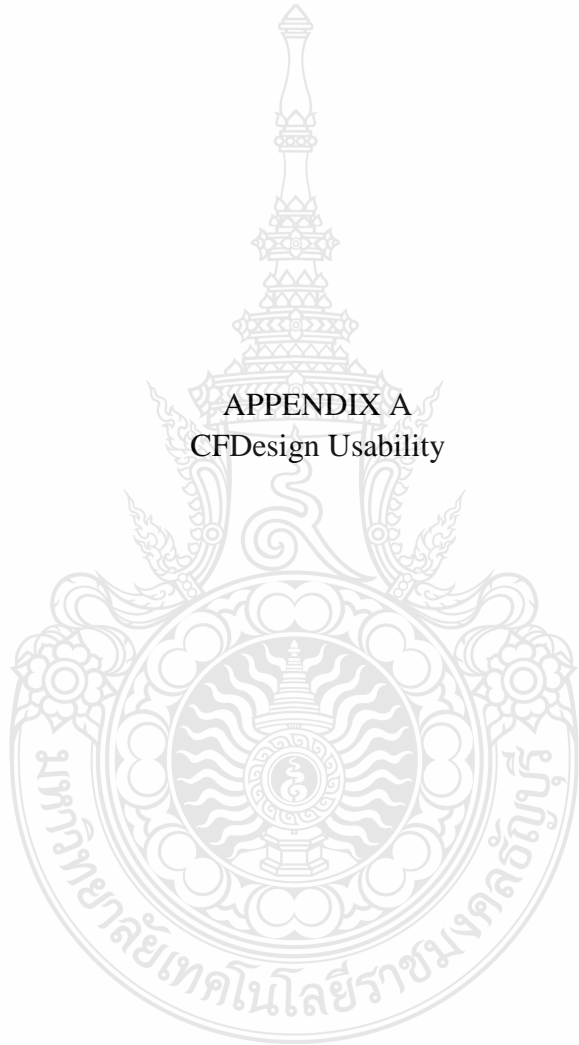
CFDesign Usability

Step 1 In the menu bar select the "New" for use the new model as shown in **Figure 1**
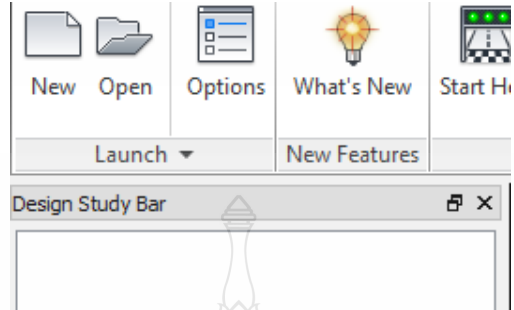
Figure 1 CFDesign Menu Bar

Step 2 In the "New Design Study" select "Browse" import the model file as shown in **Figure 2**
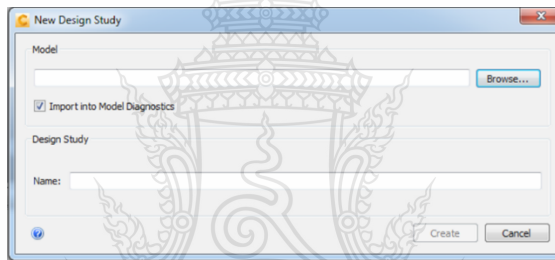
Figure 2 CFDesign Import File

Step 3 The model assessment will check the model compatible "Edge lengths, Surface sliver, Model silvers, Part gaps, Model gaps, and interference" for preparing CFD solving, as shown in **Figure 3**
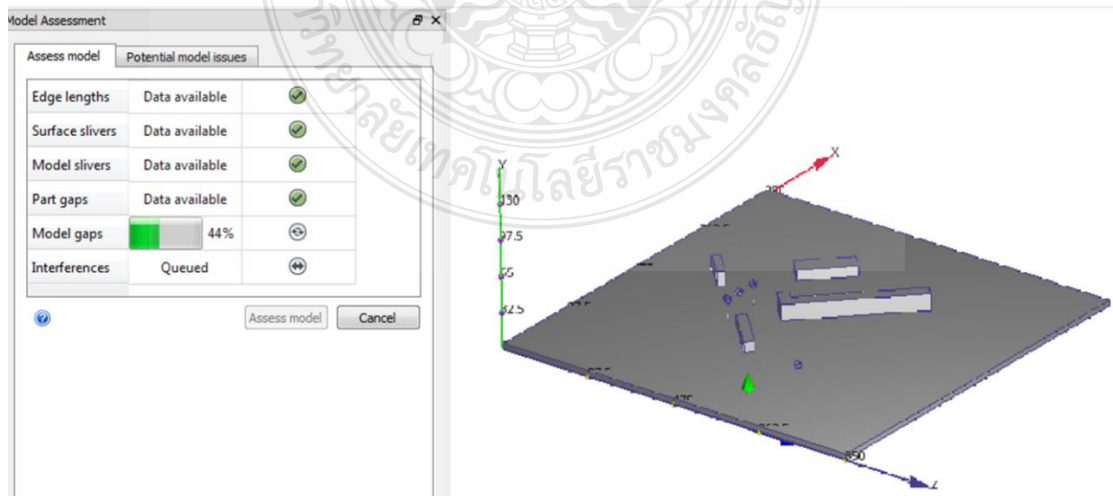
Figure 3 CFDesign Model Assessment

Step 4 Overall, the model part must be selected by the material, the wind turbine be selected by the solid part, and the air be selected by air fluid material, as shown in **Figure 4**
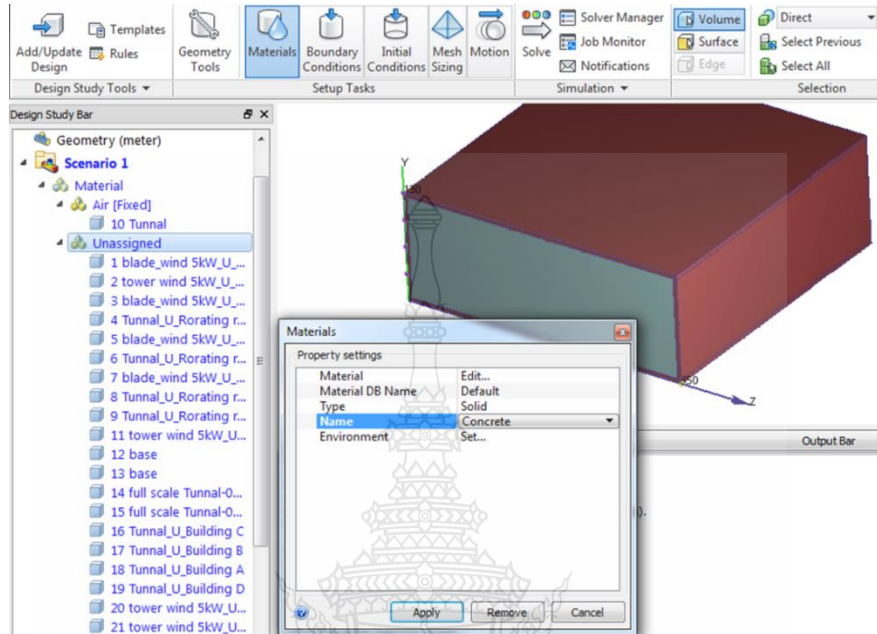
Figure 4 CFDesign Material Selected

Step 5 Select the boundary condition of the model; the inlet side of model should be selected by 4.5 m/s of air flow and the outlet side by 0 Pa of pressure, as shown in **Figure 5**
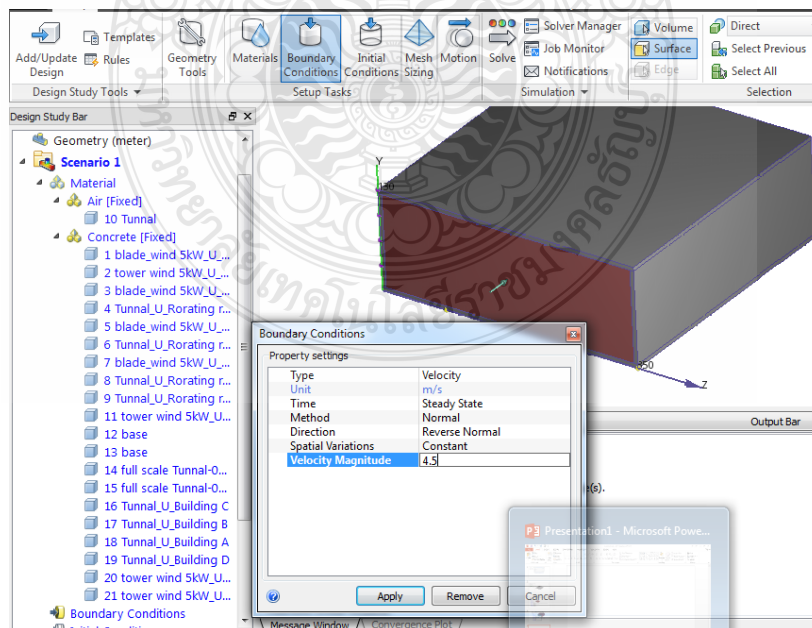
Figure 5 CFDesign Boundary Condition of the Model

Step 6 After selecting the boundary condition, the "Mashing" will be created as shown in **Figure 6**
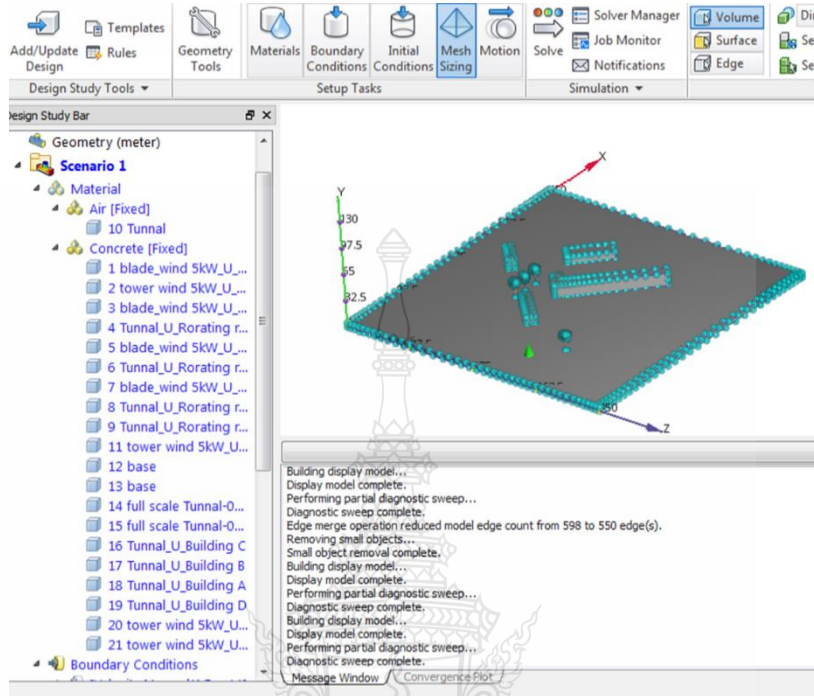
Figure 6 CFDesign Mashing

Step 7 After the model part is mashed, the model will be solved and can be changed to the "turbulence model", including the k- □, k-□, and RNG turbulence model, as shown in **Figure 7**
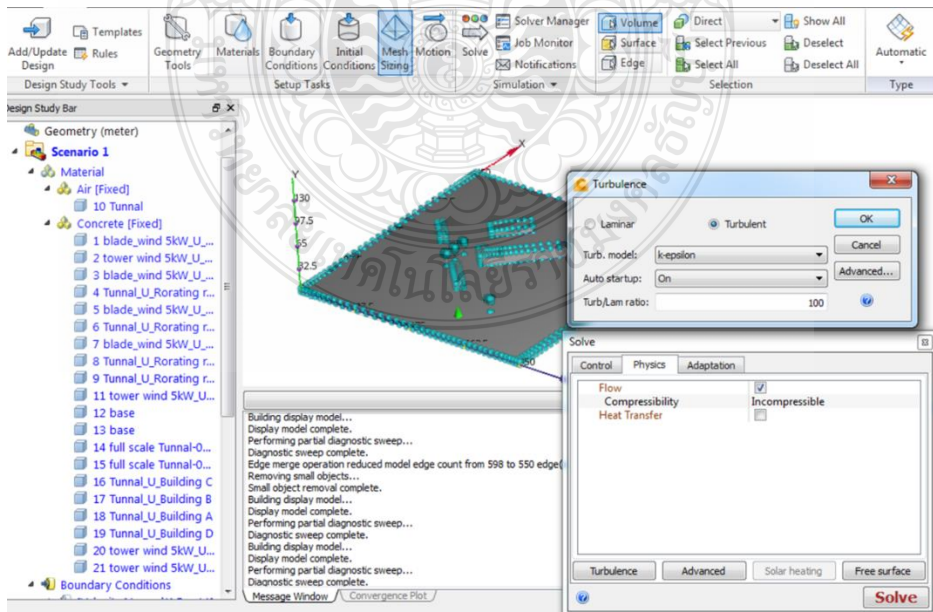
Figure 7 CFDesign Turbulent Model Selection

Step 8 After all steps are finished, the model will be solved, as shown in **Figure 8**
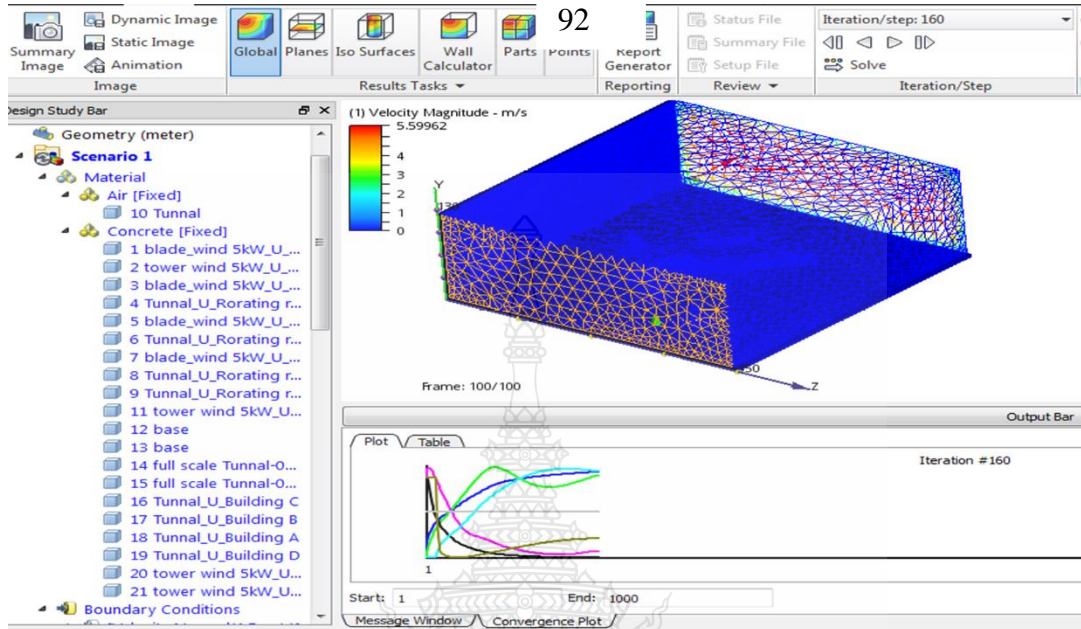
Figure 8 CFDesign solver

Step 9 After completely solving, torque and angular velocity can be found in summary result file in the CFD solver, as shown in **Figure 9**
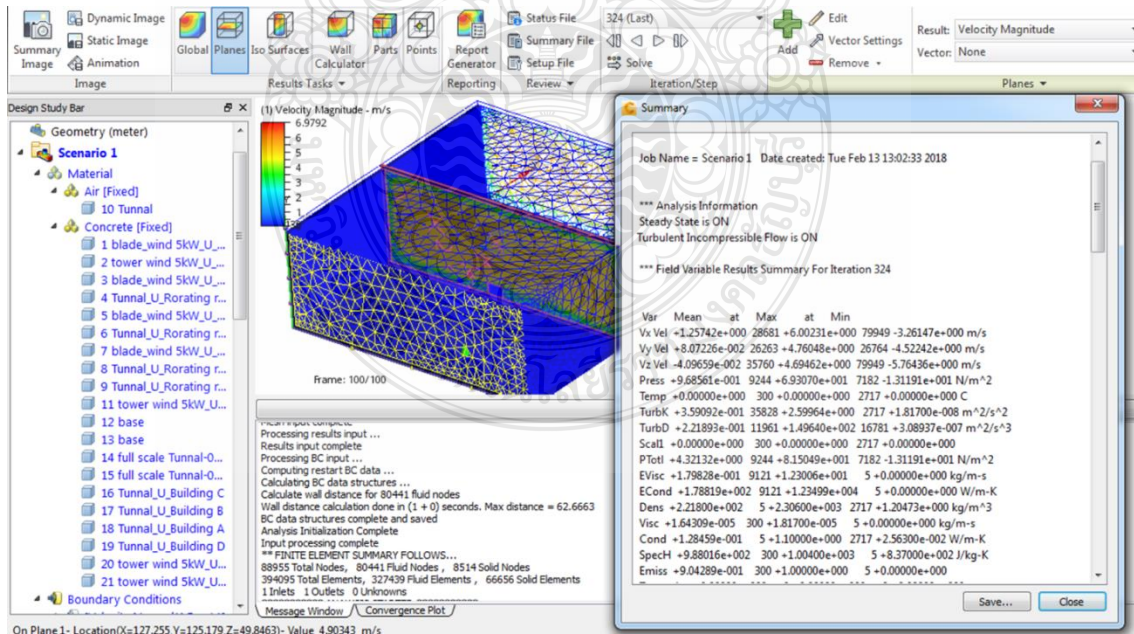
Figure 9 CFDesign Solver Result
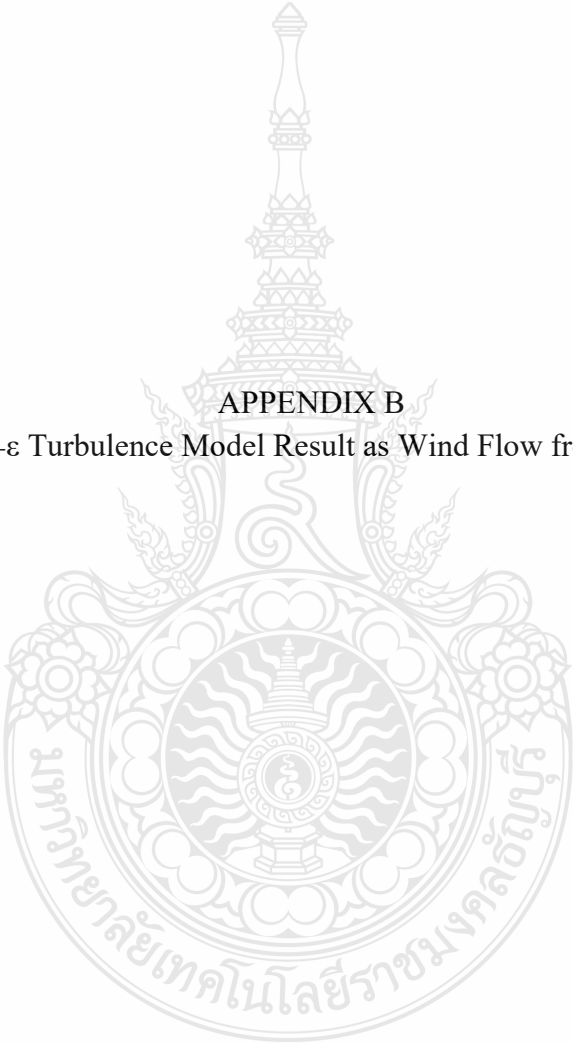
APPENDIX B
CFD k-ε Turbulence Model Result as Wind Flow from the NE

CFD k-ε Turbulence Model Result as Wind Flow from the NE

Time (sec)	Hydraulic Torque (N-m)	Rotating Speed (RPM)	Hydraulic Force X (N)	Hydraulic Force_Y (N)	Hydraulic Force_Z (N)
0.01	2.4552	0	17.4068	0.516968	-0.092353
0.01	2.67805	0	12.8947	0.0797592	-0.0759822
0.01	1.87318	0	427.809	32.5027	-21.1724
0.01	1.104	0	569.933	55.7602	-22.3992
0.02	4.54204	0.0468909	26.7915	0.581729	-0.2612
0.02	4.42764	0.035775	449.86	33.3611	-20.6451
0.02	3.1948	0.0210848	606.068	52.5289	-21.851
0.03	6.82808	0.133637	38.0461	0.725862	-0.401232
0.03	6.77508	0.138393	33.7955	0.0466406	0.228592
0.03	7.17402	0.120337	363.345	26.5138	-15.6632
0.03	5.68215	0.082101	491.109	39.2767	-17.098
0.04	8.64552	0.264044	47.0315	0.781845	-0.424631
0.04	8.54435	0.267788	42.3114	-0.0336484	0.510232
0.04	9.38421	0.257351	269.636	22.4117	-12.5488
0.04	8.64112	0.190622	361.308	30.6903	-29.3593
0.05	9.88862	0.429161	53.0728	0.779345	-0.39112
0.05	9.73415	0.430973	47.9552	-0.101556	0.752175
0.05	10.9232	0.436576	197.428	20.3871	-11.6242
0.05	9.79358	0.355655	260.543	19.7955	-22.5592
0.06	10.6586	0.61802	56.7608	0.742119	-0.336074
0.06	10.436	0.616881	51.309	-0.149072	0.92129
0.06	11.9023	0.645193	151.463	11.9446	-6.53468
0.06	10.1284	0.542699	195.547	10.3559	-11.7612
0.07	11.0965	0.821585	58.9074	0.682908	-0.271947
0.07	12.4506	0.872511	120.378	7.55813	-3.8658
0.07	10.3812	0.736138	152.345	5.4146	-7.03605
0.08	11.3148	1.03351	60.1454	0.611378	-0.202416
0.08	10.9301	1.02235	54.0468	-0.181262	1.08342
0.08	12.7221	1.1103	100.308	5.31362	-2.54294
0.08	10.5221	0.934404	125.282	3.03188	-5.04692

0.09	19.0884	1.24961	106.894	0.798177	-0.494049
0.09	17.2567	1.2311	94.9329	0.262075	0.750898
0.09	19.9854	1.35327	129.922	4.54978	-1.79553
0.09	10.5637	1.13536	108.06	1.94752	-4.04966
0.1	21.0277	1.61417	114.126	0.73117	-0.273896

CFD k-ε Turbulence Model Result as Wind Flow from the NE (Continued)

Time (sec)	Hydraulic Torque (N-m)	Rotating Speed (RPM)	Hydraulic Force_X (N)	Hydraulic Force_Y (N)	Hydraulic Force_Z (N)
54.86	0.32607	47.3015	-41.7148	-0.01713	0.048808
54.86	-0.18684	43.6589	-35.8792	-0.46882	0.240094
54.86	-0.22895	43.708	-28.7582	-0.3178	-0.49926
54.86	-0.23434	34.3317	-18.9764	-0.0853	-0.49914
54.87	0.340863	47.3046	-41.8008	-0.03141	0.10442
54.87	-0.14347	43.6572	-35.9677	-0.52435	0.187149
54.87	-0.1655	43.7058	-28.5529	-0.36638	-0.45528
54.87	-0.20811	34.3295	-19.1966	-0.07626	-0.512
54.88	0.353932	47.3079	-41.761	-0.022	0.164874
54.88	-0.10173	43.6558	-36.2388	-0.49777	0.20182
54.88	-0.0787	43.7042	-28.6284	-0.37541	-0.44529
54.88	-0.19614	34.3275	-19.2351	-0.07081	-0.50336
54.89	0.050719	47.3113	-41.8633	0.095147	0.230805
54.89	-0.06658	43.6548	-36.3143	-0.47266	0.171296
54.89	-0.02356	43.7035	-29.1373	-0.36866	-0.48159
54.89	-0.40025	34.3256	-18.6075	0.03445	-0.50251
54.9	0.22333	47.3118	-41.8715	0.127048	0.341196
54.9	-0.1739	43.6542	-36.1854	-0.49464	0.170406
54.9	-0.03955	43.7032	-29.0092	-0.43821	-0.38627
54.9	-0.6984	34.3218	-18.2727	0.062935	-0.54899
54.91	0.308476	47.3139	-41.9311	0.141496	0.380095
54.91	-0.19369	43.6525	-36.357	-0.51052	0.150612
54.91	0.04121	43.7029	-29.1237	-0.42443	-0.38628
54.91	-0.69861	34.3151	-18.2387	0.074493	-0.5323

APPENDIX C
CFD k-Ɛ Turbulence Model Result as Wind Flow from the SW

CFD k-ε Turbulence Model Result as Wind Flow from the SW

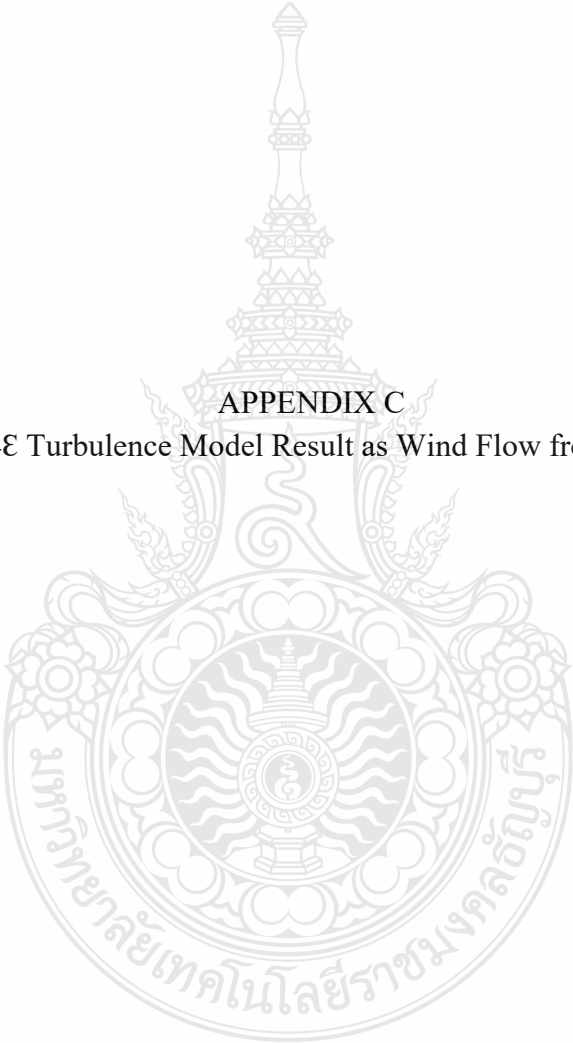| Time (sec)	Hydraulic Torque (N-m)	Rotating Speed (RPM)	Hydraulic Force_X (N)	Hydraulic Force_Y (N)	Hydraulic Force_Z (N)
0.01	2.4552	0	17.4068	0.516968	-0.09235
0.01	2.67805	0	12.8947	0.079759	-0.07598
0.01	1.87318	0	427.809	32.5027	-21.1724
0.01	1.104	0	569.933	55.7602	-22.3992
0.02	4.54204	0.046891	26.7915	0.581729	-0.2612
0.02	4.42764	0.035775	449.86	33.3611	-20.6451
0.02	3.1948	0.021085	606.068	52.5289	-21.851
0.03	6.82808	0.133637	38.0461	0.725862	-0.40123
0.03	6.77508	0.138393	33.7955	0.046641	0.228592
0.03	7.17402	0.120337	363.345	26.5138	-15.6632
0.03	5.68215	0.082101	491.109	39.2767	-17.098
0.04	8.64552	0.264044	47.0315	0.781845	-0.42463
0.04	8.54435	0.267788	42.3114	-0.03365	0.510232
0.04	9.38421	0.257351	269.636	22.4117	-12.5488
0.04	8.64112	0.190622	361.308	30.6903	-29.3593
0.05	9.88862	0.429161	53.0728	0.779345	-0.39112
0.05	9.73415	0.430973	47.9552	-0.10156	0.752175
0.05	10.9232	0.436576	197.428	20.3871	-11.6242
0.05	9.79358	0.355655	260.543	19.7955	-22.5592
0.06	10.6586	0.61802	56.7608	0.742119	-0.33607
0.06	10.436	0.616881	51.309	-0.14907	0.92129
0.06	11.9023	0.645193	151.463	11.9446	-6.53468
0.06	10.1284	0.542699	195.547	10.3559	-11.7612
0.07	11.0965	0.821585	58.9074	0.682908	-0.27195
0.07	10.7942	0.816195	53.1378	-0.17265	1.02653
0.07	12.4506	0.872511	120.378	7.55813	-3.8658
0.07	10.3812	0.736138	152.345	5.4146	-7.03605
0.08	11.3148	1.03351	60.1454	0.611378	-0.20242
0.08	10.9301	1.02235	54.0468	-0.18126	1.08342
0.08	12.7221	1.1103	100.308	5.31362	-2.54294

0.08	10.5221	0.934404	125.282	3.03188	-5.04692
0.09	19.0884	1.24961	106.894	0.798177	-0.49405
0.09	17.2567	1.2311	94.9329	0.262075	0.750898
0.09	19.9854	1.35327	129.922	4.54978	-1.79553
0.09	10.5637	1.13536	108.06	1.94752	-4.04966
0.1	21.0277	1.61417	114.126	0.73117	-0.2739

CFD k-ε Turbulence Model Result as Wind Flow from the SW (Continued)

Time (sec)	Hydraulic Torque (N-m)	Rotating Speed (RPM)	Hydraulic Force_X (N)	Hydraulic Force_Y (N)	Hydraulic Force_Z (N)
99.83	-0.00457	46.5854	34.3605	0.089538	0.064686
99.83	0.02621	44.1708	29.6374	0.170634	-1.00479
99.83	0.091633	47.535	40.2323	0.547838	-0.12502
99.84	-0.17995	40.757	23.9956	0.516273	-0.58614
99.84	-0.01161	46.5853	34.315	0.067301	0.050877
99.84	-0.07077	44.1713	29.5708	0.181165	-0.9745
99.84	-0.26722	47.5367	39.817	0.463017	0.052091
99.85	-0.13505	40.7535	23.8833	0.516258	-0.63005
99.85	-0.00332	46.5851	34.3462	0.025562	0.039276
99.85	-0.13077	44.1699	29.5813	0.238344	-1.01673
99.85	-0.75139	47.5316	39.3547	0.514452	0.068701
99.86	-0.03302	40.7509	24.0252	0.512786	-0.64599
99.86	-0.00587	46.585	34.1477	0.105168	0.072771
99.86	0.04112	44.1674	29.7848	0.212274	-1.01475
99.86	-1.01631	47.5173	38.8402	0.734958	0.092061
99.87	-0.01829	40.7503	23.9622	0.498993	-0.64891
99.87	-0.0089	46.5849	34.074	0.152007	0.091622
99.87	0.042019	44.1682	29.8637	0.21975	-1.02743
99.87	-0.7117	47.4978	38.709	0.705169	0.002594
99.88	0.012824	40.75	24.0564	0.49026	-0.64755
99.88	-0.16287	46.5847	33.9188	0.181345	0.080055
99.88	0.127362	44.169	29.9735	0.303615	-0.98618
99.88	-0.68741	47.4843	38.6724	0.744054	-0.02297
99.89	0.007563	40.7502	24.1887	0.475549	-0.61336

99.89	-0.16969	46.5816	33.9493	0.208409	0.114788
99.89	0.085476	44.1714	29.9307	0.35909	-0.98989
99.89	-0.55548	47.4711	38.8164	0.744025	-0.09302
99.9	0.016103	40.7503	24.0863	0.465979	-0.60464
99.9	-0.23662	46.5784	33.8903	0.119593	0.091097
99.9	0.091486	44.1731	29.9721	0.302837	-1.03678
99.9	-0.47753	47.4605	38.5414	0.762185	-0.05503
99.91	0.004648	40.7507	24.1469	0.442006	-0.58825
99.91	-0.15999	46.5739	34.0475	0.139447	0.120427
99.91	0.183031	44.1748	30.0886	0.259411	-1.04812
99.91	-0.25926	47.4514	38.886	0.684902	-0.0856

APPENDIX D
CFD k-ω Turbulence Model Result as Wind Flow from the SW
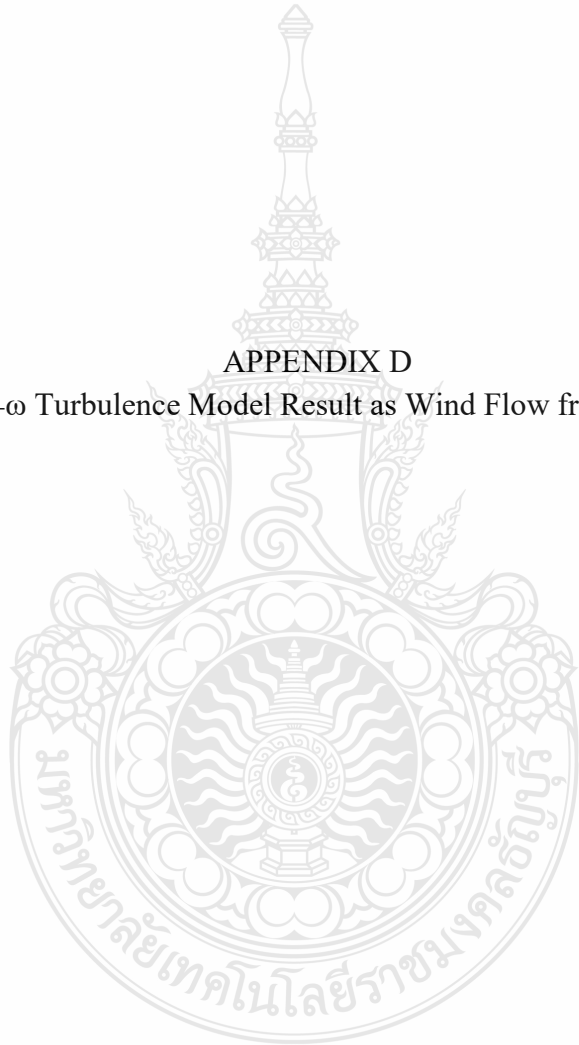
CFD k-ω Turbulence Model Result as Wind Flow from the SW

Time (sec)	Hydraulic Torque (N-m)	Rotating Speed (RPM)	Hydraulic Force_X (N)	Hydraulic Force_Y (N)	Hydraulic Force_Z (N)
0.01	2.4552	0	17.4068	0.516968	-0.09235
0.01	2.67805	0	12.8947	0.079759	-0.07598
0.01	1.87318	0	427.809	32.5027	-21.1724
0.01	1.104	0	569.933	55.7602	-22.3992
0.02	4.54204	0.046891	26.7915	0.581729	-0.2612
0.02	4.42764	0.035775	449.86	33.3611	-20.6451
0.02	3.1948	0.021085	606.068	52.5289	-21.851
0.03	6.82808	0.133637	38.0461	0.725862	-0.40123
0.03	6.77508	0.138393	33.7955	0.046641	0.228592
0.03	7.17402	0.120337	363.345	26.5138	-15.6632
0.03	5.68215	0.082101	491.109	39.2767	-17.098
0.04	8.64552	0.264044	47.0315	0.781845	-0.42463
0.04	8.54435	0.267788	42.3114	-0.03365	0.510232
0.04	9.38421	0.257351	269.636	22.4117	-12.5488
0.04	8.64112	0.190622	361.308	30.6903	-29.3593
0.05	9.88862	0.429161	53.0728	0.779345	-0.39112
0.05	9.73415	0.430973	47.9552	-0.10156	0.752175
0.05	10.9232	0.436576	197.428	20.3871	-11.6242
0.05	9.79358	0.355655	260.543	19.7955	-22.5592
0.06	10.6586	0.61802	56.7608	0.742119	-0.33607
0.06	10.436	0.616881	51.309	-0.14907	0.92129
0.06	11.9023	0.645193	151.463	11.9446	-6.53468
0.06	10.1284	0.542699	195.547	10.3559	-11.7612
0.07	11.0965	0.821585	58.9074	0.682908	-0.27195
0.07	10.7942	0.816195	53.1378	-0.17265	1.02653
0.07	12.4506	0.872511	120.378	7.55813	-3.8658
0.07	10.3812	0.736138	152.345	5.4146	-7.03605
0.08	11.3148	1.03351	60.1454	0.611378	-0.20242
0.08	10.9301	1.02235	54.0468	-0.18126	1.08342
0.08	12.7221	1.1103	100.308	5.31362	-2.54294

0.08	10.5221	0.934404	125.282	3.03188	-5.04692
0.09	19.0884	1.24961	106.894	0.798177	-0.49405
0.09	17.2567	1.2311	94.9329	0.262075	0.750898
0.09	19.9854	1.35327	129.922	4.54978	-1.79553
0.09	10.5637	1.13536	108.06	1.94752	-4.04966
0.1	21.0277	1.61417	114.126	0.73117	-0.2739

CFD k-ω Turbulence Model Result as Wind Flow from the SW (Continued)

Time (sec)	Hydraulic Torque (N-m)	Rotating Speed (RPM)	Hydraulic Force_X (N)	Hydraulic Force_Y (N)	Hydraulic Force_Z (N)
24.5	0.150145	47.2557	30.5796	0.379111	-0.10659
24.51	0.058621	39.9583	16.1805	0.24233	-0.20772
24.51	0.122748	51.8733	35.2057	-0.22254	-0.01463
24.51	-0.17256	47.9526	26.6115	0.116439	-1.54912
24.51	0.141895	47.2586	30.0846	0.373061	-0.09567
24.52	0.077241	39.9594	16.2101	0.242635	-0.19846
24.52	0.14062	51.8756	35.2283	-0.21263	-0.04716
24.52	-0.15721	47.9493	26.6781	0.109388	-1.58486
24.52	0.121513	47.2613	29.72	0.368642	-0.08885
24.53	0.06521	39.9609	16.2301	0.256557	-0.14501
24.53	0.151619	51.8783	35.1972	-0.22283	-0.0428
24.53	-0.15315	47.9463	26.6596	0.116411	-1.59781
24.53	0.095963	47.2636	29.4204	0.364843	-0.08137
24.54	0.077656	39.9621	16.3043	0.235802	-0.14619
24.54	0.174199	51.8812	35.2502	-0.22082	-0.04891
24.54	-0.26391	47.9434	26.5329	0.147941	-1.57446
24.54	-0.0373	47.2655	29.1116	0.347373	-0.10527
24.55	-0.14282	39.9636	15.8841	0.229625	-0.22106
24.55	0.200582	51.8845	35.3494	-0.21245	-0.07145
24.55	-0.28836	47.9384	26.5089	0.171592	-1.53995
24.55	-0.0073	47.2647	29.0832	0.352779	-0.08681
24.56	-0.09635	39.9609	15.9483	0.214099	-0.20039
24.56	0.159931	51.8884	35.4805	-0.20909	-0.07873
24.56	-0.44175	47.9329	26.2438	0.146891	-1.52003

| 24.56 | 0.026122 | 47.2646 | 29.1117 | 0.35383 | -0.06956 |
24.57	-0.05921	39.959	15.9347	0.186255	-0.17142
24.57	0.184423	51.8914	35.5947	-0.23033	-0.11555
24.57	-0.39043	47.9244	26.4954	0.173579	-1.53227
24.57	-0.09269	47.2651	28.8442	0.341969	-0.08755
24.58	-0.09831	39.9579	15.8235	0.156392	-0.14956
24.58	-0.00217	51.8949	35.3521	-0.18093	-0.13659
24.58	-0.2578	47.917	26.6531	0.190976	-1.55139
24.58	-0.16349	47.2633	28.6951	0.354371	-0.07379
24.59	-0.18806	39.956	15.4876	0.15181	-0.10717
24.59	0.071427	51.8949	35.4198	-0.18119	-0.1256

CFD k-ω Turbulence Model Result as Wind Flow from the SW (Continued)

Time (sec)	Hydraulic Torque (N-m)	Rotating Speed (RPM)	Hydraulic Force_X (N)	Hydraulic Force_Y (N)	Hydraulic Force_Z (N)
24.59	-0.18119	47.9121	26.7861	0.190194	-1.57767
24.59	-0.2305	47.2602	28.501	0.34894	-0.07512
24.6	-0.1624	39.9524	15.6061	0.128709	-0.13894
24.6	0.019939	51.8963	35.2005	-0.16581	-0.119
24.6	-0.26738	47.9086	26.6364	0.264386	-1.64294
24.6	-0.34012	47.2558	28.4432	0.320876	-0.03314
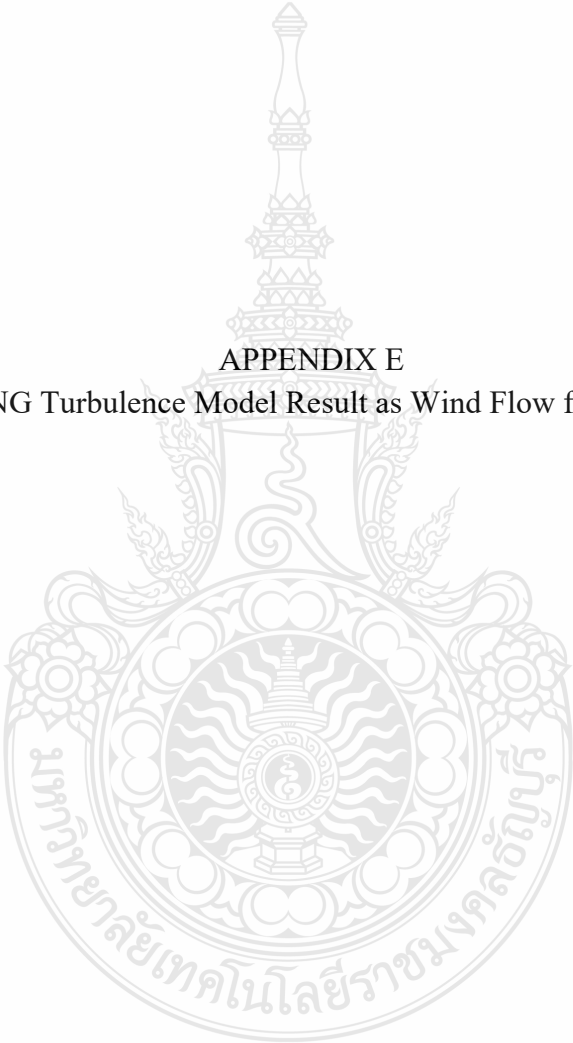
APPENDIX E
CFD RNG Turbulence Model Result as Wind Flow from the SW

CFD RNG Turbulence Model Result as Wind Flow from the SW

Time (sec)	Hydraulic Torque (N-m)	Rotating Speed (RPM)	Hydraulic Force_X (N)	Hydraulic Force_Y (N)	Hydraulic Force_Z (N)
0.01	2.4552	0	17.4068	0.516968	-0.09235
0.01	2.67805	0	12.8947	0.079759	-0.07598
0.01	1.87318	0	427.809	32.5027	-21.1724
0.01	1.104	0	569.933	55.7602	-22.3992
0.02	4.54204	0.046891	26.7915	0.581729	-0.2612
0.02	4.42764	0.035775	449.86	33.3611	-20.6451
0.02	3.1948	0.021085	606.068	52.5289	-21.851
0.03	6.82808	0.133637	38.0461	0.725862	-0.40123
0.03	6.77508	0.138393	33.7955	0.046641	0.228592
0.03	7.17402	0.120337	363.345	26.5138	-15.6632
0.03	5.68215	0.082101	491.109	39.2767	-17.098
0.04	8.64552	0.264044	47.0315	0.781845	-0.42463
0.04	8.54435	0.267788	42.3114	-0.03365	0.510232
0.04	9.38421	0.257351	269.636	22.4117	-12.5488
0.04	8.64112	0.190622	361.308	30.6903	-29.3593
0.05	9.88862	0.429161	53.0728	0.779345	-0.39112
0.05	9.73415	0.430973	47.9552	-0.10156	0.752175
0.05	10.9232	0.436576	197.428	20.3871	-11.6242
0.05	9.79358	0.355655	260.543	19.7955	-22.5592
0.06	10.6586	0.61802	56.7608	0.742119	-0.33607
0.06	10.436	0.616881	51.309	-0.14907	0.92129
0.06	11.9023	0.645193	151.463	11.9446	-6.53468
0.06	10.1284	0.542699	195.547	10.3559	-11.7612
0.07	11.0965	0.821585	58.9074	0.682908	-0.27195
0.07	10.7942	0.816195	53.1378	-0.17265	1.02653
0.07	12.4506	0.872511	120.378	7.55813	-3.8658
0.07	10.3812	0.736138	152.345	5.4146	-7.03605
0.08	11.3148	1.03351	60.1454	0.611378	-0.20242
0.08	10.9301	1.02235	54.0468	-0.18126	1.08342
0.08	12.7221	1.1103	100.308	5.31362	-2.54294

0.08	10.5221	0.934404	125.282	3.03188	-5.04692
0.09	19.0884	1.24961	106.894	0.798177	-0.49405
0.09	17.2567	1.2311	94.9329	0.262075	0.750898
0.09	19.9854	1.35327	129.922	4.54978	-1.79553
0.09	10.5637	1.13536	108.06	1.94752	-4.04966
0.1	21.0277	1.61417	114.126	0.73117	-0.2739

CFD RNG Turbulence Model Result as Wind Flow from the SW (Continued)

Time (sec)	Hydraulic Torque (N-m)	Rotating Speed (RPM)	Hydraulic Force_X (N)	Hydraulic Force_Y (N)	Hydraulic Force_Z (N)
49.84	0.603213	41.1924	25.735	0.253109	-0.48626
49.84	0.443969	46.3436	37.5176	0.007651	0.099881
49.85	-0.00506	38.3817	17.858	0.049272	-0.75258
49.85	-0.47966	50.0066	36.1899	0.139008	0.044676
49.85	0.582986	41.2039	25.4258	0.252011	-0.47742
49.85	0.357486	46.3521	37.1558	-0.04361	0.044776
49.86	-0.06043	38.3816	17.8209	0.071215	-0.80333
49.86	-0.33984	49.9975	36.4083	0.100972	0.044263
49.86	0.544418	41.215	25.0944	0.251042	-0.46859
49.86	0.170401	46.3589	37.0177	-0.02811	0.025796
49.87	-0.04427	38.3805	17.7699	0.063942	-0.81301
49.87	-0.24865	49.991	36.7074	0.076226	0.049754
49.87	0.483404	41.2254	24.7968	0.249497	-0.47283
49.87	-0.38241	46.3621	35.937	-0.09744	0.070168
49.88	-0.0424	38.3796	17.7594	0.078945	-0.8382
49.88	-0.14928	49.9862	36.8724	0.050221	0.02366
49.88	0.477033	41.2347	24.9501	0.252371	-0.46491
49.88	-0.35984	46.3548	36.1717	-0.12573	0.172355
49.89	-0.00909	38.3788	18.0045	0.090047	-0.86293
49.89	-0.07438	49.9834	37.1499	0.030549	0.000716
49.89	0.431499	41.2438	24.7572	0.253573	-0.45072
49.89	-0.64962	46.348	35.707	0.07834	0.162776
49.9	-0.07356	38.3786	17.9415	0.14845	-0.87616
49.9	-0.03232	49.982	37.2156	0.021291	-0.01757
49.9	0.216308	41.252	24.6141	0.259501	-0.40588
49.9	-0.63202	46.3356	35.8143	0.177306	0.21275

|					
49.91	-0.05831	38.3772	18.1062	0.228382	-0.886
49.91	-0.01222	49.9813	37.2111	0.003851	-0.01488
49.91	0.173416	41.2562	24.4761	0.241772	-0.38161
49.91	-0.61584	46.3235	35.4664	0.188018	0.12398
49.92	-0.14292	38.3761	18.1333	0.283415	-0.87169
49.92	-0.00624	49.9811	37.22	0.000794	-0.02599
49.92	0.099661	41.2595	24.3361	0.245744	-0.35969
49.92	-0.52021	46.3117	35.5263	0.189985	0.089948
49.93	-0.18813	38.3734	18.0739	0.278905	-0.88324
49.93	0.022721	49.981	37.3782	0.000368	-0.0451
49.93	0.169548	41.2614	24.3546	0.251521	-0.36318

CFD RNG Turbulence Model Result as Wind Flow from the SW (Continued)

Time (sec)	Hydraulic Torque (N-m)	Rotating Speed (RPM)	Hydraulic Force_X (N)	Hydraulic Force_Y (N)	Hydraulic Force_Z (N)
49.93	-0.13688	46.3018	35.8269	0.103443	0.018329
49.94	-0.33946	38.3698	18.1238	0.309502	-0.84149
49.94	-0.01208	49.9814	37.4015	0.00086	-0.04103
49.94	0.04595	41.2646	24.2071	0.249709	-0.32969
49.94	0.065066	46.2992	35.9644	0.060977	-0.0322
49.95	-0.26057	38.3633	18.0453	0.296063	-0.86257
49.95	0.024375	49.9812	37.554	-0.00599	-0.06572

APPENDIX F
List of Publications
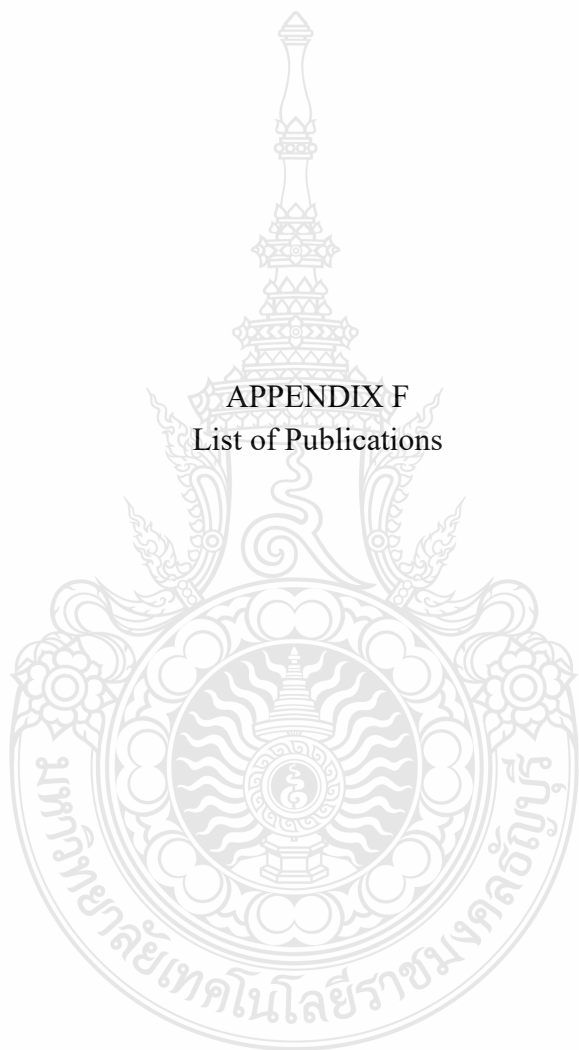
List of Publications

International Journal

K.Kongkapisuth, W.Roynarin and D.Intholo " Study of Building Effects
on Small HAWTs Performance in Building-Obstructed Wind Flow Area
by Using a CFD k-Ɛ Turbulence Model Validated with Site Measurement"
International Energy Journal 17(2017) 193-210.
Impact Factor 2015 = 0.434
Quarties 2016 = Q3
https://www.rericjournal.ait.ac.th

International Conferences

1. **Krittapas Kongkapisuth**, Wirachai Roynarin Ph.D., Decha Intholo
"Performance prediction of 5kW wind turbine wind flow as across
building obstruction using CFD, k-Ɛ Turbulence Model, technique"
Proceeding, The 1st Maejo-Enginio International Conference on
Renewable Energy (MEICRE 2017), The Empress Hotel, Chiang Mai,
Thailand, May 31-June 02, 2017, pp. 342-358.

2. **Krittapas Kongkapisuth**, Wirachai Roynarin Ph.D., Decha Intholo
"Building Obstruction Effect on Power Performance of small wind turbine
using 3 Turbulence Models CFD technique" Proceeding, International
Academy of Science, Technology, Engineering and Management
(81st IASTEM),Phuket, Thailand, October 9-10, 2017, pp. 46-54.

National Conferences

Krittapas Kongkapisuth, Wirachai Roynarin Ph.D., Decha Intholo
"The study of airflow obstruction effect from building on 5 kW wind
turbine performance by using CFD technique" Proceeding, The 9th
Thailand Renewable Energy for Communities Conference 2016
(TREC-9 2016) , Rajamangala University of Technology Lanna,
Chiang Mai, Thailand, November 29-December 01, 2016, pp. 122-128.

Biography

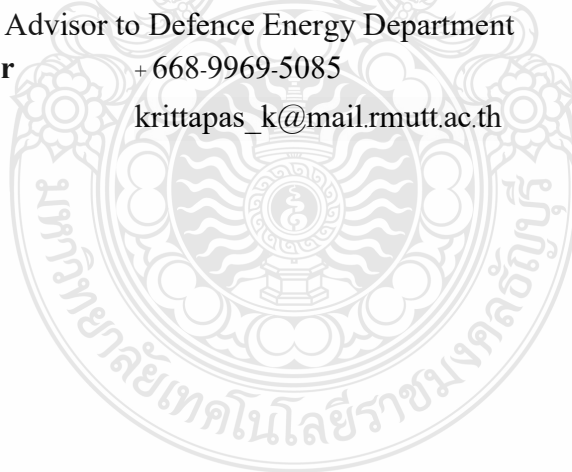|	
Name - Surname	*Lieutenant General* Krittapas Kongkapisuth
Date of Birth	10 March 1962
Address	59/31 Leabklonsong Rd., Bangchun Subdistrict, Klongsamwa District, Bangkok, Thailand 10510
Education	Bachelor of Science (Civil Engineer), Chulachomkloa Royal Military Academy Master of Science (Renewable Energy), Narasuan University Doctor of Engineering Program in Energy and Materials Engineering (International Program), Faculty of Engineering, Rajamangala University of Technology Thanyaburi (RMUTT)
Experiences Work	Director of Policy & Plan Division, Defence Energy Department Director of Renewable Energy Division, Defence Energy Department Chief of Staff, Defence Energy Department Deputy General Director, Defence Energy Department Senior Expert, Office of the Permanent Secretary for Defence Advisor to Defence Energy Department
Telephone Number	+ 668-9969-5085
Email Address	krittapas_k@mail.rmutt.ac.th

Biography

Name - Surname	*Lieutenant General* Krittapas Kongkapisuth
Date of Birth	10 March 1962
Address	59/31 Leabklonsong Rd., Bangchun Subdistrict, Klongsamwa District, Bangkok, Thailand 10510
Education	Bachelor of Science (Civil Engineer), Chulachomkloa Royal Military Academy
	Master of Science (Renewable Energy), Narasuan University
	Doctor of Engineering Program in Energy and Materials Engineering (International Program), Faculty of Engineering, Rajamangala University of Technology Thanyaburi (RMUTT)
Experiences Work	Director of Policy & Plan Division, Defence Energy Department
	Director of Renewable Energy Division, Defence Energy Department
	Chief of Staff, Defence Energy Department
	Deputy General Director, Defence Energy Department
	Senior Expert, Office of the Permanent Secretary for Defence
	Advisor to Defence Energy Department
Telephone Number	+ 668-9969-5085
Email Address	krittapas_k@mail.rmutt.ac.th